Lawrence Berkeley National Laboratory
Recent Work

Title
HYDROGEN RETENTION AND RELEASE FROM URANIUM DIOXIDE

Permalink
https://escholarship.org/uc/item/8mj1g90p

Author
Sherman, D.F.

Publication Date
1987-09-01

eScholarship.org Powered by the California Digital Library
University of California

LBL-24030 c.2

Lawrence Berkeley Laboratory
UNIVERSITY OF CALIFORNIA

Materials & Chemical Sciences Division

NOV 10 1987

Hydrogen Retention and Release from Uranium Dioxide

D.F. Sherman
(Ph.D. Thesis)

August 1987

TWO-WEEK LOAN COPY
This is a Library Circulating Copy
which may be borrowed for two weeks.

LBL-24030 c.2

Prepared for the U.S. Department of Energy under Contract DE-AC03-76SF00098

DISCLAIMER

This document was prepared as an account of work sponsored by the United States Government. While this document is believed to contain correct information, neither the United States Government nor any agency thereof, nor the Regents of the University of California, nor any of their employees, makes any warranty, express or implied, or assumes any legal responsibility for the accuracy, completeness, or usefulness of any information, apparatus, product, or process disclosed, or represents that its use would not infringe privately owned rights. Reference herein to any specific commercial product, process, or service by its trade name, trademark, manufacturer, or otherwise, does not necessarily constitute or imply its endorsement, recommendation, or favoring by the United States Government or any agency thereof, or the Regents of the University of California. The views and opinions of authors expressed herein do not necessarily state or reflect those of the United States Government or any agency thereof or the Regents of the University of California.

HYDROGEN RETENTION AND RELEASE FROM URANIUM DIOXIDE

Douglas F. Sherman

Materials and Chemical Sciences Division
Lawrence Berkeley Laboratory
University of California

and

Department of Nuclear Engineering
University of California, Berkeley
Berkeley, California 94720

August 1987

HYDROGEN RETENTION AND RELEASE FROM URANIUM DIOXIDE

Douglas F. Sherman

Department of Nuclear Engineering

University of California, Berkeley, California

ABSTRACT

A technique was developed for measuring the solubility of hydrogen in refractory ceramics, as well as the kinetics of release of the dissolved hydrogen. The ceramic samples (UO_2 in this study) are exposed to high pressure hydrogen gas at a fixed temperature for a time sufficient to achieve equilibrium. After rapid quenching, the hydrogen-saturated sample is transferred to a vacuum-outgassing furnace. The sample is outgassed in a linear temperature ramp and the released hydrogen is detected by an in-situ mass spectrometer. This technique measures the rate of release of hydrogen with a sensitivity level of about 2 ng of hydrogen(as D_2) per hour. With experiments of up to 4 hours duration this gives a total sensitivity of less than 10 ng of hydrogen per 4.5 g UO_2 sample or about 0.3 ppm atomic. In this study, experiments were conducted on both polycrystalline UO_2 and single crystal UO_2 specimens. The experimental variables in this study included temperature (1000 - 1600 °C) and infusion pressure (5 - 32 atm D_2), and for the polycrystalline specimen, the stoichiometry of the oxide. The dissolution of hydrogen in both

single crystal and polycrystalline UO_2 was found to obey Seivert's law. The Sievert's law constant of deuterium in single crystal UO_2 was determined to be: $3.0 \times 10^7 \exp(-235\ kJ/RT)$ ppm atomic/$\sqrt{atm}$ and for polycrystalline UO_2: $5.5 \times 10^4 \exp(-100\ kJ/RT)$ ppm atomic/$\sqrt{atm}$. The solubility of hydrogen in hypostoichiometric urania was found to be up to three orders of magnitude greater than in stoichiometric UO_2 depending on the O/U ratios-- thus implying the anion vacancy is the primary solution site in the UO_2 lattice. The release-rate curves for the single crystal and polycrystalline UO_2 specimens exhibited multiple peaks, with most of the deuterium released between 600 and 1200 °C for the polycrystalline samples, and between 700 and 1800 °C in the single-crystal specimens. This release of hydrogen from UO_2 could not be adequately modeled as diffusion or diffusion with trapping and resolution. It was determined that release was governed by release from traps in both the polycrystalline and single crystal UO_2 specimens. The single-crystal specimens exhibited first-order detrapping from two sites, and the polycrystalline specimens first-order detrapping from the first site and second-order detrapping from the second site that was observed at a higher outgassing temperature.

TO PATRICIA

Table of Contents

Abstract 1

Table of Contents i

Acknowledgements iv

1. INTRODUCTION 1

    1.1 Background 1

    1.2 Objectives and Experimental Matrix 2

    1.3 Review of Previous Work 5

        1.3.1 Hydrogen Solubility and Diffusion in UO_2 5

        1.3.2 Hydrogen Solubility in Other Ceramic Oxides 9

2. EXPERIMENTAL 14

    2.1 UO_2 Samples 14

    2.2 Infusion Furnace 17

        2.2.1 Description of Apparatus 17

        2.2.2 Operation 23

        2.2.3 Saturation Time and Quench Calculation 27

    2.3 Gas Release Apparatus 31

        2.3.1 Description of Apparatus 31

        2.3.2 Operation 39

        2.3.3 Estimate of D_2 Losses During Operation 42

3. RESULTS 46

    3.1 Gaussian Fits to Release Rate Data 46

3.2 Release of D_2 from Single Crystal UO_2 48

3.3 Release of D_2 from Polycrystalline UO_2 51

3.3.1 Stoichiometric UO_2 51

3.3.2 Hypostoichiometric Urania 60

3.4. Solubility Summary 65

3.4.1 Single Crystal UO_2 65

3.4.2 Polycrystalline UO_2 67

3.5 Comparison with other Ceramic Oxides and Wheeler's Results 70

3.5.1 Ceramic Oxides 72

3.5.2 Wheeler's Results 72

4. MODELING OF RELEASE KINETICS 74

4.1 Simple Diffusion Model 74

4.1.1 Solution of Diffusion Equation 74

4.1.2 Comparison of Solution with Results 77

4.2 Diffusion with Trapping and Resolution 81

4.2.1 Solution of Diffusion Equation with Trapping and Resolution 83

4.2.2 Comparison of Solution with Results 85

4.3 Detrapping Model 86

4.3.1 First and Second-Order Detrapping 87

4.3.2 Comparison of Solution with Results 88

5. DISCUSSION OF TRAPPING 104

5.1 Trapping in Uranium Dioxide 104

5.2 Trapping of Hydrogen in Metals and other Refractory Materials 104

5.3 Trapping in This Experiment 105

6. CONCLUSIONS 107

6.1 Thermodynamic Solubility of Hydrogen in UO_2 107

6.2 Chemical Nature and Location of Hydrogen in UO_2 107

6.3 Release Kinetics of Hydrogen from UO_2 108

APPENDIX A Estimate of D_2 loss during Quenching 109

A.1 Release via Simple Diffusion 109

A.2 Release via Detrapping 110

A.3 Uniform Release Model 113

APPENDIX B Experimental Release Rate Curves 115

REFERENCES 147

ACKNOWLEDGEMENTS

I would like to thank my research advisor, Professor Donald R. Olander of the Department of Nuclear Engineering, for his patient guidance and help in carrying out this research.

I would also like to thank John Souza, John Austin, and Dan Winterbauer of the mechanical shop, and Jack Harrell of the electronic shop for the fabrication of many of the parts used in this research.

I would especially like to thank Dr. Mehdi Balooch for his supervision, and greatly appreciated assistance throughout this entire research.

I would also like to thank all of my fellow students of Dr. Olander's research group who may have assisted me over the many years of this research.

Finally, I would like to thank my wife, Jeanne, whose incredible patience and support has been the main source of inspiration in finishing this work.

This work was supported by the Director, Office of Energy Research, Office of Basic Energy Sciences, Materials Science Division of the U.S. Department of Energy under contract # DE-AC03-76SF00098.

1. INTRODUCTION

1.1. Background

When heated to high temperature, improperly fabricated UO_2 fuel rods may release hydrogen-bearing gases that attack the Zircaloy cladding. This hydriding could lead to brittle failure of the cladding, releasing radioactive fission products into the primary reactor coolant. One possible source of hydrogen in the fuel (other than adsorbed H_2O) is hydrogen dissolved in the lattice of the solid. Hydrogen can be introduced into the fuel during manufacture, which includes sintering in H_2/H_2O mixtures at ≈1700 C. The hydrogen/H_2O atmosphere is used to control the stoichiometry of the resulting UO_2 pellets. In a previous study by Olander et. al,[1] the interaction of water with UO_2 was extensively studied. At present no reliable information on hydrogen solubility in UO_2 is available. Previous results by Wheeler[2] on hydrogen interaction with UO_2, which will be discussed later, are inconclusive.

Transport and solubility of tritium in UO_2 is also of interest. Tritium is produced as a ternary fission product in U-235 and substantial quantities of tritium (10,000-20,000 Ci) can exist in a reactor near the end of core life. Release of this tritium from ruptured fuel pins into the primary coolant during reactor operation can pose a potential disposal problem for contaminated coolant water as well as an atmospheric contamination problem as leaking primary coolant water evaporates into the primary containment. A proposed head-end step for fuel reprocessing called "voloxidation"[3] is based on driving tritium from sheared fuel pins by heating. The kinetics of this process are also dependent on an understanding of tritium transport in UO_2 at elevated temperatures.

Tritium behavior in other ceramic oxides[4] is also important in fusion technology as tritium is produced in the fusion reactor. Some of these oxides may be used as coating, on metallic components, or as breeder material.[5] (e.g Li_2O,[6] $LiAlO_2$[7]) The

inventory and distribution of tritium in these materials will be dependent on its high temperature transport behavior.

1.2. Objectives and Experimental Matrix

The three objectives of this research are: (a) to determine the thermodynamic solubility of hydrogen in the lattice of single crystal and polycrystalline UO_2, (b) to determine the chemical nature and location in the microstructure of hydrogen bound in single crystal and polycrystalline UO_2, and (c) to examine the characteristics of the kinetics of release of hydrogen from single crystal and polycrystalline samples of UO_2.

The experimental variables that are used to achieve these objectives include the pressure and temperature of hydrogen infusion, and the stoichiometry and morphology of the UO_2 samples.

There are two possible mechanisms for hydrogen dissolution in the UO_2 lattice. The first mechanism is one-step molecular dissolution:

$$H_2(g) = H_2(\text{dissolved}) \tag{1}$$

The equilibrium constant K_{sp} for this reaction is given by:

$$K_{sp} = \frac{C_{H_2}}{P_{H_2}} = K^o \exp(-\Delta H_s/RT) \tag{2}$$

Where C_{H_2} is the concentration of hydrogen molecules dissolved in the solid, P_{H_2} is the hydrogen gas pressure, K^o is the pre-exponential factor and ΔH_s is the heat of solution of hydrogen in UO_2. The other mechanism for dissolution is two-step atomic dissolution:

$$\tfrac{1}{2}H_2(g) = H(g) \tag{3a}$$

and

$$H(g) = H(\text{dissolved}) \tag{3b}$$

giving a total reaction:

$$\tfrac{1}{2}H_2(g) = H(\text{dissolved}) \tag{4}$$

The equilibrium constant K_{sp} for this reaction is given by:

$$K_{sp} = \frac{C_H}{(P_{H_2})^{1/2}} = K^o \exp(-\Delta H_s/RT) \tag{5}$$

C_H is the concentration of hydrogen atoms dissolved in the solid.

By varying the temperature at a particular pressure and then constructing an Arrhenius plot for the concentration of dissolved hydrogen versus temperature it is possible to determine the sign and magnitude of the heat of solution. A positive heat of solution shows that solution is endothermic with respect to the hydrogen molecule and conversely a negative heat of solution corresponds to an exothermic solution.

Eqs. (2) and (5) provide two different relations between hydrogen pressure and the concentration of the dissolved hydrogen. In Eq (2) C_{H_2} is directly proportional to the pressure of $H_2(g)$; this is known as Henry's law. In Eq (5) C_H is proportional to the square root of of the pressure of $H_2(g)$, which is known as Sievert's law. By varying the pressure at a fixed temperature it is possible to determine, from the slope of the graph of logarithm of the pressure versus concentration which state of dissolved hydrogen predominates. A slope of unity corresponds to Henry's law and molecular dissolution, and a slope of one half to Sievert's law and atomic dissolution.

Another variable that is explored is the effect on hydrogen solubility of stoichiometry of the UO_2. Unlike most ceramic oxides, UO_2 can exist in different stoichiometries depending on the prevailing oxygen potential of the ambient gas. In stoichiometric UO_2 the oxygen-to-uranium ratio is exactly 2. In hypostoichiometric urania (UO_{2-x}), that can only exist at temperatures above 1300 C, the O/U ratio is less than 2. Finally hyperstoichiometric urania (UO_{2+x}) corresponds to O/U ratios greater than 2.

In the UO_2 lattice there are only two possible possible solution sites for hydrogen: (1) The (½,½,½) interstitial site in the fluorite structure (as shown by helium

solubility studies)[8] and; (2) The anion vacancy (as suggested by Wheeler[2]). By varying the stoichiometry the vacancy concentration is greatly altered. The concentration of thermally generated (intrinsic) anion vacancies in the fluorite lattice is small in stoichiometric UO_2. However, extrinsic vacancies (required to satisfy charge neutrality in the crystal) are produced in UO_{2-x}. Conversely in UO_{2+X} there should be few anion vacancies. Thus by comparing the solubility of hydrogen in stoichiometric and hypostoichiometric UO_2 the role of anion vacancies in dissolving hydrogen in the lattice can be determined.

Another variable studied is the morphology of the ceramic; Both polycrystalline and single crystal samples have been tested. From these experiments, the effect on solubility of grain boundaries and other microstructural defects present in polycrystalline UO_2 are explored. These defects may be sites for hydrogen dissolution in polycrystalline UO_2.

Finally the release kinetics are examined for the rate-determining step of release of hydrogen from uranium dioxide. The kinetics will suggest whether release is governed by diffusion or if release from "traps" or specific binding sites in the solid is important as the previous study on H_2O release suggested.[1] Possible traps in the solid include; pores, dislocations, subgrain boundaries, impurity atoms, and precipitates.

Although hydrogen is mentioned as the species of interest, actually deuterium was used as the infusing gas in UO_2 in this study. The use of deuterium avoids the problem of measuring small hydrogen or H_2O signals by a mass spectrometer in the presence of a large hydrogen or H_2O background in the vacuum system during the outgassing of the UO_2. In addition, direct molecular beam sampling and *in situ* detection of the released deuterium or D_2O was employed in place of post-release transfer of the gas to a separate chamber for analysis.

1.3. Review of Previous Work

1.3.1. Hydrogen Solubility and Diffusion in UO_2

A considerable amount of work has been published on diffusion phenomena in uranium dioxide. But, surprisingly little work has been done on hydrogen diffusion in UO_2, with almost none on solubility of hydrogen in UO_2. Past work on tritium transport in UO_2 has been motivated almost entirely by interest in release of this radionuclide from reactor fuel.

The first work on diffusion was performed by Wheeler in 1971.[2] UO_2 single crystals were heated in hydrogen or tritium sufficiently long to achieve saturation at temperatures of 500 C to 1000 C and pressures of 0.1 to 0.9 kPa. During subsequent heating, the rate of release was measured by gas pressure increases or radioassay of the released tritium. Good agreement was obtained for different samples as well as for the two different techniques. The diffusivity, D, in cm^2/sec is given by:

$$D = 0.37\exp(-59.8kJ/RT) \tag{6}$$

The only other work measuring the diffusivity of hydrogen in UO_2 with this method was performed by Aratono and Nakashima.[9] Here a polycrystalline pellet of UO_2 was thermally infused with tritium gas for enough time to reach equilibrium before subsequent outgassing. The results that are shown in Fig. 1 are in reasonable agreement, suggesting no significant difference in hydrogen diffusion in single and polycrystalline UO_2. In addition, in both experiments the form of the hydrogen detected appeared to be molecular, with no formation of HTO.

Other work on tritium diffusivity in UO_2 by Scargill,[10] Aratono and Tachigawa,[11] and Aratono and Nakashima,[12] involved release from lightly-irradiated samples of UO_2. Scargill[10] examined release from neutron- irradiated polycrystalline and single-crystal samples of UO_2. Good agreement was obtained between the two samples but the diffusion coefficient was 4 to 7 orders of magnitude less than those of Wheeler or

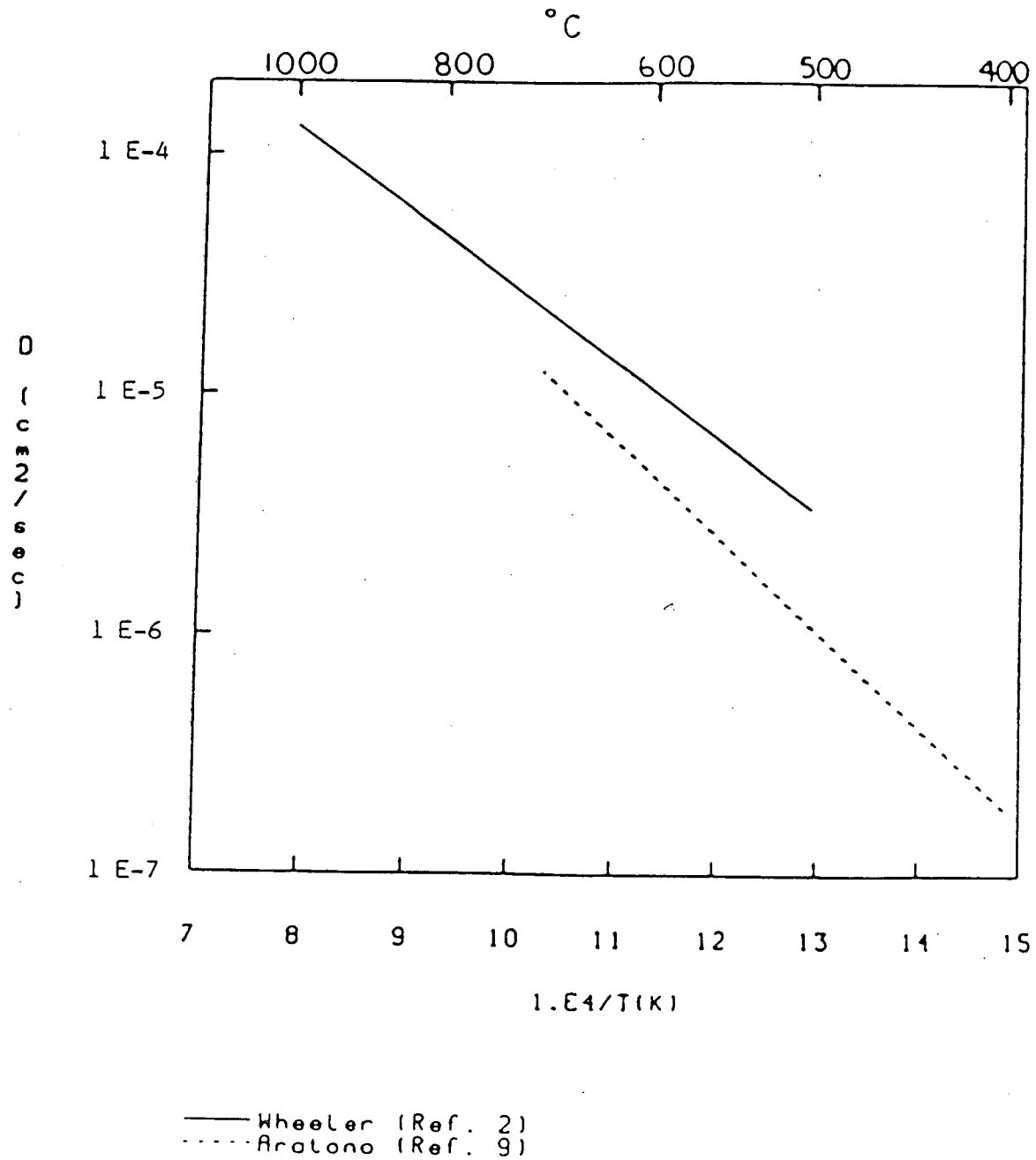

Fig. 1 Diffusivity of Hydrogen in Single Crystal(Wheeler) and Polycrystalline UO_2(Aratono)

Aratono. Up to 85% of the released tritium was in the form of HTO, but this was dependent on the water content of the sweep gas. Molecular hydrogen was predominant in the release when water vapor was absent.

Apparently anomalous results were obtained by Aratono and Tachigawa[11] for release of recoil-injected tritium from neutron-irradiated UO_2 pellets containing 0.1 w% LiF. This study gave higher diffusivities than those of Scargill but less than those of Wheeler. Finally, work has been performed by Aratono et. al[10] on out-of-pile release from irradiated UO_2 polycrystalline pellets and on in-pile release from UO_2 pellets.[12] These works have been in general agreement with that of Scargill.[10] They also observed tritium release as HTO when any water vapor was present in the sweep gas and HT in the presence of H_2. These results are summarized in Table 1.

Aside from the results of Aratono and Tachigawa[11] there appear to be two classes of diffusion of hydrogen in UO_2: A relatively fast diffusion for thermally-infused hydrogen; and a slow one for fission-produced tritium. One possible explanation advanced by Aratono and Nakashima[9] is that tritium produced in fission is in an energetic atomic form that can react with the oxygen in UO_2 to form hydroxyl bonds that can impede transport. These hydroxides are then released as HTO that is reduced to HT at the surface. The irradiation-produced fission products are not believed to be a major impedance to transport. Wheeler[2] and Scargill[10] have speculated that thermally-infused hydrogen is in molecular form, leading to more rapid diffusion than the highly reactive atomic form of the fission produced tritium.

Only Wheeler[2] has estimated solubilities of hydrogen in UO_2. The total amount of hydrogen absorbed and dissolved during heating in single crystal UO_2 was measured. Values of the hydrogen solubility varied between limits of about 0.03-0.4 μg hydrogen/g UO_2, (4-54 ppm atomic), with no systematic variation with the temperature and pressure, which were not indicated.

Table 1

Summary of Measured Tritium Diffusion Coefficients in UO_2 $D = D_o exp(-Q/RT)$				
Material	D_o (cm^2/sec)	Q (kJ/mol)	Temp. Range (°C)	Reference
UO_2-S.C.*	.037	59.8	500-1000	(2)
UO_2-P.C.*	0.15	76	400-600	(9)
UO_2-P.C.*1	.003	163	600-1000	(9)
UO_2-P.C., S.C.*1	.12	182	600-1000	(10)
UO_2 pellets*2	50	134	400-800	(11)

* - T thermally infused into UO_2

*1- T produced in UO_2 by fission

*2- T produced in UO_2 by neutron reaction with Li

Wheeler proposed that this variable hydrogen solubility was due to undetectable variations in the O/U ratio and the resulting anion vacancy concentration. The low solubility suggests that vary few sites were available. In addition, it was observed that UO_2 crystals heated in wet hydrogen resulted in smaller hydrogen contents. However no quantitative results were given.

1.3.2. Hydrogen Solubility in Other Ceramic Oxides

Interest in hydrogen transport in solids has been mainly confined to metals with little work in ceramic oxides. Although there have been some studies on hydrogen diffusion in some ceramic oxides little work has been done on solubility. Recent work on tritium transport in these materials has been motivated by an interest in their suitability as fusion reactor components. They could be used as insulators, first wall coatings, tritium barriers, and for Li_2O, and $LiAlO_2$, as breeding blanket material. Frequently industrial catalysts are ceramic oxides and there is some work on hydrogen transport in these materials. In many of these oxides the permeability of hydrogen is the predominant focus. As the permeability is the product of the diffusivity and the solubility, the solubility is also of interest.

Elleman, et. al.,[13] has studied the hydrogen transport in the ceramic oxides Al_2O_3, BeO, and Y_2O_3. Solubility data was only obtained on Al_2O_3. In addition he has reviewed the literature on hydrogen transport in other nonmetallic solids.[14]

Alumina single crystals and powder were exposed to deuterium gas at elevated temperatures for enough time to reach saturation. The samples were then outgassed and the deuterium measured with a quadrupole mass spectrometer. These measurements were difficult to make as the solubilities were near the sensitivity limit of their mass spectrometric detection system of $\approx$10 ppm atomic. An additional complication was the necessity for correcting for adsorbed hydrogen in the solubility measurements. The solubility was studied as a function of temperature. Alumina was found to be an

endothermic absorber of hydrogen with an activation energy of 76 kJ/mol. Earlier work by Roy and Coble[15] on solubility of hydrogen in pressed alumina powder disks at elevated temperatures gave comparable results, with an activation energy of 66 kJ/mol.

Hydrogen permeation of alumina was investigated[13] as a function of pressure and was found to vary as the 0.43 power of the hydrogen pressure. From these data the pressure dependence of solubility can be inferred, because the diffusivity is independent of pressure. This power dependence is close to the 0.5 value associated with hydrogen dissolution in metals, and indicates hydrogen dissolution in the solid in atomic form. In addition to Al_2O_3, efforts to measure solubility were also attempted for BeO but were found to be below the detection sensitivity of the mass spectrometric technique.

Other ceramic oxides on which their exists some hydrogen solubility data include silica(SiO_2),[14] titania(TiO_2),[16] zinc oxide(ZnO_2),[17] lithium oxide(Li_2O),[18] and zirconia(ZrO_2). For ZrO_2, only hydrogen permeability of oxide coatings on zirconium was investigated.[19] The linear pressure dependence of the permeability suggests molecular dissolution of hydrogen in ZrO_2.

There have been several studies of hydrogen solubility in silica that are summarized by Elleman.[14] Various types of glasses have been studied in temperatures ranging from 140 C to 1000 C. Generally good agreement has been found among the various investigations, considering the wide variation in properties of the different glasses. The solubility was found to increase with decreasing temperature implying that SiO_2 is an exothermic absorber. The solubility was also found to depend linearly on pressure, suggesting that hydrogen dissolves in silica in molecular rather than in atomic form.

The only work on hydrogen solubility in TiO_2 was reported by Iwaki and Mura.[16] Hydrogen uptake was measured over the temperature range of 200-500 C by monitoring the time rate of change in the electrical conductivity of powdered specimens The

authors interpreted the results in terms of chemisorption of hydrogen but crude estimates of the solubility of hydrogen could be inferred. As the samples had reached dissolution equilibrium the data implied a total (adsorbed plus dissolved) hydrogen concentration in TiO_2 of 4 x 10^3 to 12 x 10^3 ppm atomic for temperatures increasing from 350 to 500 C.

Thomas and Lander[17] examined hydrogen dissolution in ZnO by observing the conductivity changes when the oxide was exposed to hydrogen gas at high temperatures. The solubility was found to vary with pressure as $(P_{H_2})^{1/4}$. This value is expected for materials in which the conduction electrons derive principally from hydrogen ionization. The solubility was found to increase with increasing temperature suggesting that ZnO is an endothermic absorber of hydrogen.

As mentioned previously lithium oxide is a prime candidate for a a solid breeder blanket material in a fusion reactor. Hydrogen solubility in Li_2O is needed to evaluate the tritium inventory in the blanket as well as to understand the tritium release process. The solubility in sintered Li_2O pellets was measured by H. Katsuta et al.[18] using a process similar to Elleman's[13] The samples were equilibrated with both hydrogen and deuterium and then subsequently outgassed at temperatures of 500 to 700 C. Lithium oxide was found to be an endothermic absorber with a positive heat of solution of 16-19 kJ/mol. Studies of the pressure dependence of solubility in the pressure region of 7 to 100 kPs showed the solubility to vary as $(P_{H_2})^{1/2}$. This suggests that hydrogen exists in atomic form in Li_2O as in Al_2O_3. Unfortunately, other results by Ihle and Wu[20] on deuterium solubility in single crystal Li_2O at 600 C were determined to be 56 ppm atomic at 133 Pa and 5 ppm atomic at 13.3 Pa. These results show a linear pressure dependence of solubility, implying molecular rather than atomic dissolution. These differences may be because of different pressure ranges studied or material differences.

A summary of the measured hydrogen solubility results that are referenced above for: Polycrystalline Li_2O; single crystal and polycrystalline Al_2O_3; ZnO; and for

vitreous SiO_2 are shown in Table 2.

Table 2

Summary of Measured Hydrogen Solubility Coefficients in Ceramic Oxides at 1 atm

$S = S_o \exp{-\Delta H/RT}$

Material	S_o (ppm atomic)	ΔH (kJ/mol)	Temp. Range (°C)	Reference
S. C. Al_2O_3, powder	100×10^3	75.7	700-1300	(13)
Pressed Al_2O_3 pellets	204×10^3	66.7	1582-1816	(15)
Vitreous SiO_2	500	-8.4	100-1000	(14)
ZnO	98.7×10^3	76.6	400-700	(17)
Polycryst. Li_2O	453	16	500-700	(18)

2. EXPERIMENTAL

2.1. UO_2 Samples

Both single crystal as well as polycrystalline samples of UO_2 were used in this study. In addition both hypostoichiometric urania (UO_{2-x}) as well as hyper-stoichiometric urania (UO_{2+x}) were used.

UO_2 single crystal specimens were obtained from Battelle Pacific Northwest Laboratories as boules from which the single crystal samples were chipped. These samples varied in weight from 2.21 to 4.02 g with an average weight of 2.85 g, and an average equivalent sphere diameter of 8 mm. A scanning electron microscope(SEM) photomicrograph of an as-received single crystal sample is shown in Fig. 2.

The polycrystalline UO_2 pellets were obtained from Exxon Nuclear Co. and the General Electric Co. These pellets shapes were hollow cylinders with an O.D. of 10.48 mm and an I.D. of 4.76 mm, with heights ranging from 3.5 to 12 mm. The samples used varied in weight from 2.6 to 8.45 g with an average weight of 4.0 g, with an equivalent sphere diameter of 9 mm. The open and closed porosity of these polycrystalline pellets was determined using a standard technique.[21] Two samples were investigated and were found to have no appreciable open porosity and an average closed porosity of 7.0%. An SEM photomicrograph of an as-received polycrystalline sample is shown in Fig. 3.

Two hypostoichiometric samples were prepared. A cylindrical polycrystalline pellet with a diameter of 10.48 mm and height of 1 cm had a 4 mm hole drilled in the center 7 mm deep in which was placed 1 g of 1/8 inch(3.175 mm) uranium rod. The pellet was then annealed in vacuum at 1650 °C for 4 hours. After cooling, the part of the pellet with uranium metal was cleaved leaving a sample consisting of UO_2 with some diffused uranium metal. These samples of UO_2 + U were thus hypos-toichiometric urania (UO_{2-x}). An optical photomicrograph of the second sample is

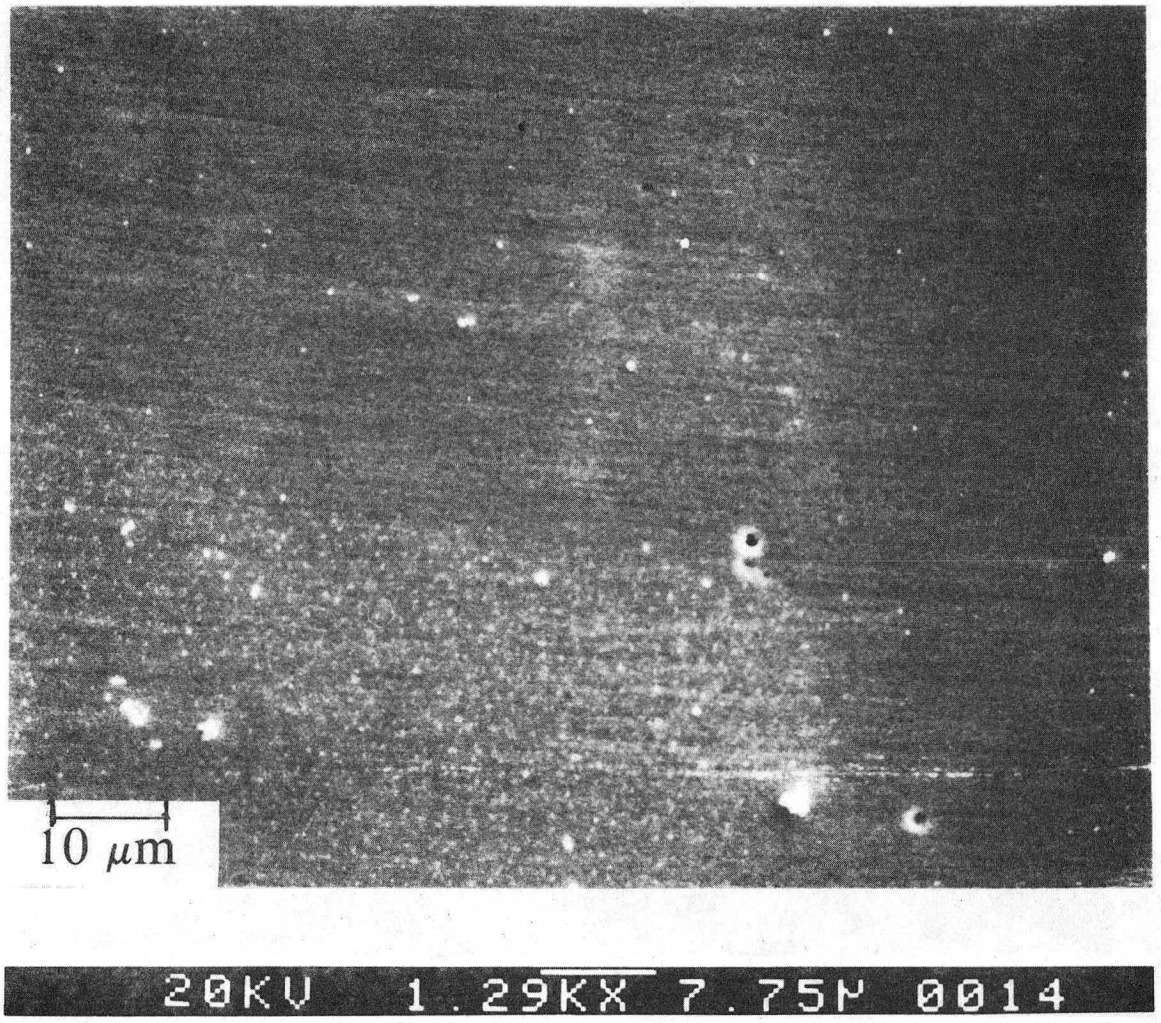

XBB 871-310A

Fig. 2 SEM Photomicrograph of an as-received single crystal UO_2 sample

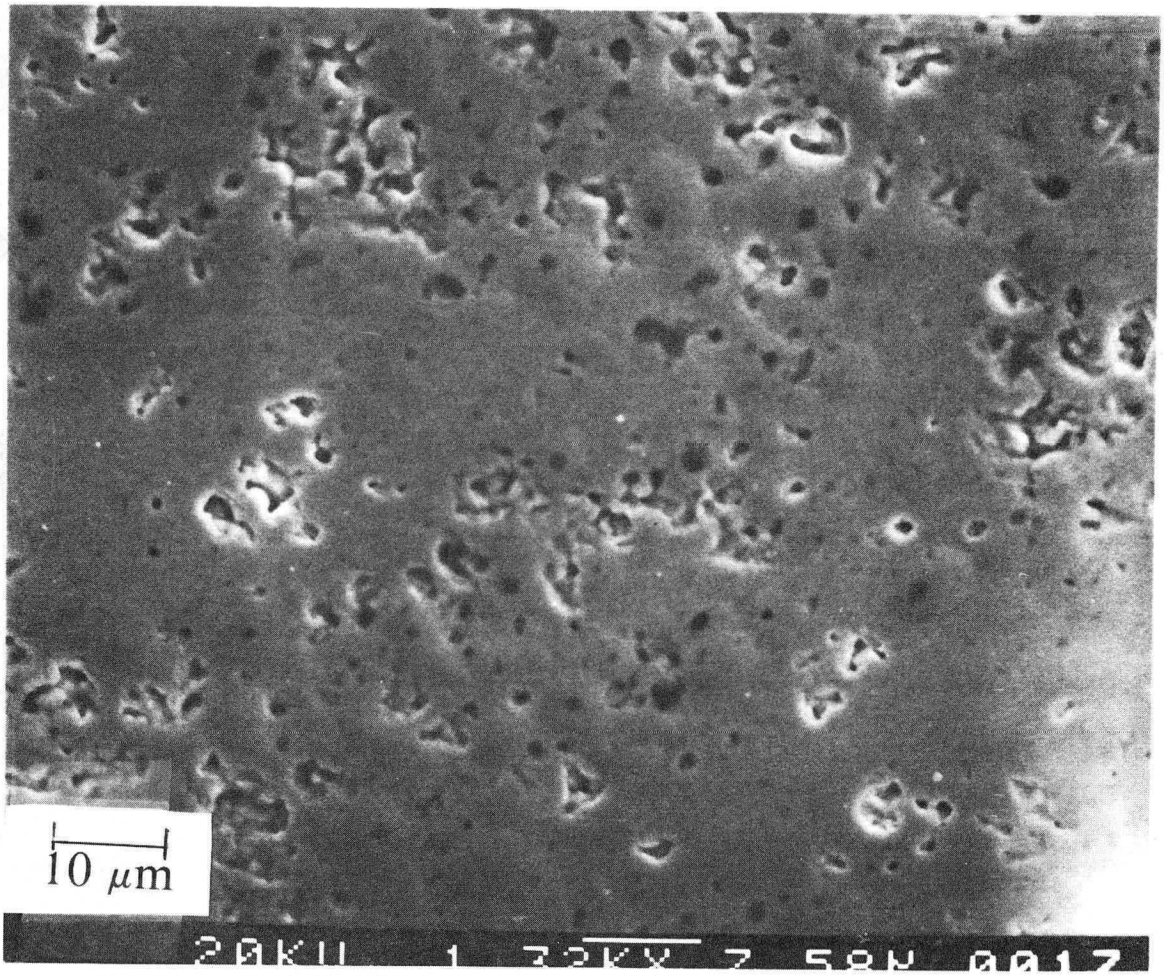

XBB 871-311A

Fig. 3 SEM Photomicrograph of an as-received polycrystalline UO_2 sample

shown in Fig. 4 with the white spots showing the uranium metal in the solid. The first sample was analyzed by heating it in a controlled H_2/ H_2O atmosphere at 1600 °C to oxidize it to stoichiometric UO_2. A measurement of the weight gain because of this oxidation gave an oxygen-to-uranium ratio of 1.976. It was not possible to similarly analyze the second sample although the oxygen-to-uranium ratio derived from the photomicrograph is about 1.90. This is less than the oxygen-to-uranium ratio expected for UO_2 at the lower phase boundary between UO_{2-x} and U of 1.94 at 1600 °C. This excess uranium is present because when the pellet was cleaved some undiffused uranium metal was accidentally included in the sample.

The hyperstoichiometric urania was produced by partially oxidizing UO_2 in air at low temperature producing UO_2 + U_3O_8, corresponding to UO_{2+x}. Some of the unused sample was analyzed by heating it in hydrogen at 1600 °C to reduce it to stoichiometric UO_2. A measurement of the weight loss because of this reduction gave an oxygen-to-uranium ratio of 2.065.

2.2. Infusion Furnace

2.2.1. Description of Apparatus

To determine the solubility of hydrogen in uranium dioxide it is necessary to infuse samples with deuterium at high temperature and pressure. To achieve this an infusion furnace shown in Fig. 5 was constructed. It consists of a suspension rig for holding up to 10 grams of solid oxide inside a molybdenum crucible that is heated inductively. This assembly is located inside a 3/8 inch (9.53 mm)thick stainless steel pressure vessel.

The stainless steel pressure vessel that was used as the infusion furnace was designed to withstand pressures above 100 atm, as well as temperatures as high as 2000 °C. The main section of the infusion furnace is a cylinder with an i.d. of 4.813 inches (12.23 cm), with a total inside length of 12 7/8 inches (32.7 cm). The top

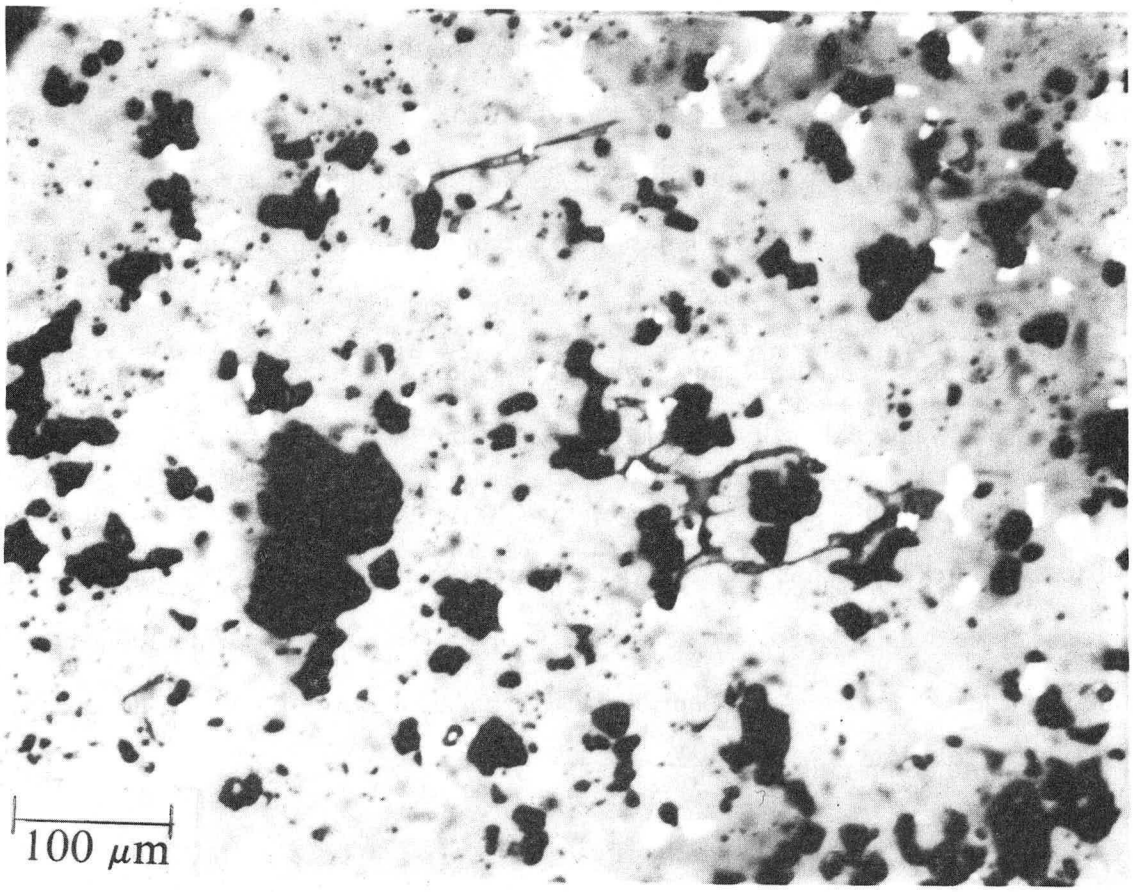

XBB 871-309A

Fig. 4 Optical Photomicrograph of a hypostoichiometric urania sample (white spots are uranium metal)

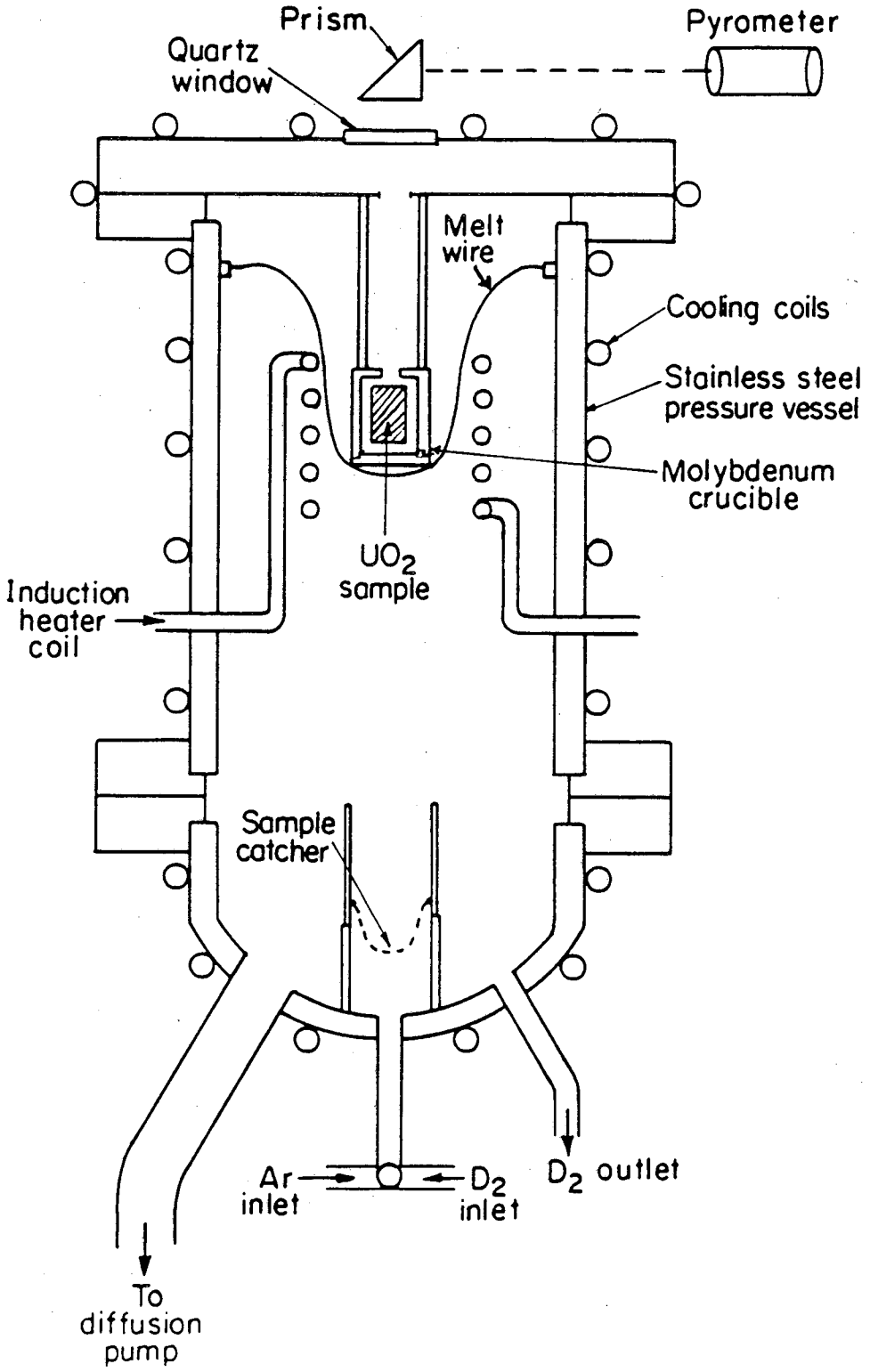

XBL 856-6337

Fig. 5 Infusion Furnace used to infuse samples with high pressure deuterium

flange is 1½ inches (3.8 cm)thick and extends 2 inches (5.1cm) from the pressure vessel. The other flanges are 1 inch (2.54cm) thick extending the same amount from the vessel. The infusion furnace was designed so that the bottom section was kept in place while the top flange could be removed allowing samples to be brought in and out of the furnace easily. The whole vessel was suspended about 30 cm above a table connected to a diffusion pump. A 5/8 inch (1.59cm) diameter hole in the top of the vessel had a ¼ inch (6.3 mm) thick quartz high pressure window enabling the temperature inside the vessel to be determined optically. Three feedthroughs were placed in the pressure vessel. One was used to pass electrical signals into the vessel, and the other two allowed for the entry and exit of the copper induction heating coil. The whole assembly was connected to a 2 inch diffusion pump through a half inch ball valve with a high pressure delrin seat. Two ½ inch (1.27 cm) holes in the bottom flange allowed for entry and exit of the deuterium gas. Cooling coils were brazed to the outside of the pressure vessel.

The method of heating used in the infusion furnace was induction heating. The induction heater coil is a solenoid that has been wound from hollow copper tubing allowing cooling water to run through it. The high frequency alternating current in the coil establishes an alternating magnetic field that has a maximum density within the coil close to the turns. This alternating magnetic field will in turn induce a current in conductors placed inside the coil. Heat will be produced in the conductor proportional to the electrical resistance of the conductor and to the square of the current flowing.

The molybdenum crucible was suspended 3 inches (7.62 cm) from the top of the pressure furnace with an intervening disk of boron nitride to electrically insulate the crucible. The crucible was held in the middle of the electrical field set up by a 7 turn 3/16 inch (4.5 mm) induction heater coil with an internal diameter of about 1.25 inches (3.8 cm). Ceramic feedthroughs electrically isolate the induction heater coil from the stainless steel walls of the infusion furnace. A Radio Frequency Co. high

frequency generator with a power output of 30 KW and frequency of 450 KHz was used as the induction heater.

A diagram of the molybdenum crucible is shown in Fig. 6. The crucible was designed to hold a pellet of 1 cm diameter by 1.25 cm in length. It's exterior dimensions were 5/8 inch (1.59 cm) diameter by 3/4 inch (1.9 cm) long. As UO_2 is an electrical insulator it is not possible to heat it with an induction heater directly. Thus, to heat the UO_2 with an induction heater it is necessary to heat it indirectly by placing it inside an electrical conductor such as molybdenum that can be heated inductively. In addition the crucible had to be a refractory material to withstand the high temperatures in this study. The UO_2 sample sat on a thin rhenium foil at the bottom of the crucible. The crucible was about 2.4 mm thick and with such a thickness was expected to give a uniform interior temperature.

The temperature of the UO_2 inside the crucible was monitored by use of an optical pyrometer. The pyrometer was sighted first through a prism, then through the high pressure quartz window at the top of the furnace and then through the black body hole at the top of the crucible. A Leeds and Northrop Co. optical pyrometer that had been calibrated using the above sighting was used. It was capable of accurately measuring temperatures from 800 to 2500 °C.

In an initial design of this experiment the UO_2 sample was suspended in the middle of a tungsten or rhenium susceptor with the sample temperature being determined by a W/3% Re- W/25% Re thermocouple. Unfortunately, because of electrical interference owing to the induction heater and other factors that led to inaccuracies in the temperature measurement, this method of heating as well as of temperature measurement was abandoned.

Because of the high diffusivity of hydrogen in UO_2 the infused specimens must be quenched rapidly to preserve the saturation hydrogen content established at the temperature and pressure of the infusion process. A calculation showing the time required

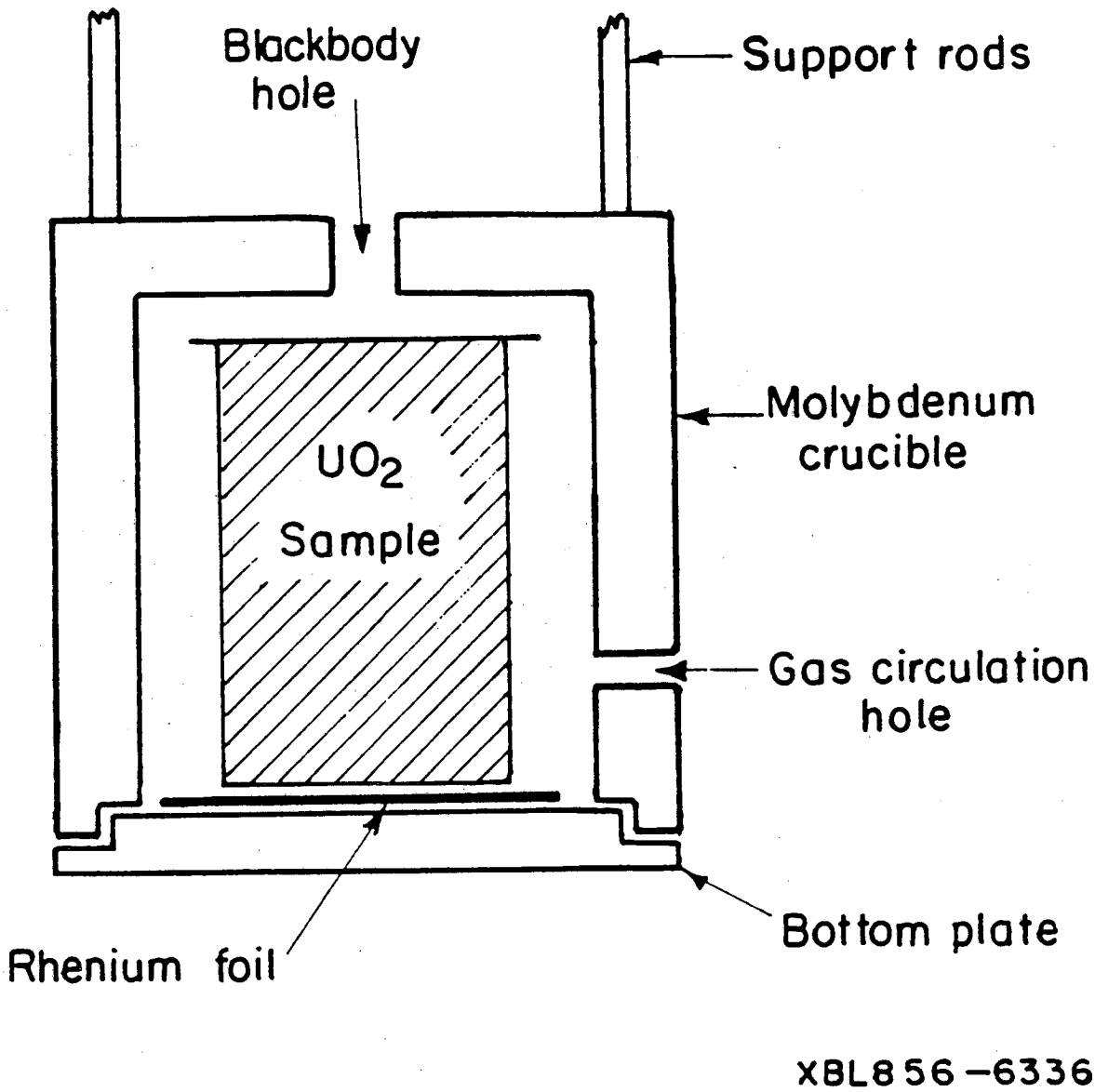

Fig. 6 Molybdenum Crucible used to hold the sample in the Infusion Furnace

to reach saturation based on the diffusion coefficient of hydrogen is shown later. The samples that rest on a rhenium foil at the bottom of the crucible rests on a trap door mechanism that is held in place by a thin tungsten wire. When it is desired to quench the sample enough current to melt the tungsten support wire is transmitted into the furnace through the wire. The bottom lid opens and the sample falls by gravity out of the crucible into a stainless steel mesh basket in the cooler region at the bottom of the furnace.

A flow diagram of the infusion system is shown in Fig. 7. As mentioned previously the infusion gas consisted of high purity D_2. Further purification of the infusion D_2 was possible by passing it through a liquid nitrogen trap. Water content of the exit D_2 gas was monitored at the exit with a General Eastern dew point hygrometer. By measuring the dew point of the gas the partial pressure of water in the gas is determined. From this partial pressure the oxygen potential of the gas can be determined that in turn will determine the stoichiometry of the UO_2. In addition, argon gas was available for testing the system. The system was equipped with pressure and temperature interlocks that could stop inflowing gas as well as power to the induction heater if an unexpected temperature or pressure transient occurred.

2.2.2. Operation

In operation the sustainable upper limit of temperature at a particular pressure was limited by the maximum power of the induction heater as well as the heat transfer characteristics inside the infusion furnace. In the previous design the furnace was to be operated in an automatic mode with the thermocouple output signal sent to a saturable core reactor that controlled the power supply of the induction heater. With the change in temperature measurement technique a manual mode was used with the power level of the induction heater being adjusted to give a particular temperature desired. Although there was some oscillation in temperature because of changes in furnace power it was possible to sustain a somewhat constant temperature over long

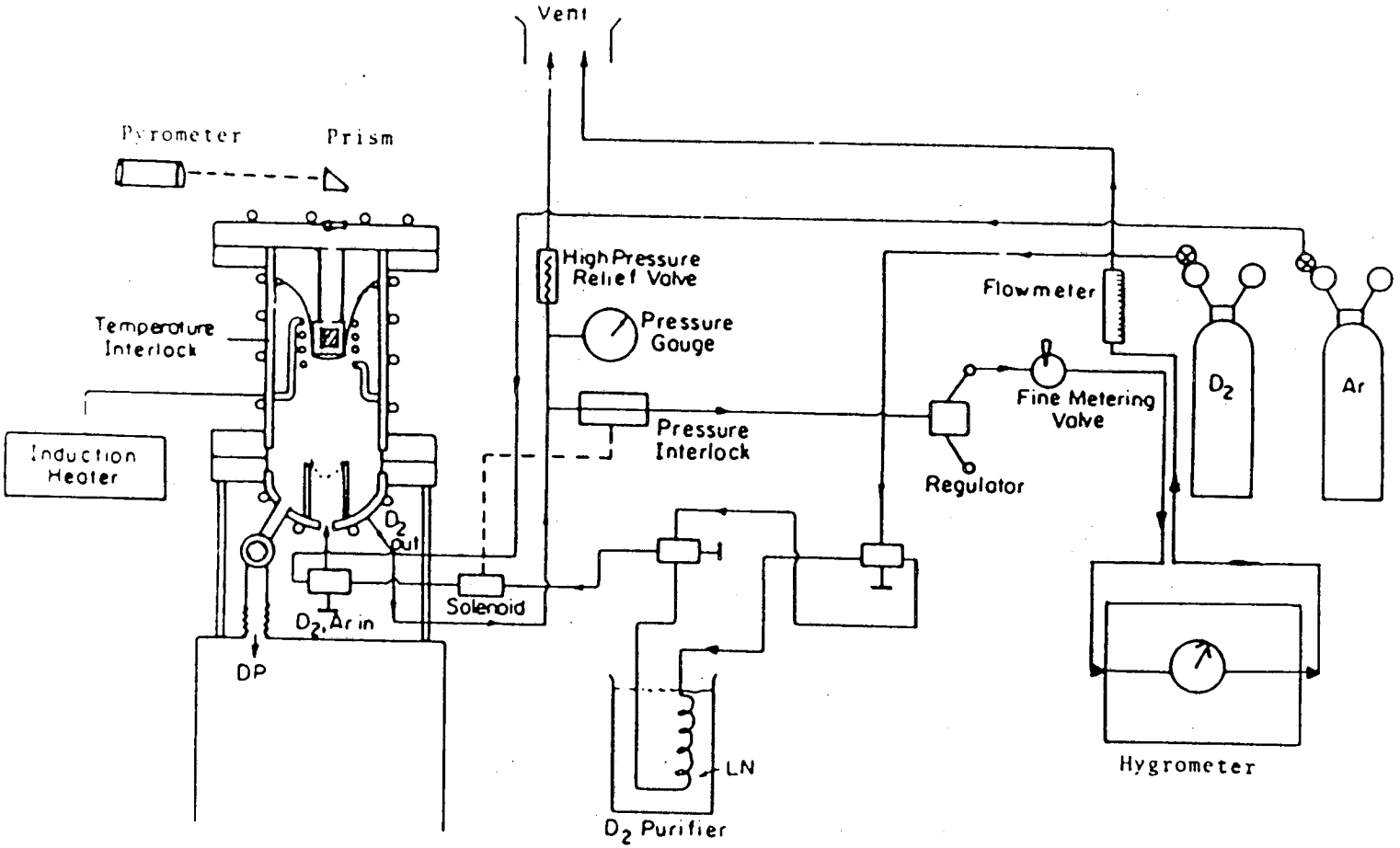

Fig. 7 Flow Chart of the gas handling system associated with the Infusion Furnace

periods of time (≈ 2 hr).

The maximum plate current achievable in the induction heater was 1.2 amps D.C. At a pressure of 10 atm. of D_2 this current corresponded to a temperature of 1800 °C in the induction furnace. The temperature of 1600 °C was chosen as the base temperature to be used as it was easily achievable at higher D_2 pressures. Although the pressure furnace could withstand pressures above 100 atm the upper limit of pressure was limited by the desired temperature at higher pressures. For a temperature of 1600 °C this limit was about 40 atm.

During operation one surprising site of heating was in the ceramic feedthroughs through which the induction heater coil enters the pressure vessel. At high induction currents heat was generated inductively in the steel surrounding these feedthroughs that necessitated additional cooling at this site to protect the neoprene O-rings in the feedthroughs. A mixture of liquid nitrogen and air directly applied was used for this cooling. This was difficult to achieve and this unexpected heating also served to limit the operation of the furnace.

As mentioned above, the water content of the D_2 was monitored after exiting from the furnace. After the D_2 pressure was reduced to 20 psig (240 kPa) it was passed through the hygrometer. The dew point of the gas ranged from -32 to -20 °C. This corresponds to partial pressures of water of 25 to 100 Pa. From these partial pressures as well as the pressure of the D_2 the oxygen potential of the gas can be determined. The corresponding oxygen potentials are -570 to -520 kJ/Mol. From the phase diagram of UO_2 the oxygen-to- uranium ratio can be determined as a function of oxygen potential and temperature. At a temperature of 1600 °C UO_2 should be perfectly stoichiometric between an oxygen potential of -250 and -700 kJ/Mol. As shown above during operation the oxygen potential of the D_2 was between these limits that implies that the UO_2 should have remained perfectly stoichiometric. The hygrometer was connected by one meter of stainless steel tubing to the heating site. Possible

absorption of water in this tubing would have suggested a lower water content in the pressure vessel than that determined by the hygrometer. If this is true possible reduction of the samples at high temperature could occur.

In the original design of the flow system it was anticipated that it would be necessary to pass the incoming D_2 through a liquid nitrogen cold trap to reduce any water vapor present. As the water content of the D_2 did not appear to be high enough to cause any oxidation of the UO_2 this step was not necessary. The pressure of the D_2 was measured at the exit of the pressure furnace and ranged from 62.5 to 500 psig (567 to 3445 kPa). The regulator was set to reduce the pressure to 20 psig (240 kPa) before entering the hygrometer before exiting through the flowmeter. The flow of the D_2 was monitored at this point and was set for most experiments at 3 liters(STP)/min.

2.2.2.1. Operational Procedure

The samples were first loaded into the molybdenum crucible set up and then placed in the induction furnace. An initial vacuum outgassing at room temperature for at least 1 hour helped remove any adsorbed water in the system or on the samples. A pressure of 10^{-6} torr (10^{-4} Pa), measured close to the diffusion pump, was obtainable. The pressure inside the pressure vessel was certainly higher, although no estimate was obtained. After this vacuum outgassing was completed the valve to the diffusion pump was closed and the system was slowly brought up to the pressure desired. Next, the power to the induction furnace was increased slowly to increase the temperature. This was done rapidly up to about 800 °C, and in steps of about 100 deg/min thereafter. The system was kept at the infusion temperature and pressure for the prescribed infusion time. It was necessary to frequently adjust the liquid nitrogen/air cooling mixture for the feedthroughs during operation. When it was desired to quench the sample, a 5 mA current was passed into the system simultaneously with the cessation of power to the induction heater. Whether the sample had really dropped could be determined by sighting through the optical pyrometer. The inflowing D_2 was

replaced with Ar and the pressure was reduced to atmospheric. After about 2 hours or sometimes longer the samples were removed and transferred by hand to the release apparatus.

2.2.2.2. Experimental Variables

As shown above four types of UO_2 were studied These include; single crystal, polycrystalline, hypostoichiometric polycrystalline and hyperstoichiometric polycrystalline UO_2 The base temperature of infusion and pressure of D_2 were 1600 °C and 10 atm respectively. Hypostoichiometric and hyperstoichiometric urania were studied only at this pressure and temperature. For single crystal and polycrystalline UO_2 the temperature dependence of solubility was studied at an infusion pressure of 10 atm D_2 at infusion temperatures of 1000 to 1600 °C. The pressure dependence of solubility for these two species was studied at an infusion temperature of 1600 °C at D_2 pressures of from 5 to 35 atm.

2.2.3. Saturation Time and Quench Calculation

The time needed to saturate the specimen with deuterium can be calculated if the diffusion coefficient of the gas in the solid is known. Using Wheeler's[2] value for the diffusion coefficient of hydrogen in UO_2, the diffusivity of the D_2 in UO_2 at the temperatures of interest can be calculated. For the maximum infusion temperature of 1600 °C the diffusivity is 7.85×10^{-4} cm^2/sec, and for the minimum temperature of 1000 °C the diffusivity is 1.28×10^{-4} cm^2/sec. From Crank[22] the characteristic time for diffusion can be determined by solving for t in $Dt/a^2 = 1$. For a single crystal sample of 4 mm radius the characteristic times will be 4 and 21 minutes for 1600 and 1000 °C respectively. For a polycrystalline sample of about 5 mm radius the characteristic times are 5 and 33 minutes. As there was some uncertainty with these diffusion coefficients an infusion time of 1 hr was chosen to provide enough margin of safety. In addition experiments with infusion times of 2 or 3 hours were performed to see if

saturation had occurred.

Previously it was mentioned that it was necessary to rapidly quench the samples to prevent alteration of the deuterium saturation concentration in the solid by the temperature history of the cooldown. Although the quench is done as quickly as possible the temperature behavior during the cooldown is significant. As a first order approximation to the quench it was possible to experimentally determine the cooldown of the sample in the crucible when it was not dropped. This zero order quench was determined by measuring the temperature as a function of time after the power was turned off. The results for several of these cooldowns are shown in Fig. 8. The results were fitted to an exponential decay with an initial cooling rate of 42.2 °C per sec. To decrease from 1600 to 1000 °C took about 18 sec or an average rate of 34 °C per sec. The somewhat slow cooling is because of the large mass of the molybdenum crucible.

During the quench as the samples fall from the crucible, cooling is limited by the heat transfer characteristics of the UO_2 and the surrounding D_2. This problem can be modeled mathematically and solved numerically.

Mathematically this problem can be modeled as a sphere of radius a and initial temperature T_{S_0} dropping from a hot zone into a stagnant gas of temperature T_0. As it falls, it loses heat by conduction/convection to the ambient D_2 and by radiation to the walls at temperature T_{00}. The temperature T_0 of the ambient D_2 was determined by modeling the heat balance inside the pressure vessel.

The conduction/convection heat transfer coefficient h, for this system, is given by;

$$N_u = \frac{(2a)h}{k_g} = C + 0.388Pr^{1/2}Re^{1/2} \quad C + .33Re^{1/2} \tag{6}$$

where the Prandtl number, Pr is 0.73 for D_2, and k_g is the thermal heat conductivity of D_2. C is a term owing to conduction that initially was set equal to 2 (for steady state) but was found to not accurately describe the problem. Instead, the conduction contribution to cooling was computed separately using the computer code HEATING6.[23]

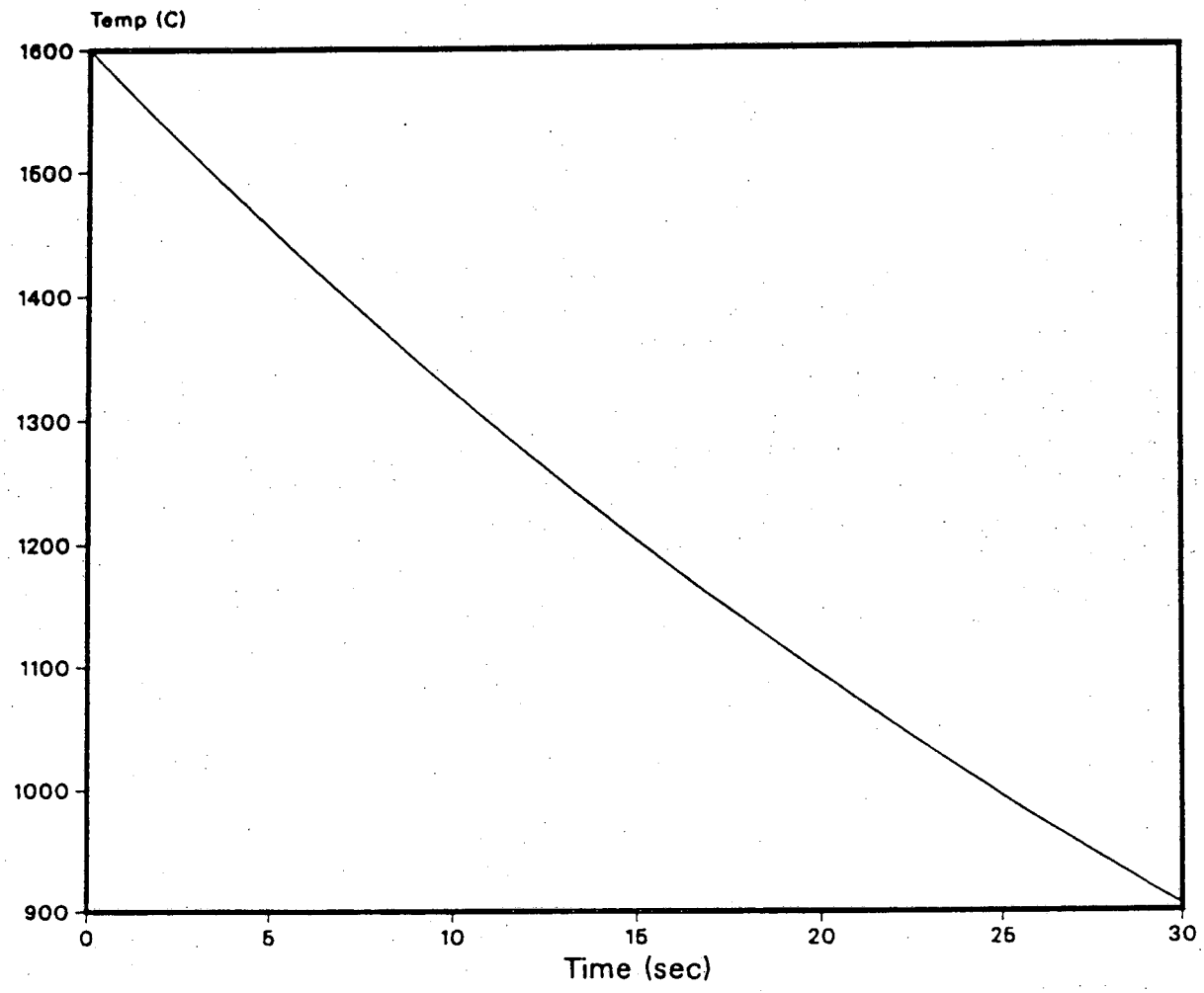

Fig. 8: Zero Order Quench
Surface Temp of UO2 Sample at 1600 C
That is Cooled Down in the Crucible

The Reynolds number Re for a free falling sphere where t is the time of the drop is given by;

$$Re = \frac{(2a)(gt)}{\nu} \tag{7}$$

where gt is the velocity, and ν is the kinematic viscosity evaluated at the mean temperature $\bar{T}$ given by;

$$\bar{T} = \frac{T_s + T_0}{2} \tag{8}$$

where T_s is the surface temperature of the sphere.

From the above three equations the heat transfer coefficient h is;

$$h = \frac{k_g(\bar{T})}{2a} \left[.33\ (2a)^{1/2} \left(\frac{gt}{\nu(\bar{T})} \right)^{1/2} \right] \tag{9}$$

where gas properties are computed at $\bar{T}$. The radiation heat loss, q_{rad} is given by the Stefan-Boltzmann law;

$$q_{rad} = \epsilon\ \sigma\ (T_s^4 - T_{00}^4) \tag{10}$$

Where ϵ 0.86 is the emissivity of UO_2, and $\sigma = 5.67 \times 10^8\ W/m^2\ K^4$. For this problem the heat conduction equation is given by:

$$\rho_S\ C_{p_S} \frac{\partial T}{\partial t} = \frac{1}{r^2} \frac{\partial}{\partial r} \left(k_s\ r^2 \frac{\partial T}{\partial r} \right) \tag{11}$$

Where T is a function of radius r, and time t. The temperature-dependent properties of UO_2 are: ρ_S, the density; C_{p_S}, the heat capacity; and k_S, the thermal conductivity. The initial condition for this equation is given by;

$$T(r,0) = T_{S_0} \tag{12}$$

where T_{S_0} is the initial surface temperature. The surface boundary condition is given by;

$$-k_S\ T(a,t) \left(\frac{\partial T}{\partial r} \right)_a = h\ [\ T(a,t) - T_{S_0}\ ] + q_{rad} \tag{13a}$$

where h is given by Eq (9) and q_{rad} by Eq (10). By symmetry the boundary condition at r=0 is given by:

$$\left(\frac{\partial T}{\partial r}\right)_0 = 0 \tag{13b}$$

This series of equations were solved for both a typical polycrystalline and single crystal UO_2 sample that has been quenched from 1600 °C. The resulting average and surface temperature for these two samples are shown in Figs. 9 and 10 along with the temperature observed above when there was no quench. In Fig. 11 the average and surface temperature for a polycrystalline sample cooled by transient conduction as above is compared with cooling by steady state conduction.

2.3. Gas Release Apparatus

2.3.1. Description of Apparatus

The gas release apparatus consists of a vacuum outgassing furnace whose function is to outgas the UO_2 samples that have been infused with D_2 in the infusion furnace. The samples rest inside a molybdenum crucible that is heated by a brew furnace. The gases that are released in this outgassing are then detected by an *in-situ* mass spectrometer.

A schematic of the vacuum outgassing furnace is shown in Fig. 12. The samples are placed inside a molybdenum crucible that was 1.27 inch O.D. (3.23 cm), 1.11 inch I.D. (2.82 cm), and 5.55 inches long (14.1 cm), and electron beam welded to a 3.5 in. wide molybdenum flange. Rhenium foil was used to line the bottom of the crucible to prevent any reaction between UO_2 and the crucible at higher temperatures.

A brew furnace in which the crucible was placed, is heated by a tungsten mesh element, 3 in. diameter and 6 in. long. The temperature was controlled by the voltage applied to the heating element that was surrounded by a series of tungsten radiation shields to minimize the heat loss and to protect the outer shell of the furnace, that was

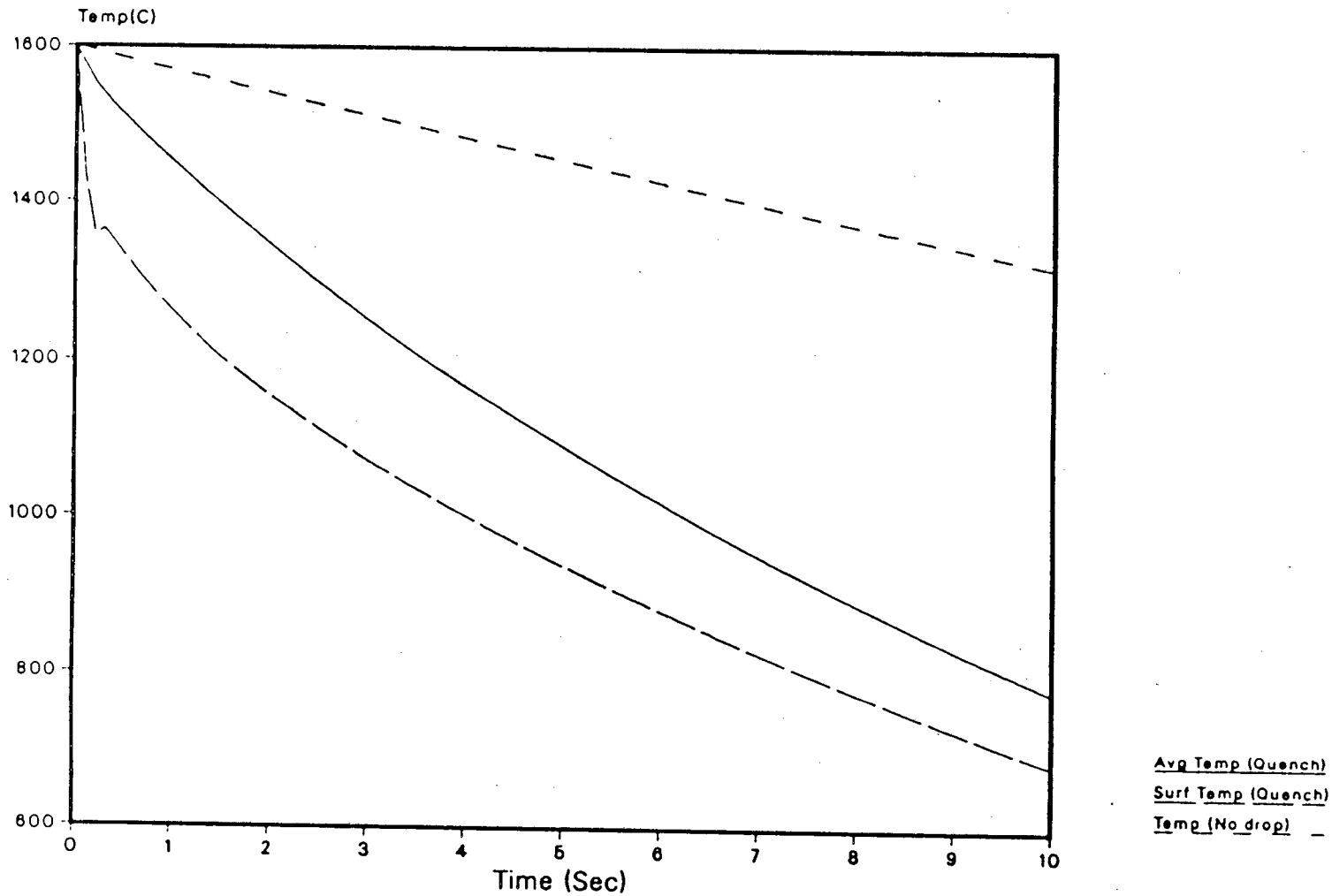

Fig. 9: Polycrystalline UO2 of R= 0.45 cm
Surface and Average Temperature during Quench
Compared with Temperature when not Dropped

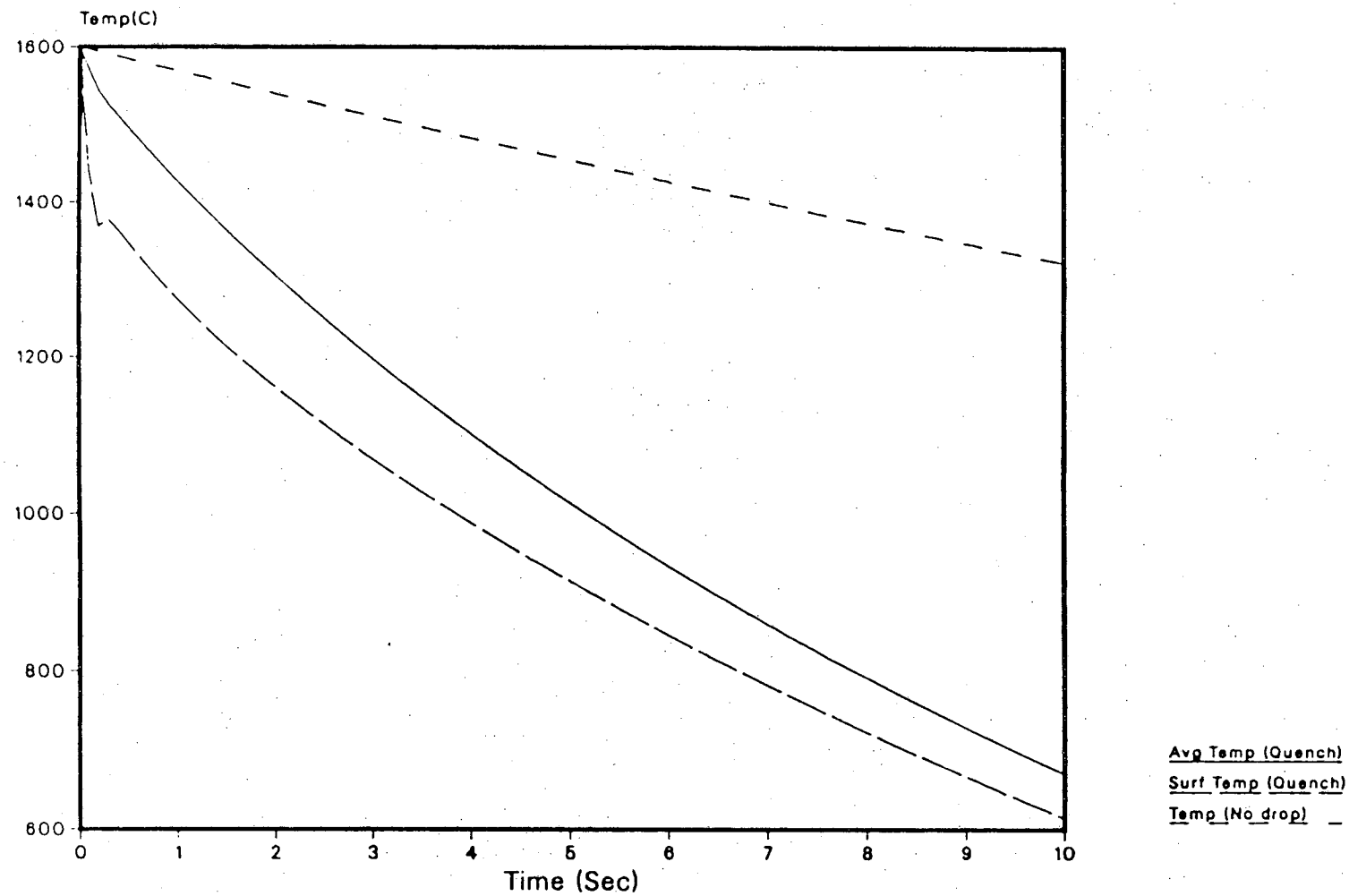

Fig. 10: Single Crystal UO2 of R= 0.4 cm
Surface and Average Temperature during Quench
Compared with Temperature when not Dropped

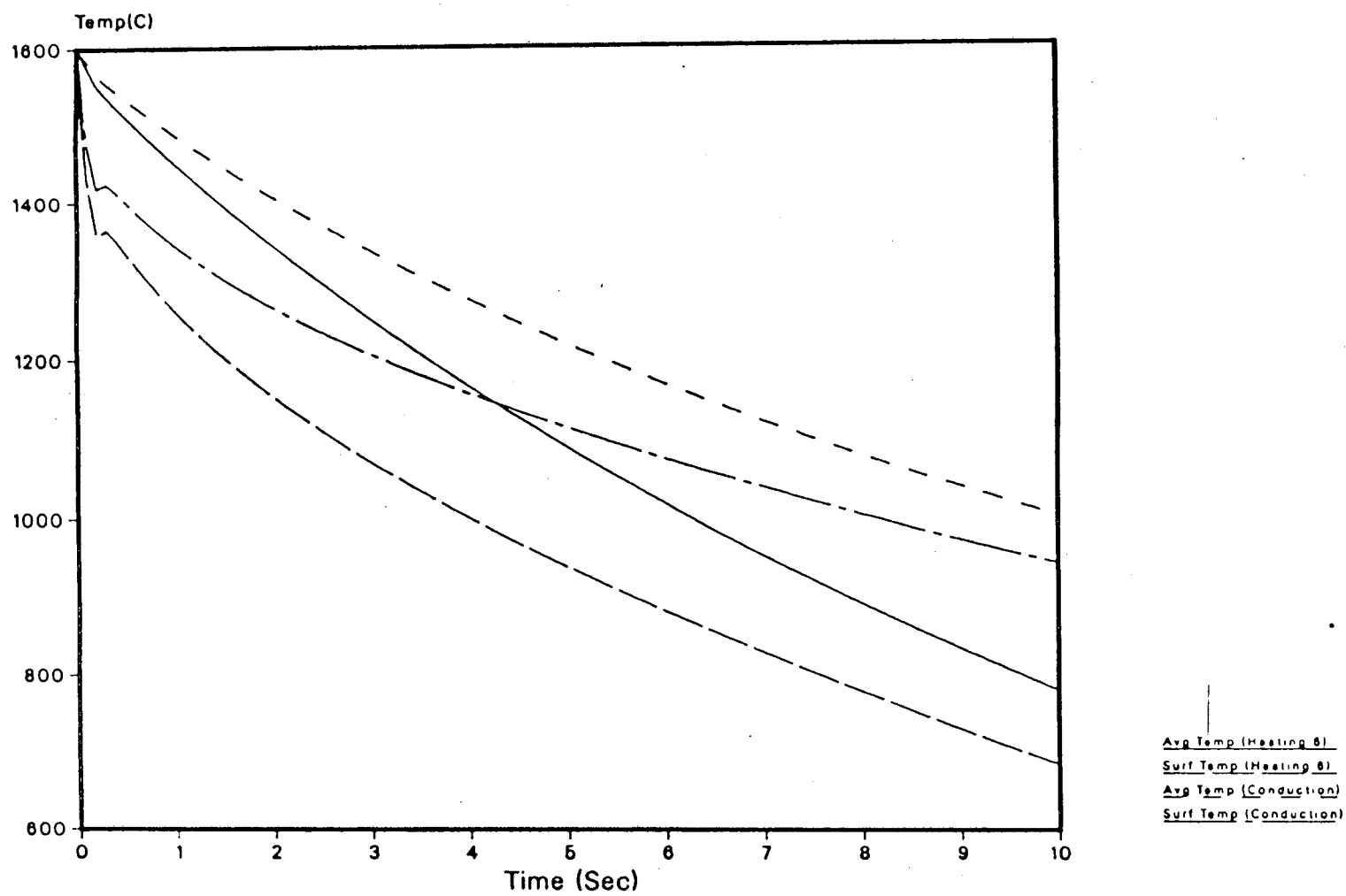

Fig. 11: Polycrystalline UO2 of R= 0.45 cm
Comparison of Cooling with Heating 6 Transient Conduction
and Cooling by Steady State Conduction

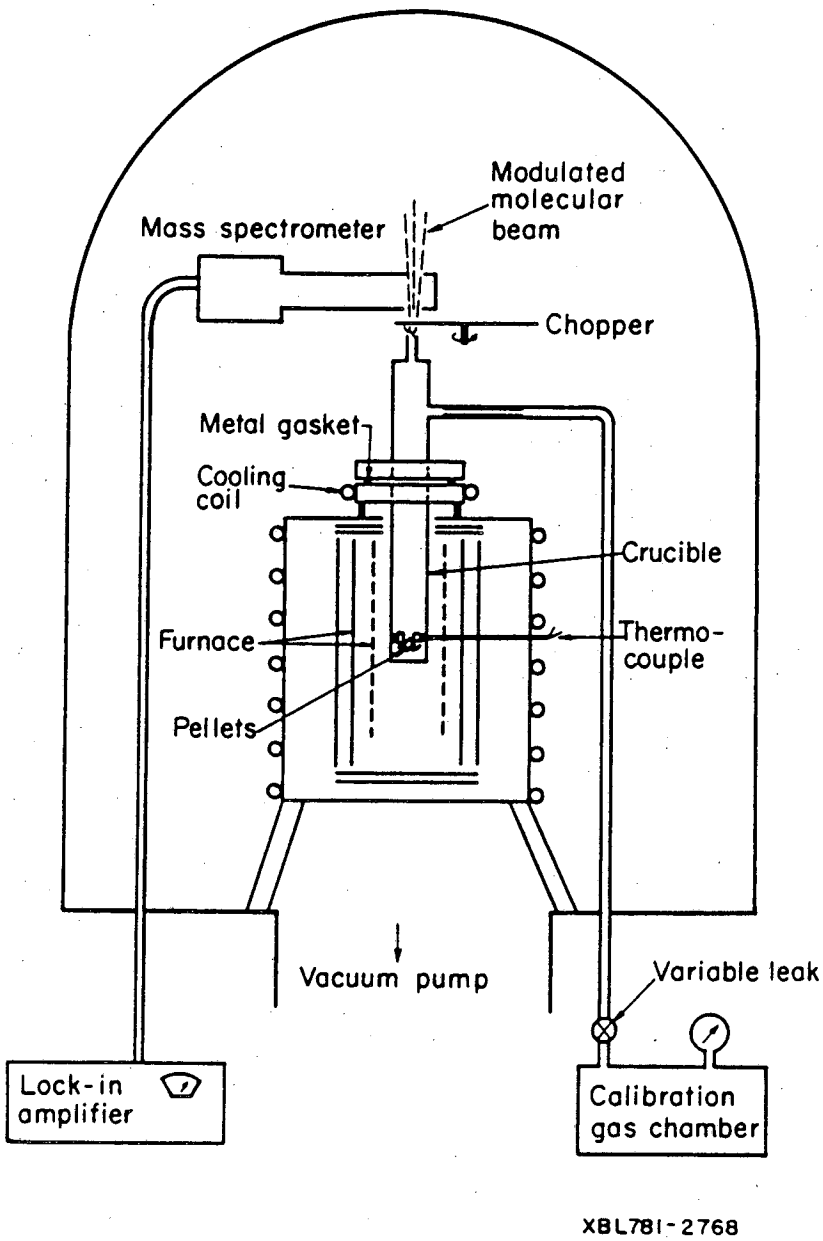

Fig. 12 Vacuum Outgassing Furnace used to outgas deuterium-infused samples

cooled by water. The entire furnace was contained in a bell jar that was under a vacuum for operation. A pressure of 10^{-6} torr (10^{-4} Pa) could be obtained using a 6 in. diffusion pump. The temperature of the samples was measured at the outside wall of the crucible by a W/3% Re-W/5% Re thermocouple.

As the samples are heated, the released gases leave the crucible via a small-bore capillary tube that is aimed directly at the ionizer of a quadrupole mass spectrometer one centimeter away. In this way, the gases are delivered in free-molecule flow to the mass spectrometer detector. All components outside the molybdenum crucible are constructed of stainless steel. The only exception is the oxygen-free copper gasket sealing the flanges at the top of the crucible. This use of stainless steel helps to avoid any reduction of any D_2O released from the pellets. Cooling of the bottom of the molybdenum flange helped to protect the weld joint at that point from direct radiation from the furnace. To prevent adsorption of condensible D_2O or D_2 on cold metal surfaces the capillary assembly is independently heated to about 100 °C. The capillary assembly consists of a small cylinder welded to a small-bore capillary tube. The small cylinder is 6.7 cm long and has an O.D. of 1.9 cm. The small-bore capillary tube is 4.3 cm long and has an I.D. of 2.0 mm.

The steady state pumpout time of the crucible-capillary assembly is the ratio of the signal intensity in molecules/sec to the steady state molecular population in the assembly. This time has been calculated to be less than 0.6 sec. Thus the system samples all the gases released from the UO_2 samples with a very small time constant. The signal derived from the mass spectrometer via the lock-in amplifier is proportional to the instantaneous rate of release of the species of interest from the sample in the crucible.

The rate at which gases leave the crucible via the sampling tube is measured using a modulated molecular beam technique. Before the molecular beam formed by effusion from the sampling tube reaches the ionizer of the mass spectrometer, it is

periodically interrupted by a three-bladed chopper rotating at a modulation frequency of 50 Hz. The output signal of the mass spectrometer (tuned to mass 4 for D_2 and 20 for D_2O) is an a.c. signal from the direct (modulated) gas flow from the sampling tube superimposed on a d.c. background signal owing to D_2 or D_2O that has not yet been pumped out of the vacuum system. The output signal from the mass spectrometer is fed into a lock-in amplifier, that discriminates against the d.c. component of the signal and responds only to that part of the signal that has a frequency equal to that of the 50 Hz reference signal from the beam chopper. The modulated beam technique permits measurement of signals that are only 0.1% of the d.c. background signal.

To quantitatively convert the mass spectrometer output signal to release rate of D_2 or D_2O from the UO_2 samples, calibration of the system is required. For this purpose, the crucible is fitted with an input line coming from a chamber outside the vacuum system that contains a calibration gas (see fig. 12). By allowing the calibration gas to flow into the crucible at a known rate and recording the mass spectrometer signal owing to this flow, absolute calibration of the mass spectrometer can be accomplished. The end of the calibration line runs into the side of the capillary assembly, thus giving the calibration line the same geometric view of the mass spectrometer ionizer. To avoid backflow of released gas up the calibration line, the tube that connects the calibration line to the capillary assembly has a 1.2 cm long section with a .38 mm diameter tube.

Normally calibration is performed with the same gaseous species that is released form the pellets. In general, the rate of pressure drop in a calibration chamber of known volume is measured to determine the flow rate out of the chamber. It was found in a previous study[1] that it was necessary to use neon instead of D_2O as the calibration gas. This is because the latter strongly adsorbs on cool metal surfaces and reliable determination of flow rate by measurement of pressure decrease in the known calibration tank volume was difficult to achieve. It was determined experimentally that

the flow rate through the variable leak used to regulate flow of calibration gas is proportional to the chamber pressure and inversely proportional to the square-root of the molecular weight. Thus for equal pressures in the calibration chamber, the flow rate of neon is equal to the flow rate of D_2O. For the same calibration chamber pressures (and hence equal flow rates), the mass spectrometer signal for D_2O was found to be about 3 time that of Neon. This factor was used to convert the neon calibration signal to an equivalent D_2O sensitivity of the mass spectrometer. When D_2 was used as the calibration gas a similar although less severe problem occurred. It was found that on heating an empty crucible after calibration with D_2 that some previously adsorbed D_2 was released. Therefore, as with D_2O, it was necessary to use an indirect method of calibration. For D_2, helium was used as the calibration gas. As with D_2O for the same calibration chamber pressures the mass spectrometric signal for D_2 was found to be about 3 times that of helium. Thus a factor of three could be used to convert the helium calibration signal to an equivalent D_2 sensitivity of the mass spectrometer. This difference is because of a lower mass spectrometer sensitivity for helium than for D_2.

The calibration line had a length of 70 cm consisting of both copper and stainless steel ¼ inch tubing with an I.D. of 4.45 mm. The end of this line had a shut off valve to isolate the system inside the bell jar during outgassing. In addition to this valve, flow into the calibration line was regulated by a Granville Phillips variable leak. The calibration chamber consisted of a Wallace & Tiernan absolute pressure gauge and some associated tubing leading to the variable leak. The total volume of this chamber and tubing was 400 cm^3. It was possible to fill this chamber with the appropriate calibration gas and to then independently pump it out after the calibration was complete.

In an earlier publication using a similar apparatus,[24] spurious results were obtained in an experiment measuring D_2O release from UO_2. On raising the temperature of the furnace large signals were observed regardless of the mass number to

which the mass spectrometer was tuned to (including mass 9, where no signal is expected). These signals were because of electronic pickup from the furnace current by the mass spectrometer. To avoid this problem, the mass spectrometer was encased in an aluminum sheath.

2.3.2. Operation

2.3.2.1. Operational Procedure

The infused samples that have been loaded into the molybdenum crucible in the release apparatus first undergo a vacuum outgas at a pressure of 10^{-6} torr (10^{-4} Pa) for a period of 3 to 18 hrs. This vacuum outgas helped to remove any adsorbed water on the samples and the low pressure was necessary for proper operation of the mass spectrometer.

After the outgassing the mass spectrometer system was turned on and allowed to warm up for about a half hour. Before the temperature of the system was raised it was necessary to calibrate the system. The pressure gauge outside the bell jar was set at a pressure of 11 torr of helium for D_2 calibration, or neon for D_2O calibration. The gas was allowed to flow into the release apparatus at a rate of about .05 torr/minute for D_2. This corresponds to 7×10^{17} mol/sec or 282 μg/hr of D_2. This flow rate resulted in an output calibration signal of from 1 to 30 millivolts. The large differences in this signal was because of small changes in the geometry of the detection system from one experiment to another and because of degradation in the gain of the mass spectrometer over time. This flow rate and signal corresponds to a calibration of from 3 to 94 (ng/hr)/μv. The average for all the experiments was 23 (ng/hr)/μv. A similar calibration for Ne was performed.

After this calibration it was necessary to remove any of this calibration gas from the system before beginning to heat the samples. This took about 5 minutes, although the heating of the crucible was not begun for at least 30 minutes to be certain that no

residual calibration gas was present in the system.

To verify that the detection system was not responding to spurious electronic noise owing to the furnace or some other source a blank was run using an empty crucible. A background signal owing to electrical noise of up to 1.0 μv was obtained during this blank run at temperatures up to 1800 °C. With the above calibration this corresponds to a signal level of about 20 ng/hr. As an additional precaution an experiment was run with an as received sample of UO_2 that had not been infused with D_2. The results were the same as with the empty crucible with an average signal level of about 20 ng/hr.

In an initial experiment the temperature of the crucible was slowly raised until an appreciable signal of D_2 was obtained. This temperature was found to be about 500 °C. The temperature was then raised at the rate of 400 °C/hr to a maximum temperature of 1800 °C. This maximum temperature was chosen because of electronic pickup from the furnace at high temperature and for safe operation of the mass spectrometer. Additionally at higher temperature appreciable vaporization of the UO_2 could occur. If the release of D_2 was not complete the temperature was maintained at 1800 °C until completion. If the release was completed at an earlier temperature then the experiment was concluded at a temperature below 1800 °C, although never lower than 1520 °C. In later experiments to conserve time initially the temperature was quickly (≈ .1 hr) raised to 500 °C before starting the temperature ramp.

At the conclusion of the experiment another calibration was run. This calibration differed as much as 20% from the one done before the temperature was increased. An average of the two calibrations was used thus giving an error of ± 10% in the results.

In practice it was not possible to maintain the temperature ramp at exactly 400 °C/hr always because of experimental limitations. The temperature was monitored at 3 minute intervals and an attempt was made to keep this difference at 20 °C every 3 minutes. When the actual temperature difference differed from this amount then the

temperature ramp was changed to keep the overall temperature ramp at the specified rate. Although the change every 3 minutes sometimes was as small as 5 or as large as 40 °C, within a few 3 minute intervals the 400 °C/hr temperature ramp was reestablished. In one hour increments of the experiment the specified temperature ramp was maintained within 1%.

During operation the background level was continuously monitored by shifting the mass filter to mass 9 and using that signal as the background level. This mass 9 signal averaged about 1 μv giving a background level of about 20 ng/hr. The difference between the mass 4 signal and the mass 9 signal gave the actual D_2 signal. Because of electronic noise it was not possible to determine a difference less than about 0.05 to 0.1 μv. The upper limit was applicable at higher temperatures. Given the above calibration this would give a release rate sensitivity limit of about 2 ng/hr. Since the experiments ran for about 3 ½ hours this detection method had a total sensitivity limit of less than 10 ng of deuterium. For a UO_2 sample of about 4 g this gives a sensitivity limit of 0.2 ppm atomic.

In the first few experiments appreciable amounts of D_2O were detected. It was found using another blank that this D_2O signal was due almost totally to the tail of the mass 18 water signal at mass 20. By restricting the mass filter only true D_2O signals were then detected, which were found to be less than 0.5% of the total Dsub2 release.

In addition to the system being able to respond to signals as low as 0.05 μv, it was able to respond to signals as large as 500 millivolts--7 orders of magnitude greater. During a typical experiment the maximum signal level of about 5 millivolts was achieved, although the actual amount varied depending on the experiment as well as the calibration level of the system. For polycrystalline samples maximum D_2 signals of 20 μg/hr were obtained, and for single crystal samples a maximum of 1 μg/hr was obtained.

2.3.3. Estimate of D_2 Losses During Operation

During operation it is possible that some of the D_2 that is outgassed from the sample can be lost before it reaches the capillary tube. It is at this point right before entering the capillary tube that the calibration gas enters the capillary assembly. From this point both outgassed D_2 and He calibration gas will have the same view of the mass spectrometer and any losses after this point will be accounted for by the calibration. The two possible mechanisms in which outgassed D_2 can be lost are through backflow into the calibration line and permeation through the molybdenum crucible. An estimate can be made for both losses.

2.3.3.1. Loss Through Flow into Calibration Line

For flow through a capillary tube of radius a and length l to a vacuum from a reservoir at a pressure P(torr), the intensity ν in molecules/sec is given by

$$\nu = \frac{3.5\text{x}10^{22}\, P_{torr}}{\sqrt{M\,T}}\ \frac{8a}{3l}\ \pi a^2 \tag{14}$$

where $\frac{8a}{3l}$ is the Clausing factor, πa^2 is the area of the capillary hole, M is the molecular weight of the gas (4 for D_2) and T is the temperature of the gas. From this equation the ratio of the beam intensity going through the top capillary to that lost through the side calibration tube is given by

$$\frac{\nu_{cal}}{\nu_{top}} = \frac{a_{cal}^3}{a_{top}^3}\ \frac{l_{top}}{l_{cal}} \tag{15}$$

Where the subscript cal refers to the calibration tube. This ratio of intensities is calculated to be 0.025 using Eq (15). Thus only 2.4% of the total flow out of the crucible-capillary chamber will enter the side calibration tube. As the calibration tube was not pumped by the vacuum system the actual amount should be less.

2.3.3.2. Loss of Deuterium by Permeation through the Crucible Wall

To calculate the permeation of D_2 through the molybdenum crucible wall it is necessary to calculate the D_2 pressure inside the crucible. Since the release characteristics of D_2 for polycrystalline and single crystal samples were substantially different it is necessary that they be separately considered.

For the polycrystalline samples a typical experiment resulted in a total release of 10 μg of D_2. About 90% of this release occurred between 750 and 1150 °C in a period of one hour. An assumption can be made that the release rate is constant at 10 μg/hr for one hour. Given this assumption gives an efflux of 4.18×10^{14} mol D_2/sec from the capillary at the top of the crucible. Given a temperature at the top of 100 °C, Eq (14) yields a pressure in the crucible of:

$$P_{D_2} = 2.37 \times 10^{-4} \text{ torr or } 3.16 \times 10^{-2} \text{Pa}$$

From this pressure and the known permeability of D_2 in molybdenum, $\mathbf{PP}_{D_2}$, of[25]

$$\mathbf{PP}_{D_2} = 1.8 \times 10^{17} \exp\left(\frac{-89950}{RT}\right) \frac{(\text{D mol.})(\text{mm})}{(\text{cm}^2)(\text{sec})(\text{Torr})^{1/2}} \tag{16}$$

where R is in J/K. The total flux J_D in atoms/sec-cm^2 through the crucible wall of thickness t is given by

$$J_D = 2\mathbf{PP}_{D_2} \frac{(P_{D_2})^{1/2}}{t} \tag{17}$$

As an approximation it can be assumed that about 2/3 of the crucible area is the temperature T of the outgas. This gives an area of ≅ 80 cm^2. Given the area and the flux, the total released in the outgas can be determined from the product of the flux and the area and time. For the typical experiment mentioned above with a crucible thickness of 2.05 mm the product of the flux and the time yields a total loss by permeability through the crucible of 0.47 μg D_2. For this experiment this is 4.5% of the total release.

For the single crystal samples a typical experiment resulted in a total release of 0.6 μg of D_2. As in the polycrystalline samples about 90% of this release occurred in a one hour period, although between temperatures of 1250 and 1650 °C. The release can be approximated as a constant release of 0.6 μg/hr for one hour. This assumption gives an efflux of 2.51×10^{13} mol D_2/sec. Using Eq (14) as before yields a pressure in the crucible of:

$$P_{D_2} = 1.42 \times 10^{-5} \text{ torr or } 1.90 \times 10^{-3} \text{Pa}$$

For permeation of hydrogen in molybdenum Frauenfelder[26] found that permeation at constant pressure exhibited maxima at low pressures and high temperatures where the effect of dissociation becomes significant. In addition at pressures of 10^{-5} torr or less measured permeation rates were substantially lower than predicted owing to the slower rates of the surface processes at these low pressures. At this pressure and temperature both effects are important. From Frauenfelder's data an average flux for a one mm thickness of molybdenum for this pressure and temperature range is

$$J_D = 1.2 \times 10^{14} \frac{\text{atoms D}}{\text{cm}^2 \text{ hr}}$$

Given the above area and thickness this yields a total loss by permeation through the crucible of 7.8 ng D_2, or 1.3% of the total released.

Other experiments with single crystal samples had somewhat lower release rates that would also give small losses because of surface effects. Additionally some experiments with polycrystalline samples had releases at lower temperatures where permeability rates would be small. In summary the losses because of permeability, although not zero, are experimentally insignificant.

for number sequence only

3. RESULTS

3.1. Gaussian Fits to Release Rate Data

The release rate curves vs. time obtained experimentally were fit using Gaussian functions. Although this data analysis method is not based on a physical model of the release process, it helps organize the data for subsequent analysis.

A Gaussian curve G(t), with an area A can be expressed by

$$G(t) = \frac{A}{\sigma\sqrt{2\pi}} \exp\left\{-\tfrac{1}{2}\left(\frac{t-\epsilon}{\sigma}\right)^2\right\} \tag{18}$$

where ϵ is the time at which the peak release rate is reached, and σ is a function of the peak width. It is related to the area, A, and maximum amplitude of the peak, H by

$$\sigma = \frac{A}{H\sqrt{2\pi}}$$

Thus a particular peak is characterized by three parameters; the area, the amplitude, and the time of the maximum release. The total area under the release rate curve represents the solubility of D_2 in the solid.

The release rate vs. time curves all contained more than one peak, each of which was fitted independently. Since the amplitude and position of each peak as well as the total area were generally well known this analysis was tractable. A Monte Carlo method was used to vary these parameters in an interval around initial guesses. This method uses random numbers to give randomly spaced guesses within a particular interval for each parameter individually. Summing up the respective Gaussians for each peak gives a calculated release curve for which a least square difference from the experimental release curve is computed. An example of a best-fit Gaussian curve for the typical polycrystalline UO_2 release curve of experiment 2 is shown in Fig. 13. In addition to the experimental release curve the four individual peaks are shown. Tables 3 and 4 were constructed from these Gaussian fits to the experimental release curves. All the experimental release rate curves obtained are shown in Appendix B.

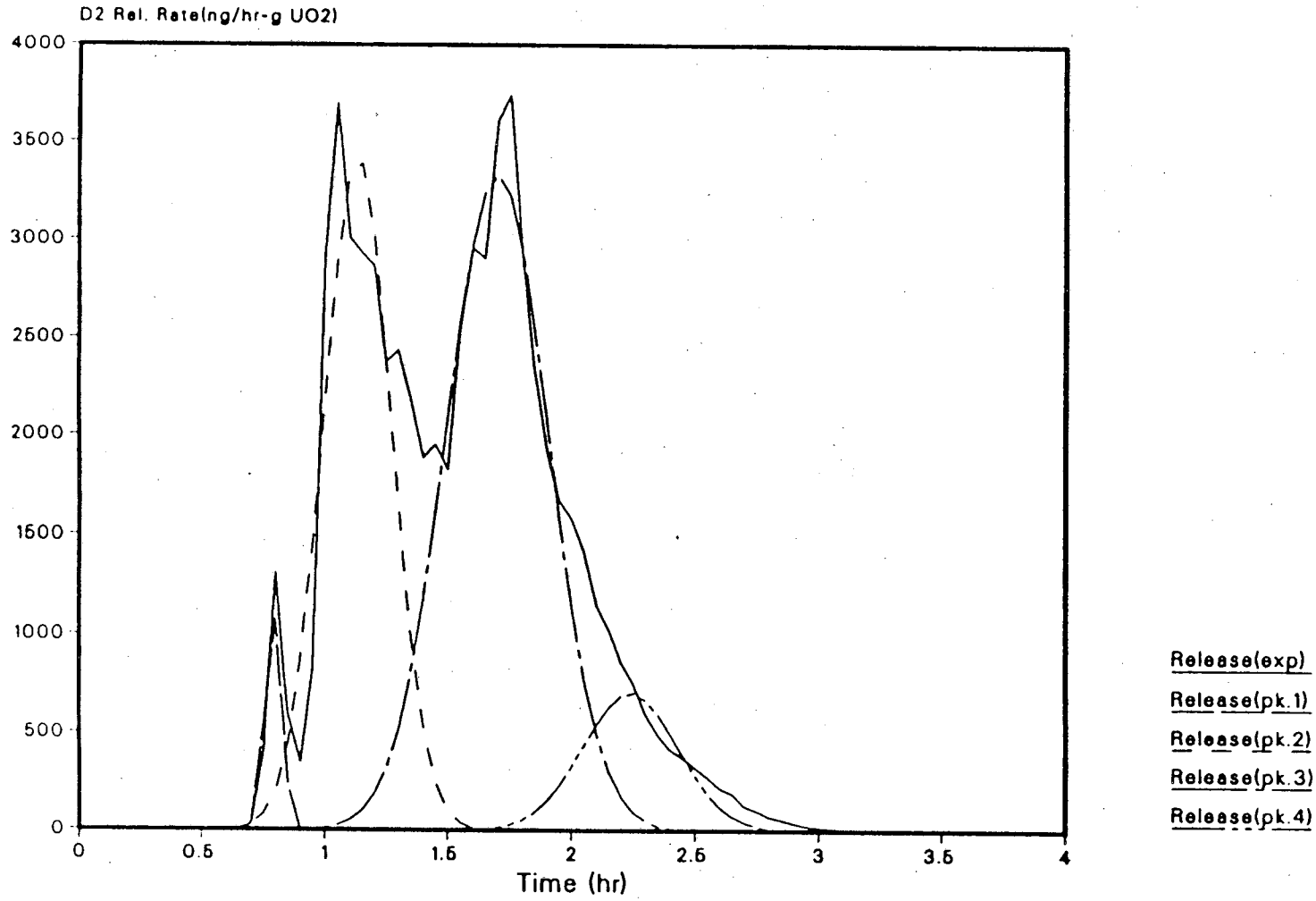

Fig. 13: Gaussian Fit to Expt. 2 Release Curve
PK1: 670 C, 95 ng; PK2: 792 C, 1195 ng
PK3: 1009 C, 1722 ng; PK4: 1237 C, 342 ng

3.2. Release of D_2 from Single Crystal UO_2

A total of 9 experiments were conducted with single crystal UO_2 samples. A summary of all 9 of these experiments is shown in Table 3. This table shows for each experiment the infusion temperature, pressure and the time these conditions were maintained. The temperatures of the respective peaks as well as the areas of each peak and the total areas are also shown. Six experiments were conducted at infusion temperatures of 1200 to 1600 °C at an infusion pressure of 10 atm of D_2. Three additional experiments at infusion pressures of 5.42 to 26.8 atm D_2 at an infusion temperature of 1600 °C were conducted.

A typical release curve for a single crystal sample is shown in Fig. 14. This figure shows the net D_2 release rate in (μg/hr)/g UO_2 as a function of time of the outgas. The net release is the actual release rate minus the background. The temperature ramp shown by a dashed curve is also a function of time. The release rate curve shown has two peaks. The first small peak with a peak D_2 release rate of 0.03 (μg/hr)/g UO_2 occurs at a temperature of about 900 °C and a second considerably larger peak with a peak release rate of 0.24 (μg/hr)/g UO_2 occurs at 1400 °C. The total D_2 release is about 0.2 μg/g UO_2 or 27 ppm atomic. This figure represents the total solubility of D_2 at 1600 °C and a pressure of 10 atm in single crystal UO_2.

The presence of two peaks in this release curve is inconsistent with a simple diffusion release process from a solid. As will be shown later, the temperature at which the second peak occurs is also inconsistent with a simple diffusion model based on Wheeler's[2] value for hydrogen diffusion in UO_2, thus implying that some other mechanism must control release in this system.

The total D_2 release varied from 0. for experiment 22 to 0.340 μg/g UO_2 for experiment 27.

For the experiments conducted at 10 atm of D_2 two peaks were detected. For

Table 3

SINGLE CRYSTAL UO_2 SUMMARY
GAUSSIAN FITTED PEAKS

EXPT #	INFUSION T(C)	INFUSION P(atm)	INFUSION t(hr)	PEAK TEMPS(C) 1	PEAK TEMPS(C) 2	PEAK TEMPS(C) 3	D_2 DISSOLVED Per PK(ng/g) 1	D_2 DISSOLVED Per PK(ng/g) 2	D_2 DISSOLVED Per PK(ng/g) 3	TOTAL DISSOLVED(ng/g)
18	1600	10.	1¼		874	1545		25	204	229
19	1600	10.	1¼		874	1402		21	157	178
20	1500	10.	1¼		1240	1428		60	11	71
21	1400	10.	2		1108	1490		24	10	34
23	1300	10.	2		1103	1407		1.	9	10
22	1200	10.	2							0
24	1600	5.42	1¼	737	995	1601	15	30	110	154
26	1600	20.0	1¼	748	905	1659	10	20	228	265
27	1600	26.8	1¼	859	1531	1736	73	235	31	340

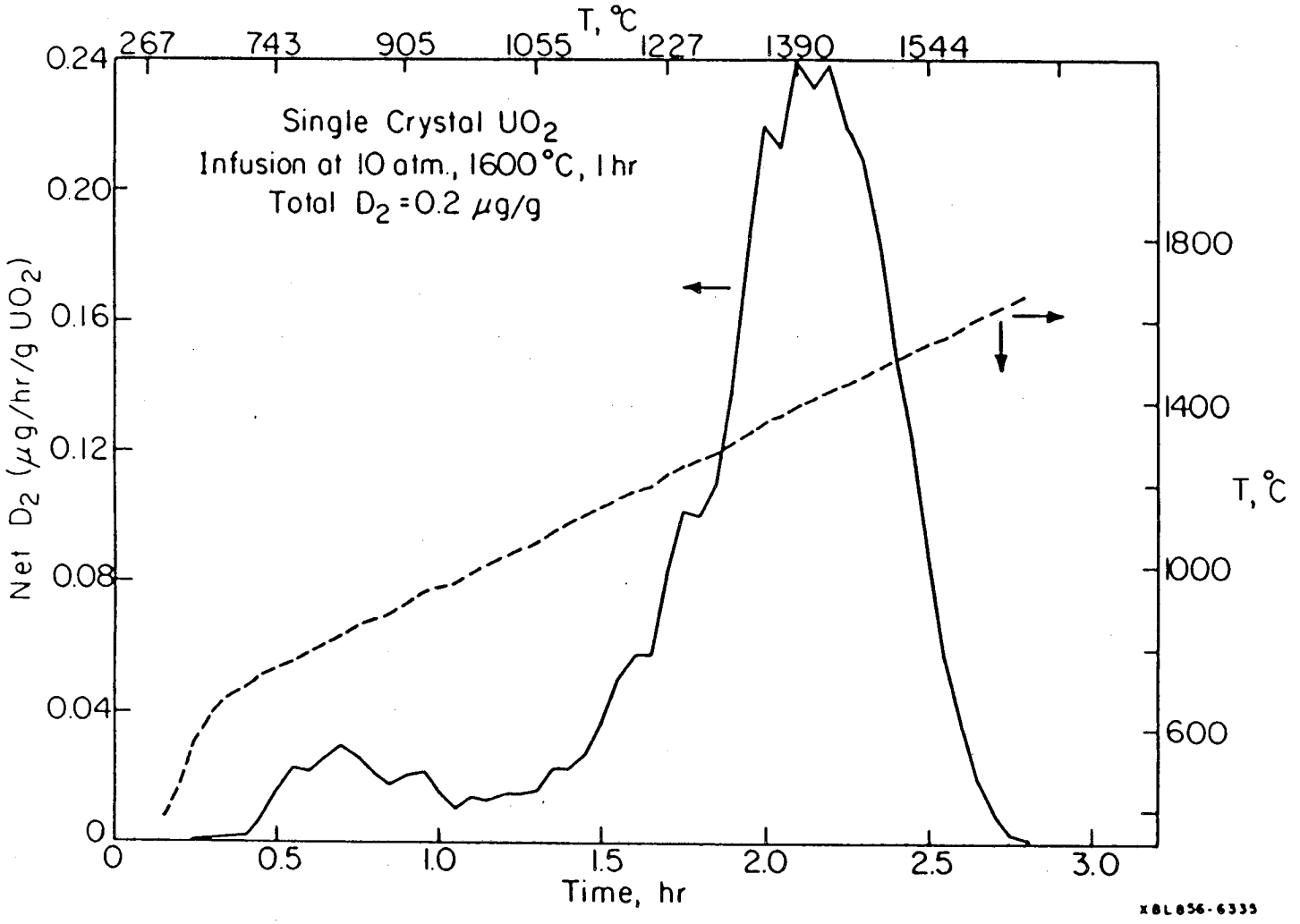

Fig. 14 Deuterium Release Curve for Expt. 18

three of these experiments the first peak was the smaller one with most the release occurring at the higher temperature of the second peak. In experiment 20 and 21 this order was reversed but on closely examining experiment 21 it is possible that this curve may represent only one peak with a peak temperature of about 1400 °C For the three other experiments conducted at 1600 °C at pressures other than 10 atm of D_2 three peaks were observed. On a closer examination the first two peaks of experiments 24 and 26 could be considered to be one peak. Similarly in experiment 27 the second and third peak could also be considered to be one peak. With these interpretations, a pattern of a first small peak at 850- 1100 °C and a larger peak at 1400-1700 °C holds for 6 of the 8 experiments in which D_2 release was observed, with Expts. 20 and 21 being an exception to this rule. For experiments at the same infusion temperature and pressure, (Expts. 18 and 19), the peak temperatures and relative areas are about the same.

3.3. Release of D_2 from Polycrystalline UO_2

A total of 23 experiments were performed on polycrystalline UO_2. Fifteen experiments were conducted at infusion temperatures of 1000 to 1600 °C at an infusion pressure of 10 atm of D_2. Five additional experiments at infusion pressures of 5.42 to 32.0 atm D_2 at an infusion temperature of 1600 °C were conducted. In addition three experiments using hypostoichiometric and hyperstoichiometric urania samples were performed at an infusion pressure of 10 atm of D_2 and an infusion temperature of 1600 °C.

3.3.1. Stoichiometric UO_2

A typical release curve for a polycrystalline UO_2 sample is shown in Fig. 15. This curve shows three discernible peaks. The peaks are more distinct than those for the single crystal samples, and the second and third peaks are more comparable in magnitude than the two peaks found in the single crystal samples. Another important

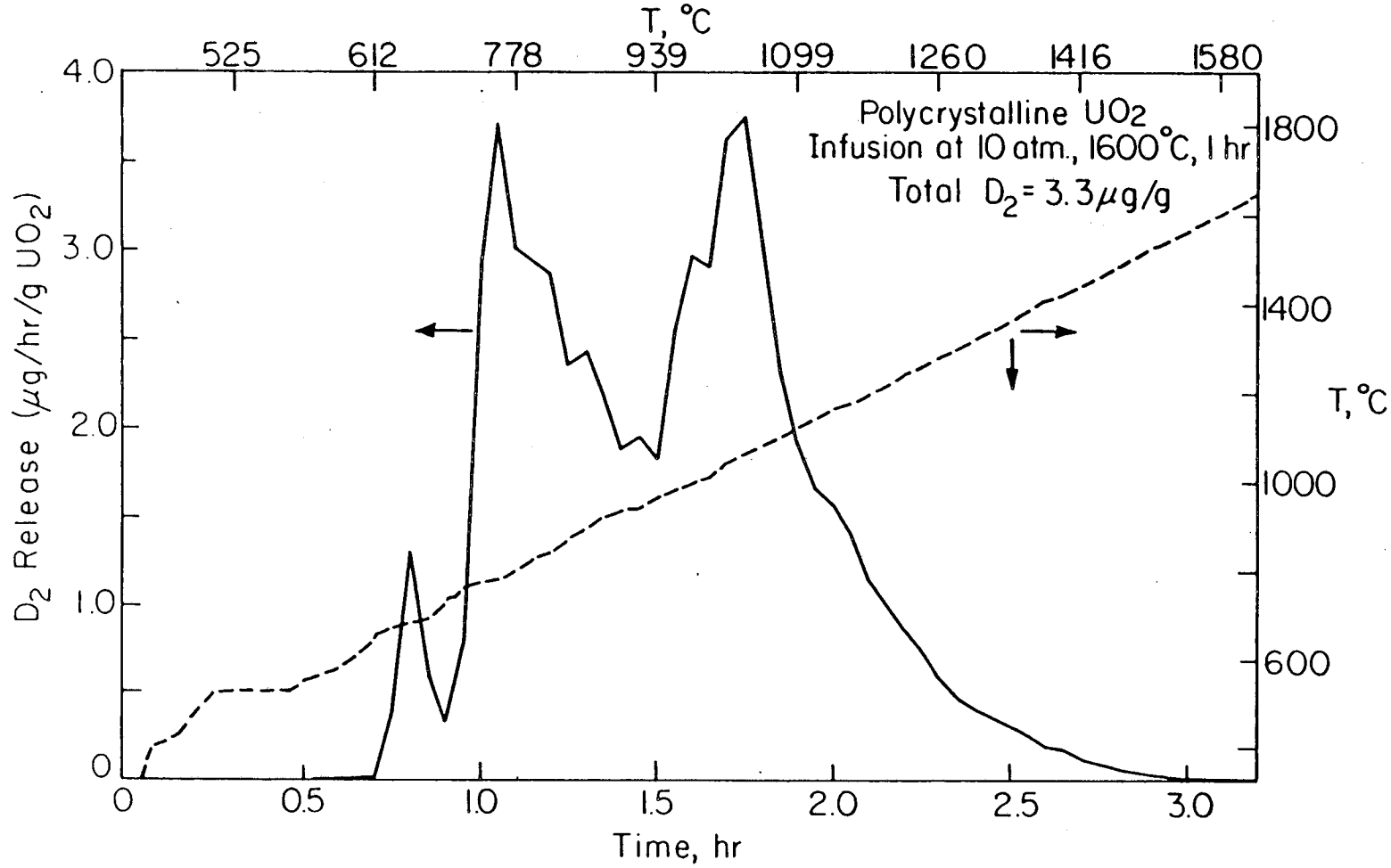

XBL856-6333

Fig. 15 Deuterium Release Curve for Expt. 2

difference is that the release rate as well as total release from polycrystalline UO_2 is at least 10 times greater than from single crystal UO_2. The second and third peaks correspond to a peak D_2 release rate of about 3.8 (μg/hr)/g UO_2 and the first peak is about 1.2 (μg/hr)/g UO_2. The temperature of the peaks also differs from single crystal UO_2. The second and third peaks occur at 800 and 1000 °C instead of at 1400 °C in single crystal UO_2. Additionally the first peak at 700 °C is not present in most of the single crystal experiments.

A summary of all the above experiments is shown in Table 4. As in Table 3, the total area represents the solubility of D_2 at the infusion temperature and pressure of the particular experiment. The experiments are grouped into four sections. The top section shows the experiments where the effect of temperature of infusion at fixed D_2 pressure was examined. The second section examines the effect of pressure of infusion at constant temperature. The third section examines the effects of variations in experimental conditions other than T, P, and t as well as hyperstoichiometric urania, and the last section examines hypostoichiometric urania and UD_3.

In Fig. 15, which depicts the results of experiment 2, only three peaks are immediately apparent, although in Table 4 this experiment is shown to have 4 peaks. Upon a closer analysis it was determined that it was possible to separate the last peak into two separate peaks. In other experiments this fourth peak was also present, although sometimes only as a shoulder on the third peak.

In addition to the effect of temperature, the effect of infusion time was studied in the first group of experiments. For experiments at 1600, 1400, 1200, and 1000 °C the time of infusion was increased from 1 to 2 hours. For the 1400 °C infusion an additional experiment with an infusion time of 3 hours was performed. As is evident from experiment 3 there was no significant difference between the one and two hour infusion times at 1600 °C implying that saturation equilibrium had been achieved after one hour. But for the 1400 1200, and 1000 °C infusion experiments saturation was not

Table 4

POLYCRYSTALLINE UO_2 SUMMARY
GAUSSIAN FITTED PEAKS

EXPT		INFUSION			PEAK TEMPS(C)				D_2 DISSOLVED Per PK(ng/g)				TOTAL
#	Specimen	T(C)	P(Atm)	t(hr)	1	2	3	4	1	2	3	4	DISSOLVED (ng/g)
1	UO_2	1600	10.	1	699	836	1056	1277	76	526	1107	267	1980
2		1600	10.	1	670	792	1009	1237	95	1195	1722	342	3320
3		1600	10.	2		875	999	1260		300	1280	141	1734
4*1		1600	10.	1	682	787	926	1109	125	431	923	612	2097
5*0		1400	10.	1		847	944			171	196		378
17		1400	10.	2	696	797	961	1097	84	269	549	77	979
30		1400	10.	3	771	888	1064	1260	96	304	142	384	926
8*0		1300	10.	1			1011				282		289
6		1200	10.	1		898	1060			241	129		370
16		1200	10.	2		891	985			181	228		415
10*0		1000	10	1		816	963			61	116		178
11		1000	10	2		828	987			174	281		456
12	UO_2	1600	5.4	1	727	789	920	1123	124	265	942	802	2165
28		1600	16.5	1	761	878	1030	1183	594	1281	1278	790	3950
13		1600	20.	1	675	788	893	1230	269	1363	6170	781	8649
29		1600	25.	1	714	797	903	1261	128	828	1885	675	3597
14		1600	32.	1	716	849	1015	1225	186	1226	1727	1749	4924
9*2,*3	UO_2	1200	10.	1			942	1216			636	73	700
31*3		1600	10.	1	720	875	1061	1258	46	500	467	507	1518
15*4		1600	10.	1	671	749	890	1077	220	966	4666	1266	7256
35*3	$UO_{2.065}$	1600	10.	1	604	774	991		100	1157	253		1509
32	$UO_{1.976}$	1600	10.	1	555	863	1101		6.11E3	5.98E4	1090		4.60E4
33*3	$UO_{1.90}$	1600	10.	1	488	845	994		1.55E5	5.32E4	13300		221E4
34	UD_3			1	638				1.E5				1.E5

*0 Equilibrium not achieved

*1 Outgassed at 200 K/h instead of 400 K/h

*2 Infusion conditions 1/2 hr at 1600, 1/2 hr at 1200

*3 Specimen cooled down in the crucible

*4 Specimen preheated to 1800 C° for 1 hrs in vacuum

*5 Powdering of specimen during infusion

achieved until 2 hours. An infusion time of three hours produced no significant difference for the 1400 °C infusion experiment. This long saturation time of (greater than an hour for infusion temperatures less than 1400 °C) is contrary to what was expected from the earlier calculation of saturation time based on Wheeler's[2] diffusion coefficient of hydrogen in UO_2. In that analysis (Sec. 2.2.3) the saturation time was calculated to be about 10 minutes for this infusion temperature.

Another variable studied was the effect of the temperature ramp rate (ie, dT/dt) on the release curve. In experiment 4 an outgassing rate of 200 °C/h instead of the usual 400 °C/h was used. The resulting release curve is shown in Fig. 16. This figure shows the resolution of the four peaks is a little better than in the other experiments at 1600 °C infusion conditions but the difference is not significant.

For experiments in which the infusion pressure was greater than 10 atm of D_2 (Nos. 13,29,14) similar release curves to those at 10 atm were observed. The only difference is that the third peak was observed to be somewhat broader, clearly requiring its separation into two peaks.

One major characteristic of the release curves is that the number of peaks and their temperature seems to be dependent on the temperature of infusion. In experiments where the infusion temperature is 1400 °C or greater at least three peaks are present. The first peak at a release temperature of 660-770 °C in the lower-temperature infusion experiments is completely absent. A release curve for the 1000 °C infusion of experiment 11, shown in Fig. 17 is typical of a low temperature infusion experiment. Although it is possible to resolve this peak into two peaks, it is probable that there is only one peak at ~ 950 °C, unlike the three peaks observed in the higher temperature infusion experiments.

In the third group of experiments the effect of quenching, temperature history, pretreatment, and hyperstoichiometry were studied. In experiment 9 and 31 the samples were not quenched normally but were allowed to cool in place. In experiment 31

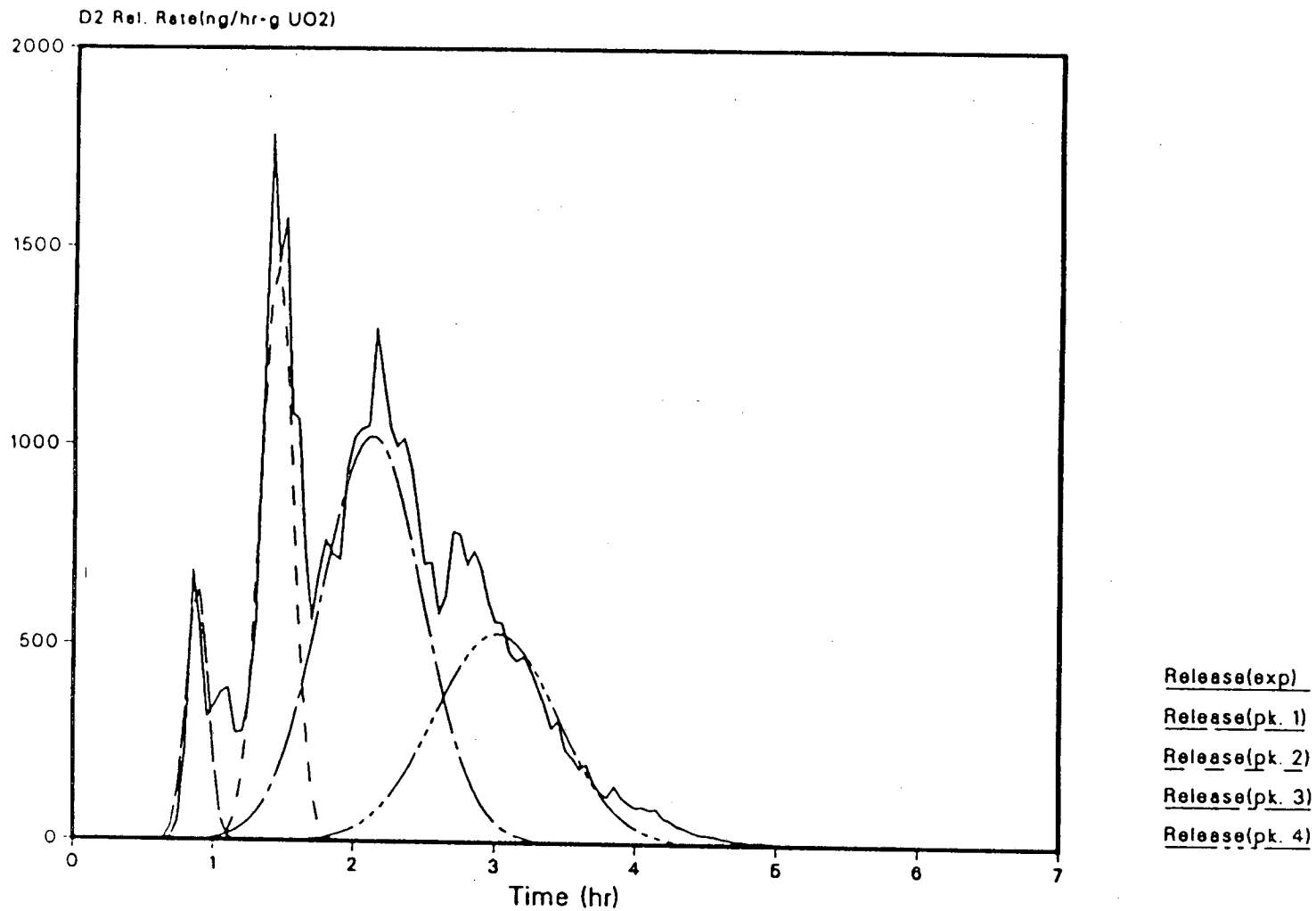

Fig. 16: Expt. 4; Release Curve with Long Outgas
Four Gaussian Fitted Peaks:
Pk 1; 682 C, Pk 2; 787 C, Pk 3; 926 C, Pk 4; 1109 C

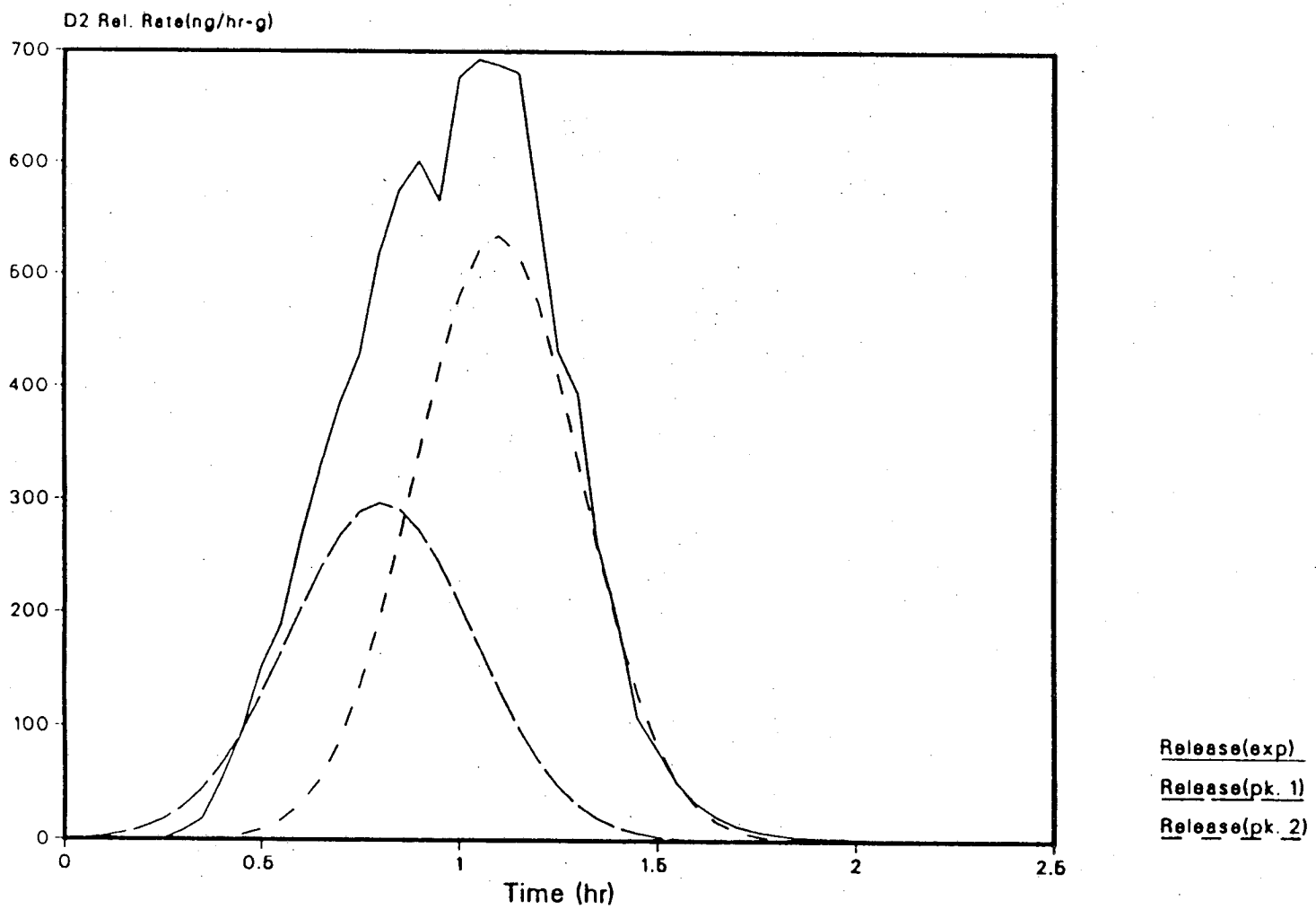

Fig. 17: Release Curve for Expt. 11
Infusion: 10 atm D2, 1000 C, 2 hr
Two Gaussian Fitted Peaks; 868 C, 987 C

the total released was about 25% less than that in the experiments with an infusion temperature of 1600°C where the samples were quenched normally. In experiment 9, in addition to slow quenching, the effect of temperature history was examined by heating the sample for ½ hr at 1600 °C then lowering the temperature to 1200 °C for the next ½ hr. If the infusion process was totally irreversible then this experiment should have given a release curve similar to an experiment with a 1600 °C infusion temperature. This was not observed although the total release was about 80% greater than in the normal 1200 °C infusion experiments suggesting some irreversibility. As the final temperature was 1200 °C, the effect of the slow quench on the quantity of D_2 dissolved was not significant.

In experiment 15 the effect of preheating the sample was examined. An as-received sample was heated in vacuum in the outgassing furnace to about 1800 °C for about 3 hours to cause the grain size to increase. An optical photomicrograph of this sample that has been etched to show the grains is shown in Fig. 18 with a typical grain size of about 15 microns. As the grain size is not significantly greater than an as-received sample, some other effect of the 1800°C anneal must be responsible for the much larger D_2 solubility observed in this experiment.

In experiment 35 a hyperstoichiometric urania sample fabricated as described previously with an oxygen-to-uranium ratio of 2.065 was infused with 10 atm of D_2 at 1600 °C. Additionally the sample was not dropped. The resulting release rate curve is similar to that of experiment 31 and other experiments with similar infusion temperature and pressure. The total release is comparable to experiment 31 where the sample was not dropped, although the second peak is much larger in experiment 35 than in 31. It appears that the added oxygen in this sample had no appreciable effect on the observed D_2 solubility.

In summary, for stoichiometric UO_2 the release rate curve exhibits from one to four peaks dependent on the temperature of infusion. For higher infusion temperatures

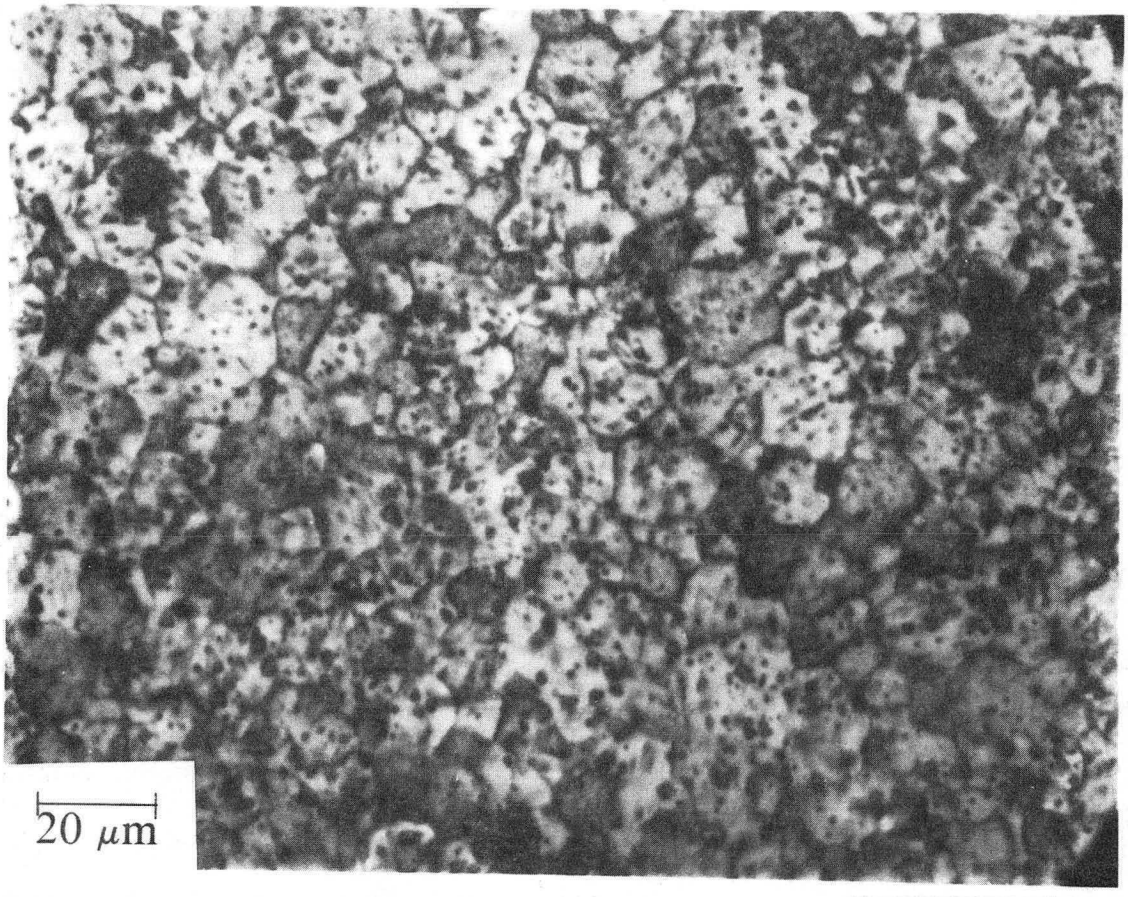

XBB 871-308A

Fig. 18 Optical Photomicrograph of a preheated polycrystalline UO_2 sample chemically etched to show the grain-boundaries

a first peak at 660- 770 °C is present. A second peak at 750- 900 °C is present in all the experiments as is a third peak at 890- 1060 °C. A fourth peak at a temperature of 1100- 1260 °C is also present in the higher temperature infusion experiments, being particularly noticeable at higher pressure infusion experiments.

3.3.2. Hypostoichiometric Urania

As mentioned previously in experiments where the infusion temperature was 1400 °C or greater, a first peak at 660- 770 °C is present. The results for the hypostoichiometric urania samples give a possible explanation for this particular peak.

As was described previously two samples of hypostoichiometric urania were examined, one with a oxygen-to-uranium ratio of 1.976 and the other about 1.90. The first corresponds to experiment 32 and the other, experiment 33. The release rate curve of experiment 32 is shown in Fig. 19. This curve is similar to that of the stoichiometric UO_2 sample except the release rate is about 20 times greater in magnitude. The first peak is about 50 times greater than the average stoichiometric UO_2 first peak. So is the second peak. From Table 4 it is seen that for experiment 33 the first peak has a total D_2 release of 155 μg/g UO_2, about 1500 times greater than for the typical stoichiometric sample. As in experiment 32 the second peak is also large, as is the third peak. The total solubility of D_2 in this sample was 221.4 μg/g UO_2. As mentioned previously the hypostoichiometric urania UO_{2-x} has a large population of extrinsic anion vacancies. Clearly this increase in anion vacancies has increased the solubility of deuterium in the solid.

Aside from the increased vacancies, another factor is involved in the large increase in solubility in the hypostoichiometric urania samples. This large solubility is particularly evident in the first peak in experiment 33. A possible source of this D_2 release is from the dissociation of UD_3 The chemistry of uranium deuteride was reported by Katz[27] with its formation given by this reaction:

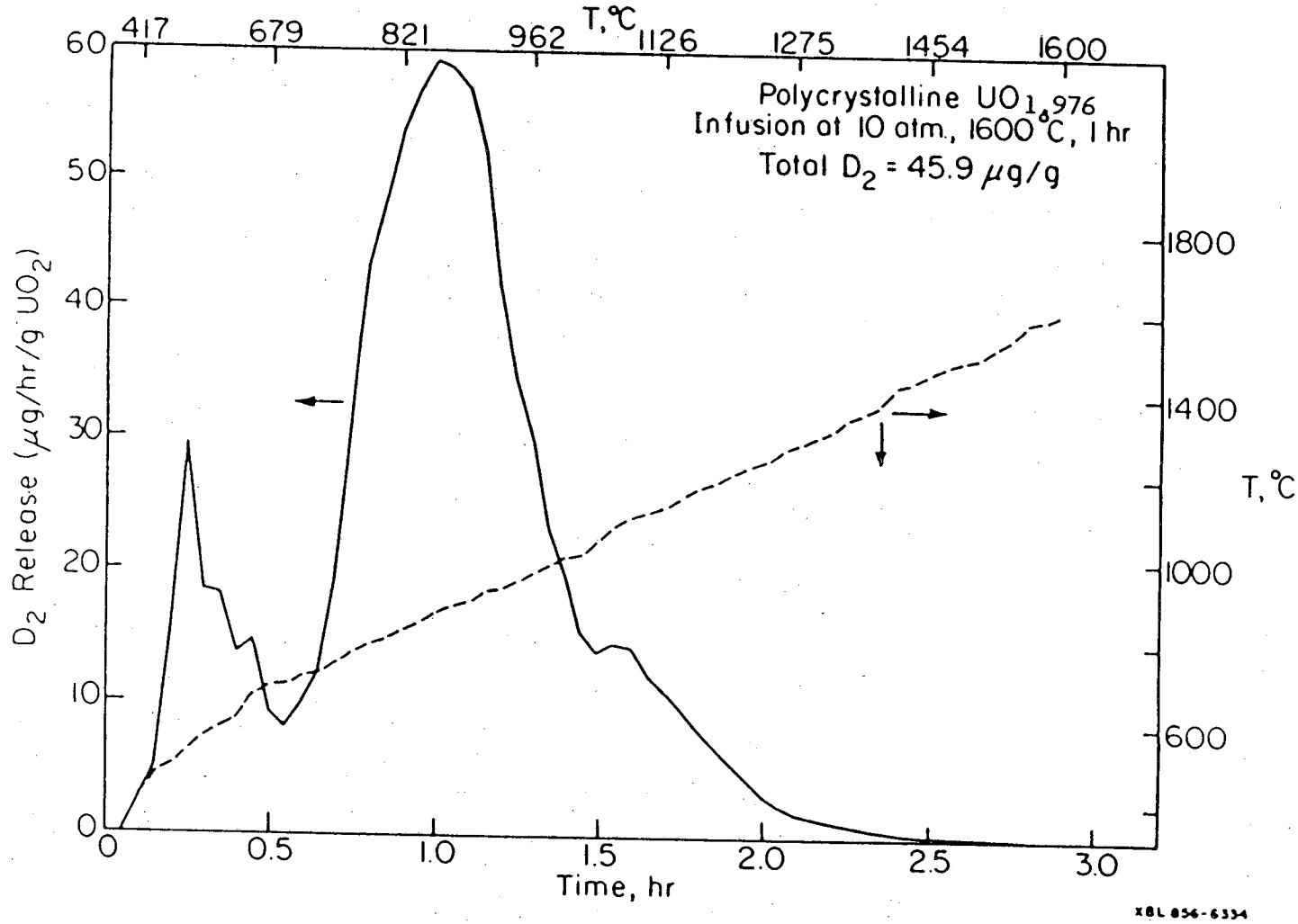

Fig. 19 Deuterium Release Curve for Expt. 32

$$U + 3/2\ D_2 \rightarrow UD_3 \tag{17}$$

This reaction proceeds to completion at 250 °C. Additionally it will decompose at temperatures above 450 °C.

To understand how UD_3 was formed in these experiments it is necessary to review the phase diagram of UO_2, shown in Fig. 20.[28] At temperatures below 1200 °C UO_{2-x} is present as two separate phases, UO_2 solid and uranium metal. Above this temperature it is possible to form a separate UO_{2-x} phase and uranium liquid, depending on the oxygen-to-uranium ratio. For experiment 32 this single phase UO_{2-x} would be present at 1600 °C and in experiment 33, additional uranium liquid is present. If a stoichiometric UO_2 sample is heated above 1200 °C and if the oxygen potential is sufficiently low it is possible to reduce the sample to hypostoichiometric urania. Previously it was mentioned that during infusion the oxygen potential was determined to be insufficient to reduce the sample although it was possible that the oxygen potential at the heating site was less than that measured. If this is so it is possible that the sample could have been reduced. On cooling of this hypostoichiometric sample, uranium would be precipitated. As the sample cools further below 450 °C the uranium metal can react with the D_2 gas present to form UD_3.

To test this hypothesis regarding the source of the first peak, experiment 34 was conducted. In this experiment a 3 g sample of U was heated in 500 torr of D_2 at 250 °C for about 2 hours in the outgassing furnace. The sample was cooled and after evacuating the D_2 the sample was then outgassed. The results are shown in Fig. 21. Only one peak was observed at a temperature of 638 °C. This peak corresponds to the dissolution of UD_3. The temperature at which this occurs corresponds usually to the first peak mentioned earlier, although in the hypostoichiometric samples the temperature of the first peak was somewhat less. For the samples that were initially hypostoichiometric, the amount of UD_3 formed would be considerably greater than that in pure UO_2 because of the excess uranium. Other evidence of this UD_3 formation was

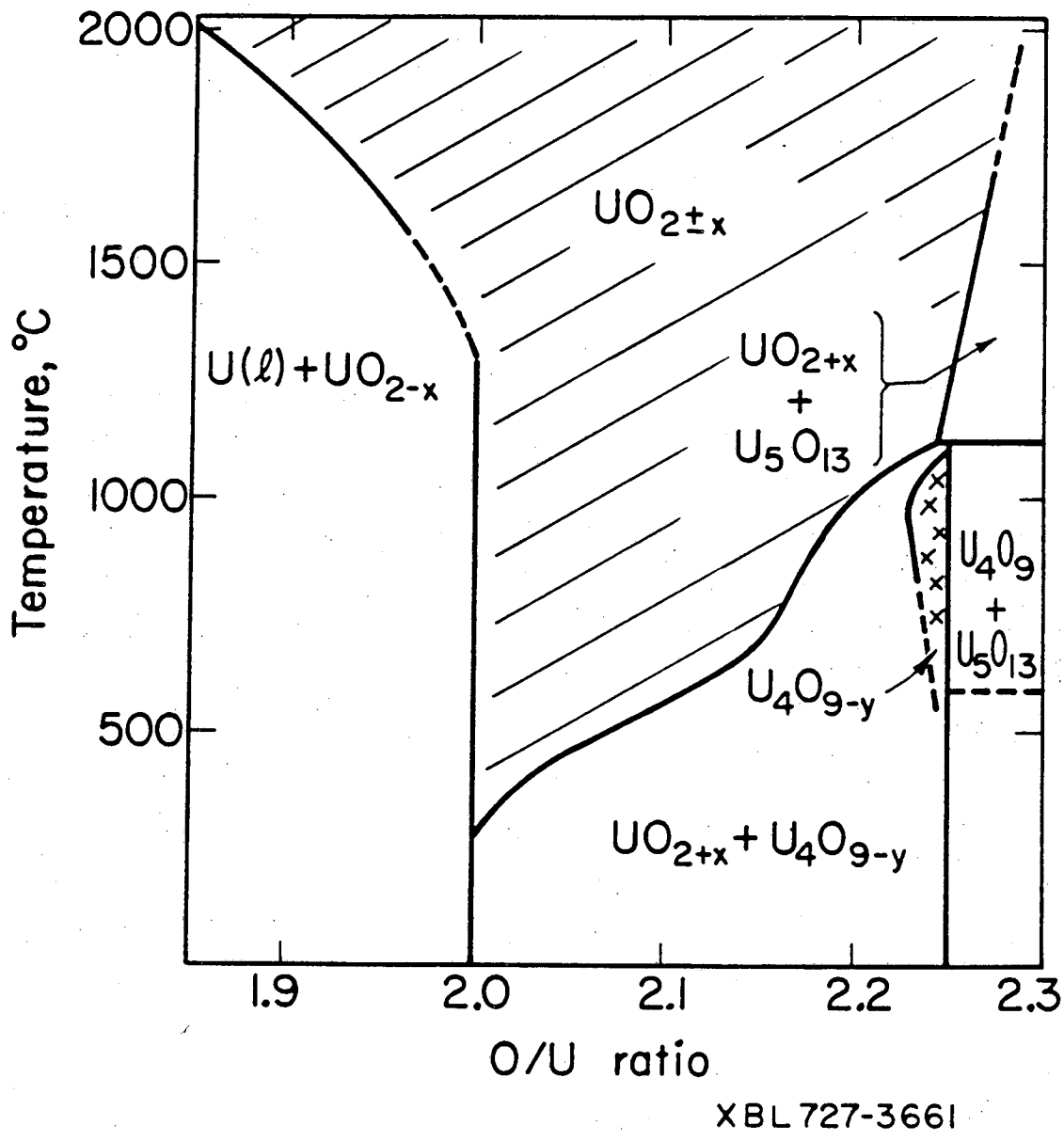

Fig. 20 Uranium-Oxygen Phase Equilibrium System

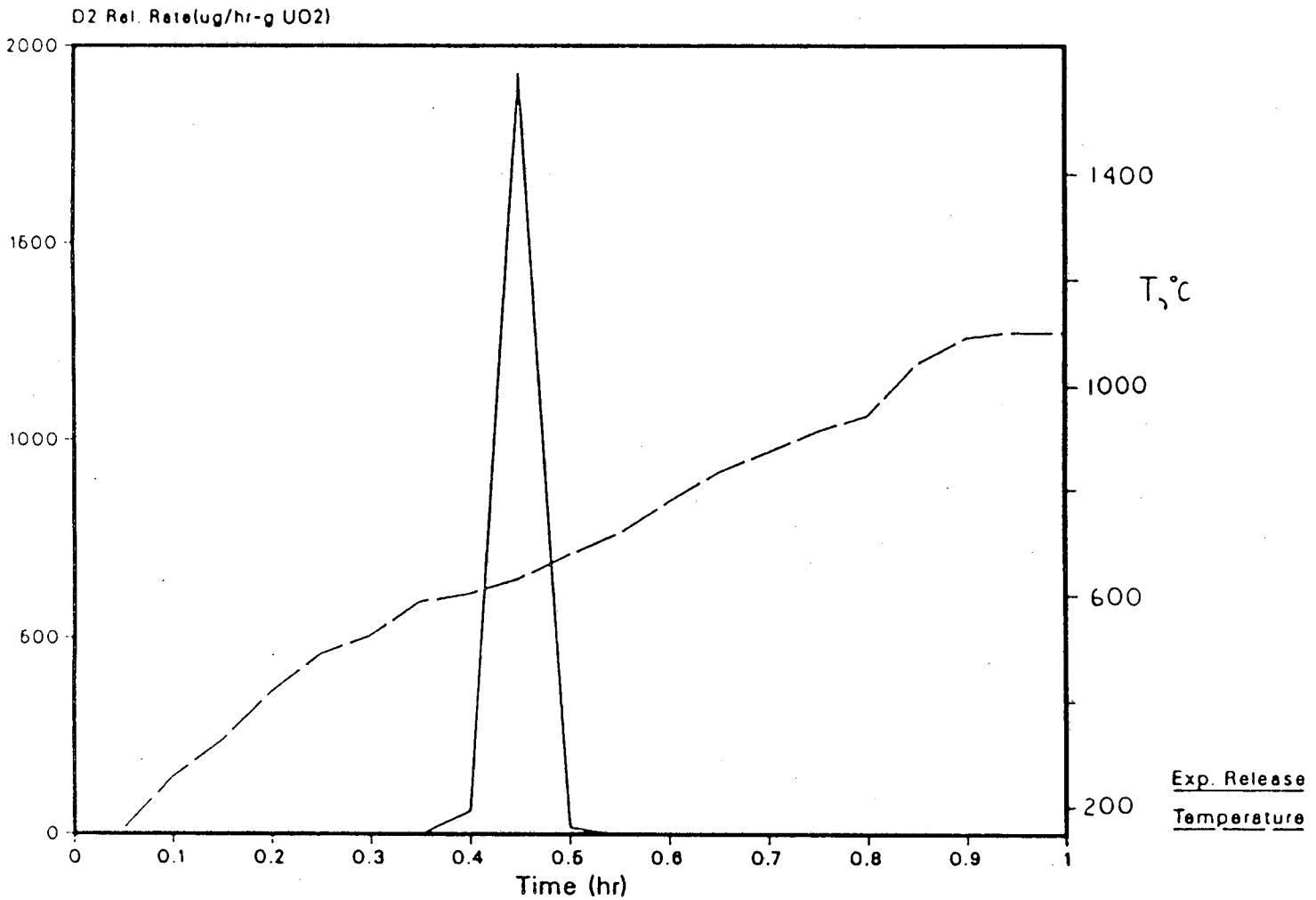

Fig. 21 EXPT 34
Dissolution of UD3
Pk Temp= 638C; Total D2 Rel= 100.6 ug

the powdering of the sample in experiment 33, which is due to formation of UD_3.

With an oxygen-to-uranium ratio of about 1.90 it is possible that up to 150,000 ppm atomic of D_2 (or 1100 μg/g UO_2) could be released if all the excess uranium reacted to form UD_3, 7 times greater than was observed. For experiments such as 2, where 100 ng of D_2/g UO_2 was released (owing to possible UD_3 formation), a similar analysis assuming only one percent of the excess uranium reacting to form UD_3 gives an oxygen-to-uranium ratio of 1.999. These calculations demonstrate that even a small extent of hypostoichiometry in which UD_3 is formed during the quench can result in a very large apparent solubility of deuterium in urania.

3.4. Solubility Summary

The total area under the net release rate curve, represents the solubility of D_2 in the particular UO_2 sample at the given infusion temperature and pressure. In these results it was assumed that the loss of D_2 during quenching was negligible. This assumption is discussed further in Appendix A. This information shown in Tables 3 and 4, for single crystal and polycrystalline UO_2, respectively, is analyzed below.

3.4.1. Single Crystal UO_2

An Arrhenius plot of the D_2 solubility in single crystal UO_2 is shown in Fig. 22. This shows the five experiments with an infusion pressure of 10 atm of D_2 at temperatures from 1300 to 1600 °C. These points have been fitted to a straight line giving a heat of solution, ΔH_s, of +235 kJ/mol. The positive sign shows that UO_2 is an *endothermic* absorber of hydrogen. The fit to these points is good with a small uncertainty. The solubility at this pressure, can be expressed as:

$$\left[\frac{\mu g\ D}{g\ UO_2}\right]_{10\ atm} = 7.0\text{x}10^5 \exp\left(\frac{-235\ kJ}{RT}\right)$$

where R is the gas constant, and T the infusion temperature in K.

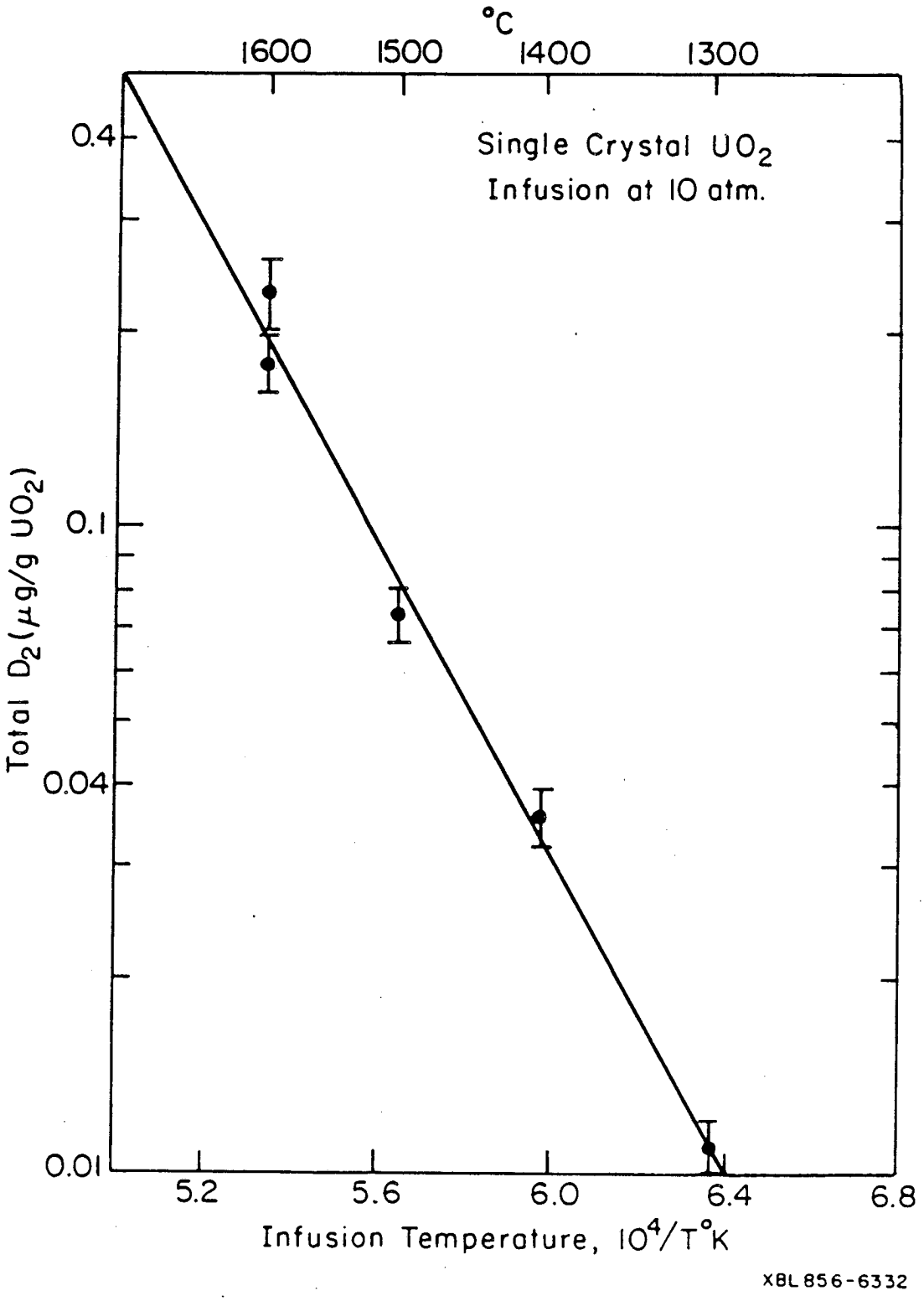

Fig. 22 Arrhenius plot of Deuterium Solubility in Single Crystal UO_2; ΔH_s= +235 kJ/Mol

In Fig. 23 a plot of the log of the solubility as a function of the log of the infusion pressure in atm of D_2 is shown. This is for the 5 experiments at an infusion temperature of 1600 °C. These 5 points have been fitted to a straight line giving a slope of 0.48 ± 0.01. This slope of nearly one half suggests a square root dependence of the solubility with pressure that from the argument in Sec. 1.2 implies that Sievert's Law is followed. Thus from Eq (3), the dissolution of hydrogen in UO_2 is a two-step atomic process, implying hydrogen will be present in atomic form in the UO_2 lattice. From this square-root dependence of the solubility with pressure, the Sievert's law constant of D in UO_2 is determined to be:

$$S = C_D(\text{ppm atomic}) / \sqrt{P} = \left(\frac{270}{2}\right)\left[\frac{\mu g\ D}{g\ UO_2}\right]_{P=10\ atm} / \sqrt{10}$$

or

$$S = 3.0 \times 10^7 \exp\left(\frac{-235\ kJ}{RT}\right) \frac{\text{ppm atomic}}{\sqrt{atm}}$$

Examining individual peaks for these single crystal release experiments gives no added information. The first peak in particular has no recognizable dependence on pressure or temperature.

3.4.2. Polycrystalline UO_2

An Arrhenius plot of the equilibrium concentration of deuterium in polycrystalline UO_2 exposed to D_2 gas at 10 atm is shown in Fig. 24. This shows the ten experiments with an infusion pressure of 10 atm of D_2 at temperatures from 1000 to 1600 °C. These points have been fitted to a straight line giving a resultant heat of solution, ΔH_s, of ≅ 100 kJ/mol. The positive sign shows that polycrystalline UO_2 is an *endothermic* absorber of hydrogen, as was single crystal UO_2. The fit to the points is not as good as for single crystal UO_2, although excluding the points that probably did not achieve saturation, as well as the possibly spurious results at an infusion temperature

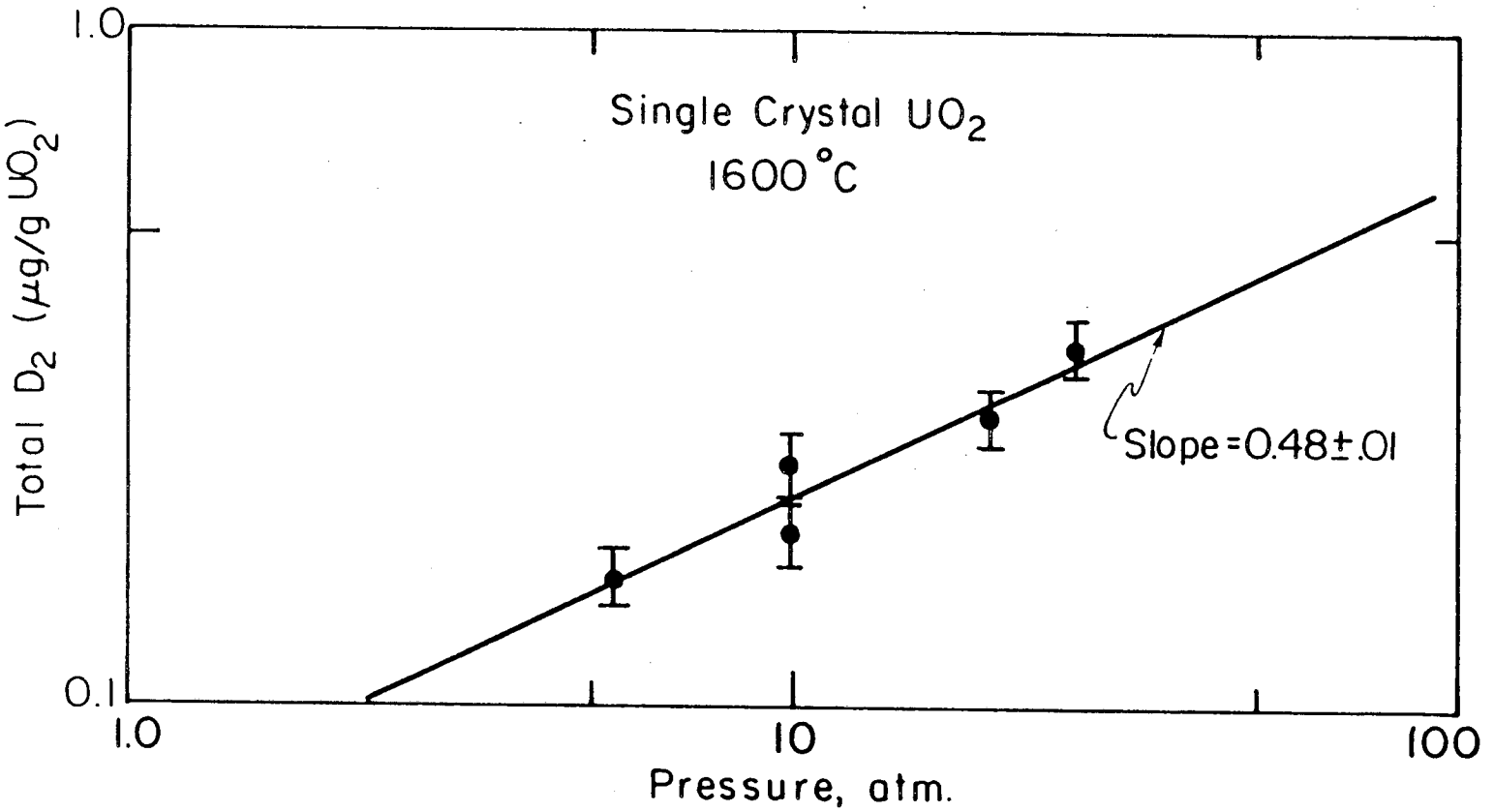

XBL 856-6330

Fig. 23 Log of Deuterium Solubility in Single Crystal UO_2 as a function of the Log of the Infusion Pressure

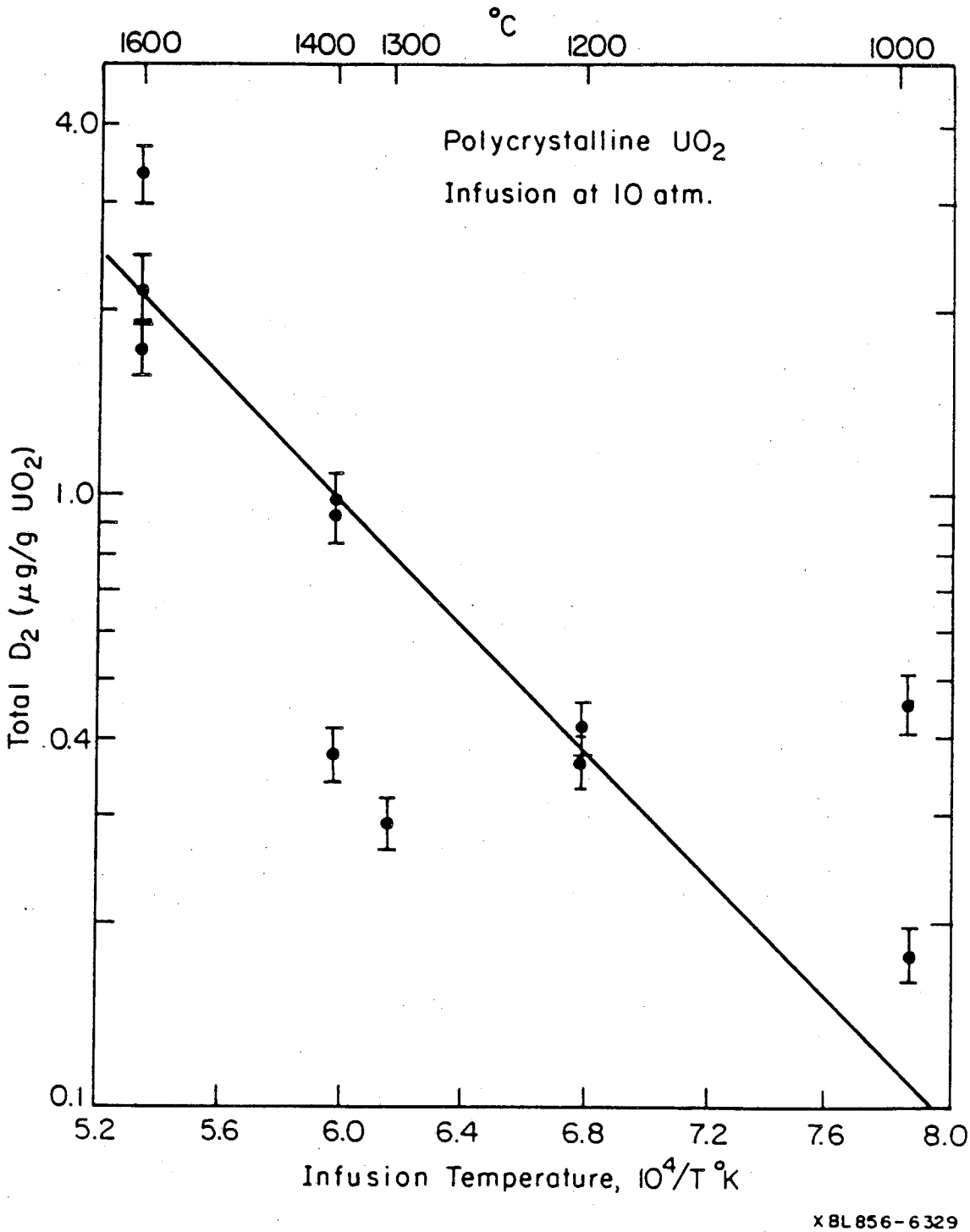

Fig. 24 Arrhenius Plot of Deuterium Solubility in Polycrystalline UO_2; $\Delta Hs = +100$ kJ/Mol

of 1000 °C, gives a good fit with the same slope. The solubility at this pressure, S of D_2 in μg/g UO_2 can be expressed as:

$$\left[\frac{\mu g\ D}{g\ UO_2}\right]_{10\ atm} = 1.3x10^3 \exp\left(\frac{-100\ kJ}{RT}\right)$$

In Fig. 25 a plot of the log of the solubility as a function of the log of the infusion pressure at 1600°C is shown. Eight of these 9 points have been fitted to a straight line giving a slope of 0.52 ± 0.13. The point representing the experiment with an infusion pressure of 20 atm of D_2 has been ignored in this fit. This slope of one half as for single crystal UO_2 implies atomic dissolution of hydrogen in polycrystalline UO_2. The Sievert's law constant for polycrystalline UO_2 is:

$$S = 5.5x10^4 \exp\left(\frac{-100\ kJ}{RT}\right) \frac{ppm\ atomic}{\sqrt{atm}}$$

An examination of the pressure and temperature dependence of the individual peaks gives some added information, but this will be deferred until a model is proposed for the origin of separate peaks in the release rate curve.

3.5. Comparison with other Ceramic Oxides and Wheeler's[2] Results

Although the solubility results of this study can be compared with those of other ceramic oxides[13–18] there are no comparable release rate results. Although there is data on outgassing experiments conducted at constant temperature for some of these ceramics, simple diffusion always has been assumed to govern the release of hydrogen from these solids[13,14,18]. The presence of multiple peaks in the outgassing curves as in this study has not been found in any of these cases including that of Wheeler[2] for hydrogen in UO_2.

3.5.1. Ceramic Oxides

The results for hydrogen solubility in ceramic oxides was summarized in Table 2. One main difference between the other ceramic oxides and UO_2 is the heat of solution

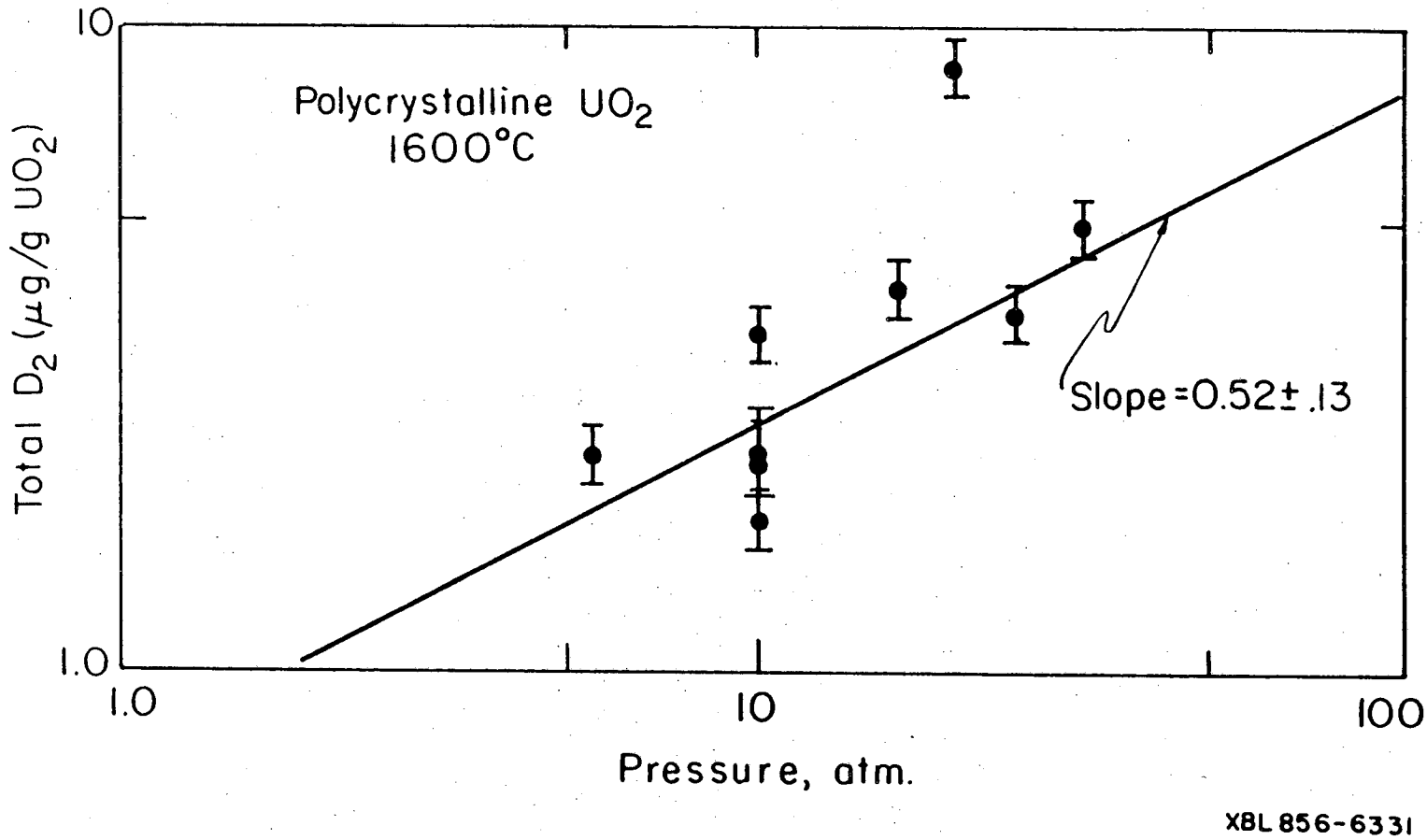

Fig. 25 Log of Deuterium Solubility in Polycrystalline UO_2 as a function of the Log of the Infusion Pressure

of hydrogen, ΔH_s. In the ceramic oxides the ΔH_s is between 8 and 76 kJ/mol. in contrast to 100 and 235 kJ/mol for polycrystalline and single crystal UO_2, respectively. This large ΔH_s, particularly for single crystal UO_2, suggests great difficulty in dissolving hydrogen in the UO_2 lattice in comparison with other ceramic oxides. Only for Al_2O_3 is data available for both the single crystal and polycrystalline form of the solid. The difference in the solubility between single crystal and polycrystalline UO_2 is greater than for Al_2O_3. although both show higher solubility in the polycrystalline material rather than the single crystal solid.

A graph showing an Arrhenius plot of the solubility at one atm of hydrogen for the ceramic oxides of Table 2 and uranium oxide from this study is shown in Fig. 26. The solubility of UO_2 is less than any of the other ceramics shown in the figure. Other ceramics mentioned previously (e.g. titania) also have larger hydrogen solubility than reported here for hydrogen in UO_2.

3.5.2. Wheeler's results

It is difficult to compare these results with that of Wheeler[2] as no pressure or temperature dependence of his results on hydrogen solubility were given. Only the statement that hydrogen solubility varied between 4 and 54 ppm atomic for single crystal UO_2 at temperatures of ~ 500 to 1000°C is given in Ref. 2. Assuming that the infusion pressure is one atm of hydrogen, the resulting Sievert's Law constant is somewhat greater than those determined here.

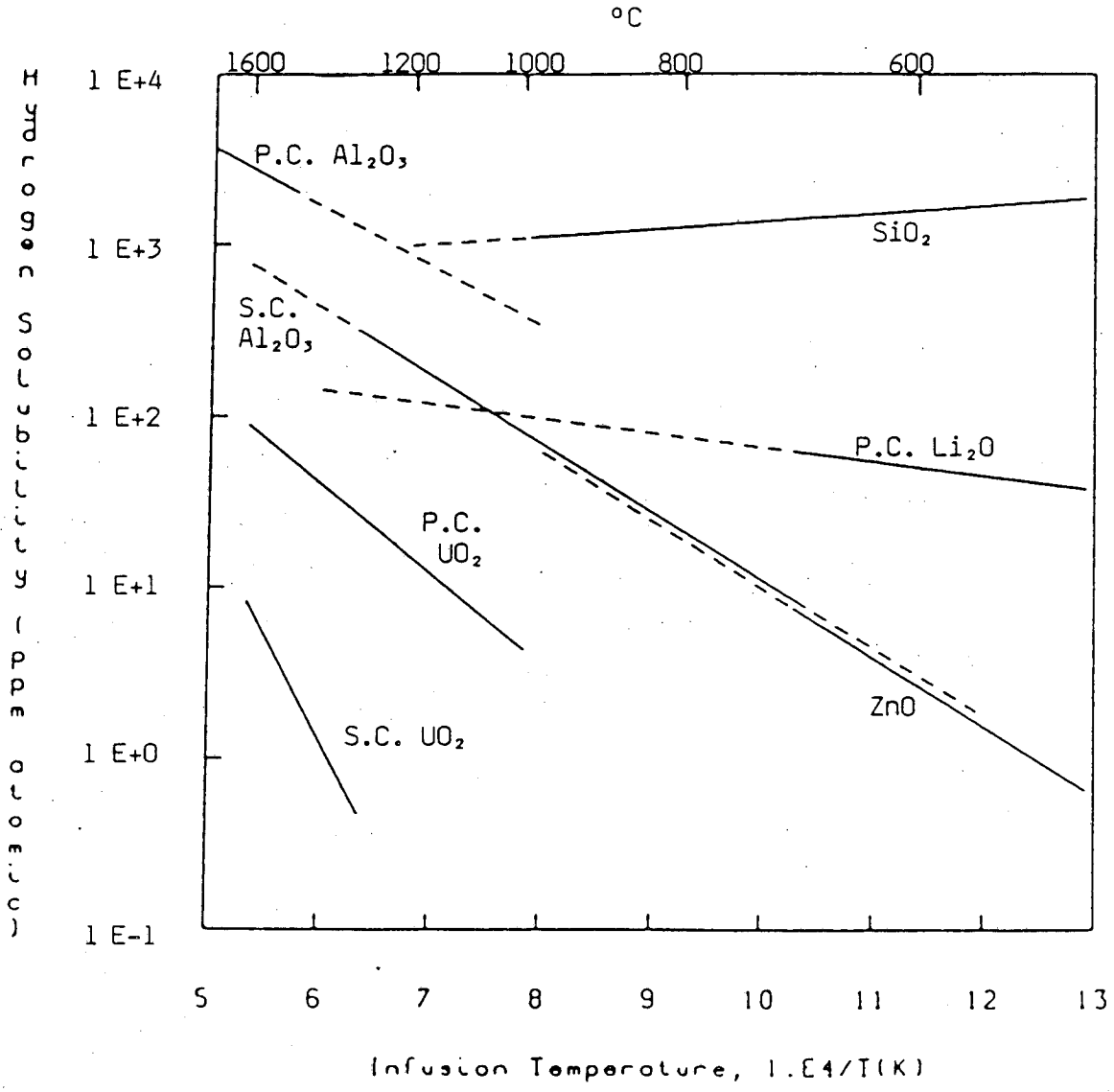

Fig. 26 Arrhenius Plot of the Solubility at one atm. of Hydrogen in Ceramic Oxides(Refs. in Table 2) and for Uranium Oxide from this study

4. MODELING OF RELEASE KINETICS

4.1. Simple Diffusion Model

A first model to be analyzed for the release of D_2 from the UO_2 samples is that of simple diffusion. This model assumes that D_2 is released from the sample during the outgas by diffusion; it was used by Wheeler in his analysis of release of hydrogen from UO_2.[2]

The diffusion equation for the mobile deuterium atoms in a sphere is given by:

$$\frac{\partial c}{\partial t} = \frac{D(T)}{r^2} \frac{\partial}{\partial r}\left(r^2 \frac{\partial c}{\partial r} \right) \tag{19}$$

Where c is the solute concentration and D(T) is the diffusivity, a function of T, the temperature of the solid at a particular time. The initial condition is:

$$C_0 = C_{Sat}\,(T_0) \tag{20}$$

where C_0, is the initial uniform concentration equal to the saturation concentration, C_{Sat}, at the infusion temperature, T_0 corresponding to the conditions of infusion. The surface boundary condition in this vacuum outgas is given by:

$$c\,(a,t) = 0 \tag{21a}$$

where a is the radius of the sphere. By symmetry the boundary condition at r=0 is:

$$\left(\frac{\partial c}{\partial r} \right)_0 = 0 \tag{21b}$$

4.1.1. Solution of Diffusion Equation

In this outgassing case, the dependence of temperature on time and the temperature ramp rate, β, is given by:

$$T = T_s + \beta t \tag{22}$$

where T_s is the temperature at t = 0 at the start of the ramp.

This analysis must recognize that the diffusion coefficient is a function of tem-

perature, that, with Eq (22), makes it a function of time. The diffusivity D is related to the diffusivity D_0 at the infusion temperature T_0 by:

$$D = D_0 \exp\left\{-\frac{E_D}{R}\left(\frac{1}{T} - \frac{1}{T_0}\right)\right\} \tag{23a}$$

Where E_D is the activation energy of diffusion. As the temperature is given as a function of t by Eq (22) the diffusivity can be expressed as a function of t by:

$$D = D_0 f_D(t) \tag{23b}$$

The function f_D can be determined from Eqs. (22) and (23a).

This problem can be simplified by defining three dimensionless groups for the time, for the radius, and for the concentration. For the time a new variable, τ can be defined as:

$$\tau = \frac{D_0 t}{a^2} \tag{24a}$$

and for the radius a new variable ρ is given by:

$$\rho = \frac{r}{a} \tag{24b}$$

and finally for the concentration, a new variable C is given by:

$$C = \frac{c}{C_0} \tag{24c}$$

With C_0 given by Eq (20).

Substituting Eqs. (23b) and (24a-c) into Eq (19) gives:

$$\frac{\partial C}{\partial \tau} = f_D \frac{1}{\rho^2} \frac{\partial}{\partial R}\left(\rho^2 \frac{\partial C}{\partial \rho}\right) \tag{25}$$

with the initial condition of Eq (20) now given by

$$C = 1 \text{ at } \tau=0 \tag{26a}$$

and the boundary conditions of Eqs (21a-b) now given by

$$C = 0 \text{ at } \rho=1 \tag{26b}$$

and

$$\frac{\partial C}{\partial \rho} = 0 \text{ at } \rho=0 \tag{26c}$$

To solve Eq (25) analytically, it is necessary to numerically integrate f_D over τ giving a new variable, θ:

$$\theta = \int_0^{\tau} f_D(\tau')\, d\tau' \tag{27}$$

With this relation the solution of Eq (25) from Carslaw & Yeager[29] is given by:

$$C = \frac{-2}{\pi\rho} \sum_{n=1}^{\infty} \frac{(-1)^n}{n} \sin(n\pi\rho) \exp{-(n^2\pi^2\theta)} \tag{28}$$

Although this gives the solution as a function of the dimensionless radius, ρ, and through Eq (27) the dimensionless time τ, what is required in this model is the time dependency of the release rate, R.

$$R = -DS \left(\frac{\partial C}{\partial r} \right)_{r=a} \tag{29a}$$

Where S is the surface area. Here the release rate, R is given as a function of τ by:

$$R = -R_0\, f_D(\tau) \left(\frac{\partial C}{\partial \rho} \right)_{\rho=1} \tag{29b}$$

Where R_0 is a reference release rate and is given by:

$$R_0 = \frac{3D_0C_0}{a^2} \tag{29c}$$

When C_0, the initial concentration is given in μg D_2/g UO_2, and D_0 in cm^2/sec, then the units of R_0 are (μg D_2/sec)/g UO_2. The gradient of the concentration at the surface in Eq (29b) is a function of time and can be evaluated by differentiating Eq (28) yielding:

$$\left(\frac{\partial C}{\partial \rho} \right)_{\rho=1} = -2 \sum_{n=1}^{\infty} \exp(-n^2\pi^2\theta) \tag{30}$$

This expression can be evaluated at τ by relating θ to τ by Eq (27). Substituting this equation into Eq (29b) with R_0 given by Eq (29c) gives the release rate, R, as a function of τ:

$$R = \frac{6D_0C_0}{a^2} f_D(\tau) \sum_{n=1}^{\infty} \exp\left\{-n^2\pi^2\left(\int_0^{\tau} f_D(\tau')\right)\right\} \tag{31}$$

4.1.2. Comparison of Solution with Results

Using the diffusivity of hydrogen in UO_2 determined by Wheeler[2] and temperature ramp of Eq (22) in Eq (31) yields a release curve as a function of time. In the diffusion model the initial concentration is assumed to be the total measured deuterium released per gram of UO_2. The results of this analysis shown with the corresponding experimental results are shown in Figs. 27 and 28 for experiments 2 and 18. The unsuitability of this model is evident; as the diffusion model gives only one peak at 620 °C for both the polycrystalline and single crystal samples. Moreover, this peak occurs at at a lower temperature than most of the polycrystalline release, and at a much lower temperature than the single crystal release.

The simple diffusion model can give only one release peak, in contrast to what was observed. But it is possible that by varying the diffusivity, a better fit to the release data could be obtained. This was done for both a single crystal and polycrystalline release experiment.

In the model discussed above for a particular solid of radius a and initial concentration C_0 only two parameters, D_0 and E_D, determine the shape of the release curve as a function of temperature. By varying these two parameters it is possible to fit a single release peak. The parameters were varied by a Monte Carlo method as described previously for the Gaussian fit to the release curves.

For the polycrystalline UO_2 outgas of Expt 2 (Fig. 13), a fit to the first peak (after the hydride peak) was attempted. This would imply that some other mechanism was involved in the last two peaks of Fig. 13. The results for this fit along with the peak that was obtained using Wheeler's values for the diffusivity are shown in Fig. 29. The diffusivity parameters for the best fit to this peak are 8.9 $\times 10^8$ cm^2/sec for the pre-exponential factor, D_0, and 280 kJ/mol for the diffusion activation energy, E_D.

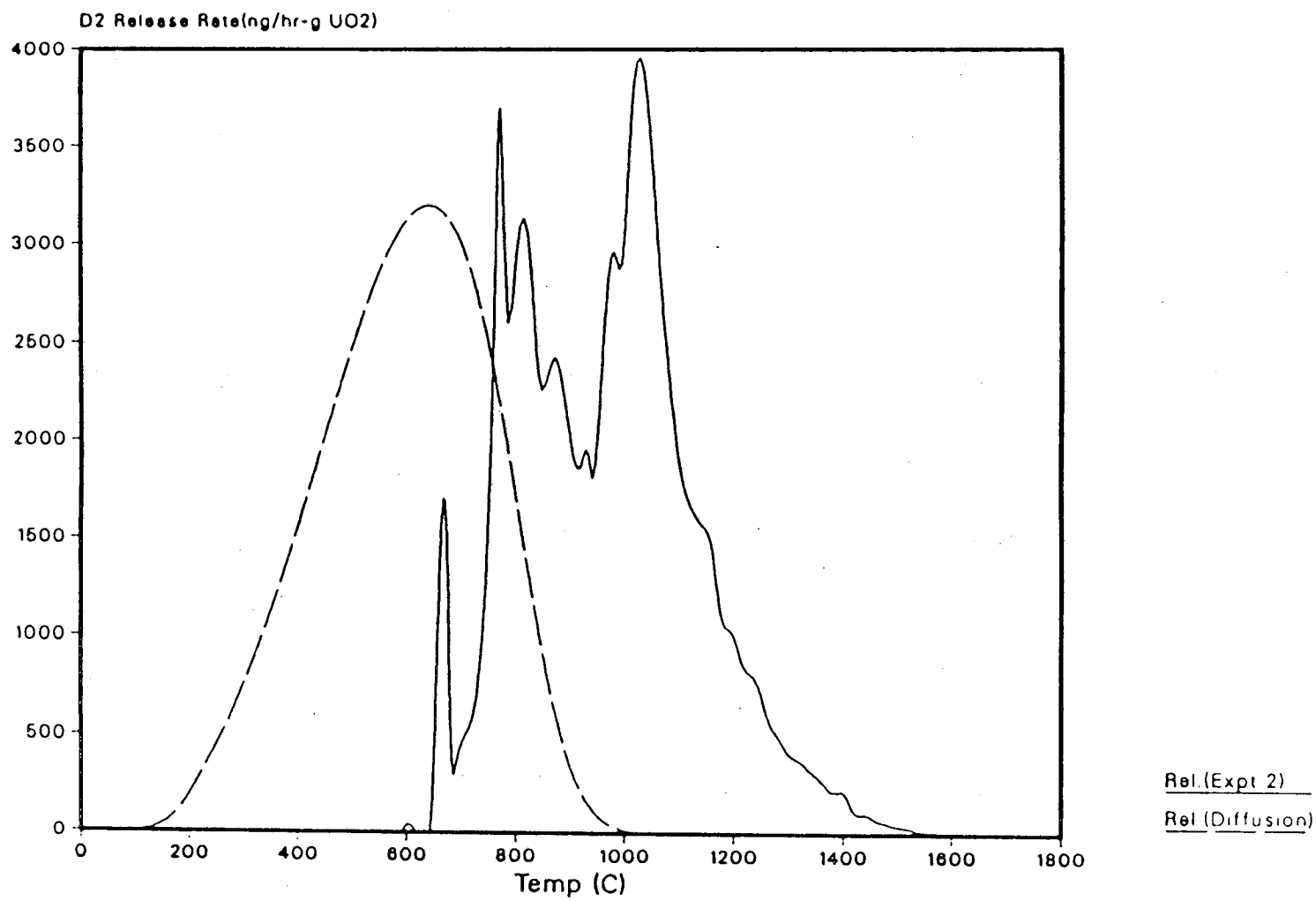

Fig. 27: Comparison of Expt 2 Release Results
With Rel. Calc. Assuming Simple Diffusion using Wheeler's Data:
DO= 0.37 cm2/sec and Ed= 60 kJ/Mol

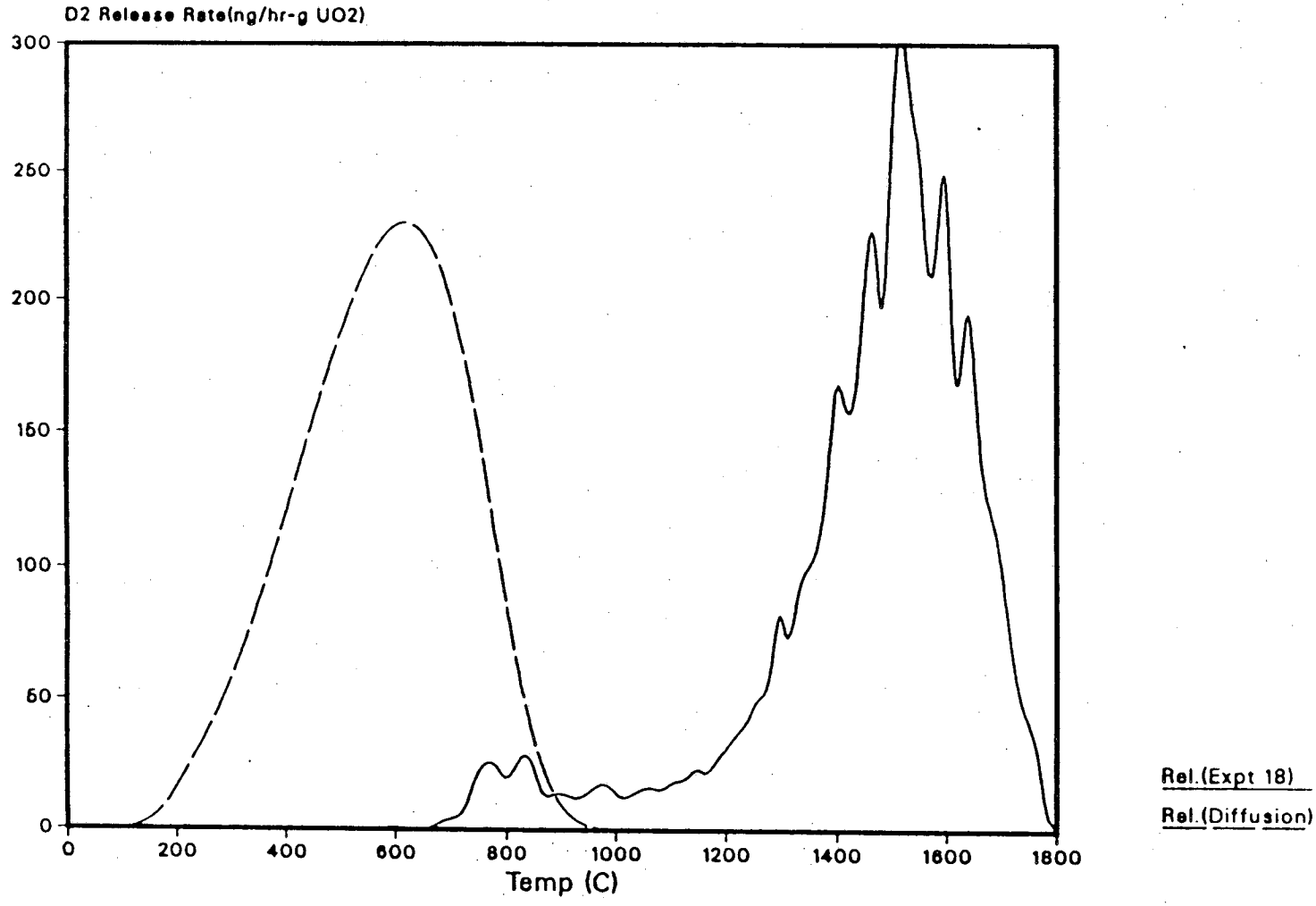

Fig. 28: Comparison of Expt 18 Release Results
With Rel. Calc. Assuming Simple Diffusion using Wheeler's Data:
D0= 0.37 cm2/sec and Ed= 60 kJ/Mol

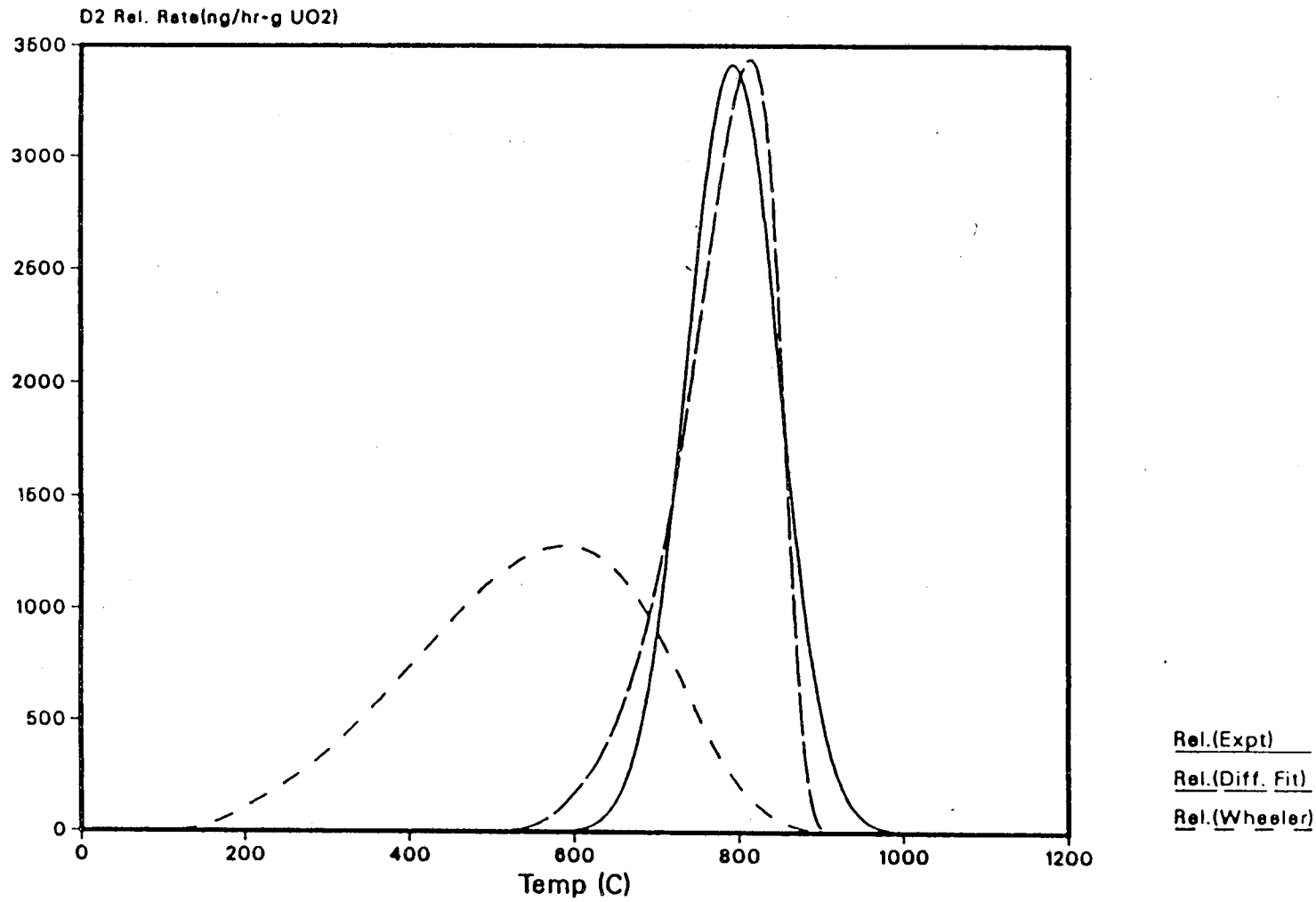

Fig. 29: Diffusion Model Best Fit to 2nd Peak of Expt 2
Compared to Peak Calc. using Wheeler's Diffusivity Data
Best fit: D0= 8.9 E+8 cm2/sec, Ed= 280 kJ/mol

For the single crystal experiments a fit to the second peak of experiment 18 was attempted, as this peak is the major one in this release experiment. The results of this fit are shown in Fig. 30, with D_0 given by 1.77 x10^4 cm^2/sec, and E_D by 319 kJ/mol.

These parameters for the best fits differ considerably from those of Wheeler. The activation energies of 280 and 309 kJ/mol are large for the diffusion of hydrogen in solids, being more comparable to self-diffusion of cations such as U^{+4} in UO_2.

The preexponential factor D_0 can be shown by absolute rate theory for interstitial or vacancy diffusion of an impurity atom in a lattice to be about equal to $a_0^2\nu$, where a_0 is the lattice constant and ν the vibration frequency of the impurity atom. For UO_2 a_0 is 5 A° and ν is within an order of magnitude of 10^{13} sec^{-1}. With these values D_0 should be about 0.02 to 0.2 cm^2/sec. These are rough estimates but nonetheless are more than 4 orders of magnitude smaller than the best fit value of D_0 for experiment 18 shown above. Thus although a fit to one peak with a diffusion model is possible, the abnormal diffusivity parameters obtained suggest the unsuitability of this model to explain these release results.

To further verify this conclusion, release curves from other experiments were investigated, with similar results. Finally, the possibility that release from the polycrystalline sample was governed only by diffusion to the grain boundaries was investigated. Even with this unrealistic assumption a pre-exponential factor of about 10^5 cm^2/sec is obtained. This is still to large, again showing that the diffusion model is not applicable to these results.

4.2. Diffusion with Trapping and Resolution

A second model that was proposed for the release of D_2 from the UO_2 samples is that of diffusion with trapping and resolution. This model is similar to the simple diffusion model except with the inclusion of trapping and resolution of the migrating deuterium atoms in the UO_2. This model has been applied to release of fission gases

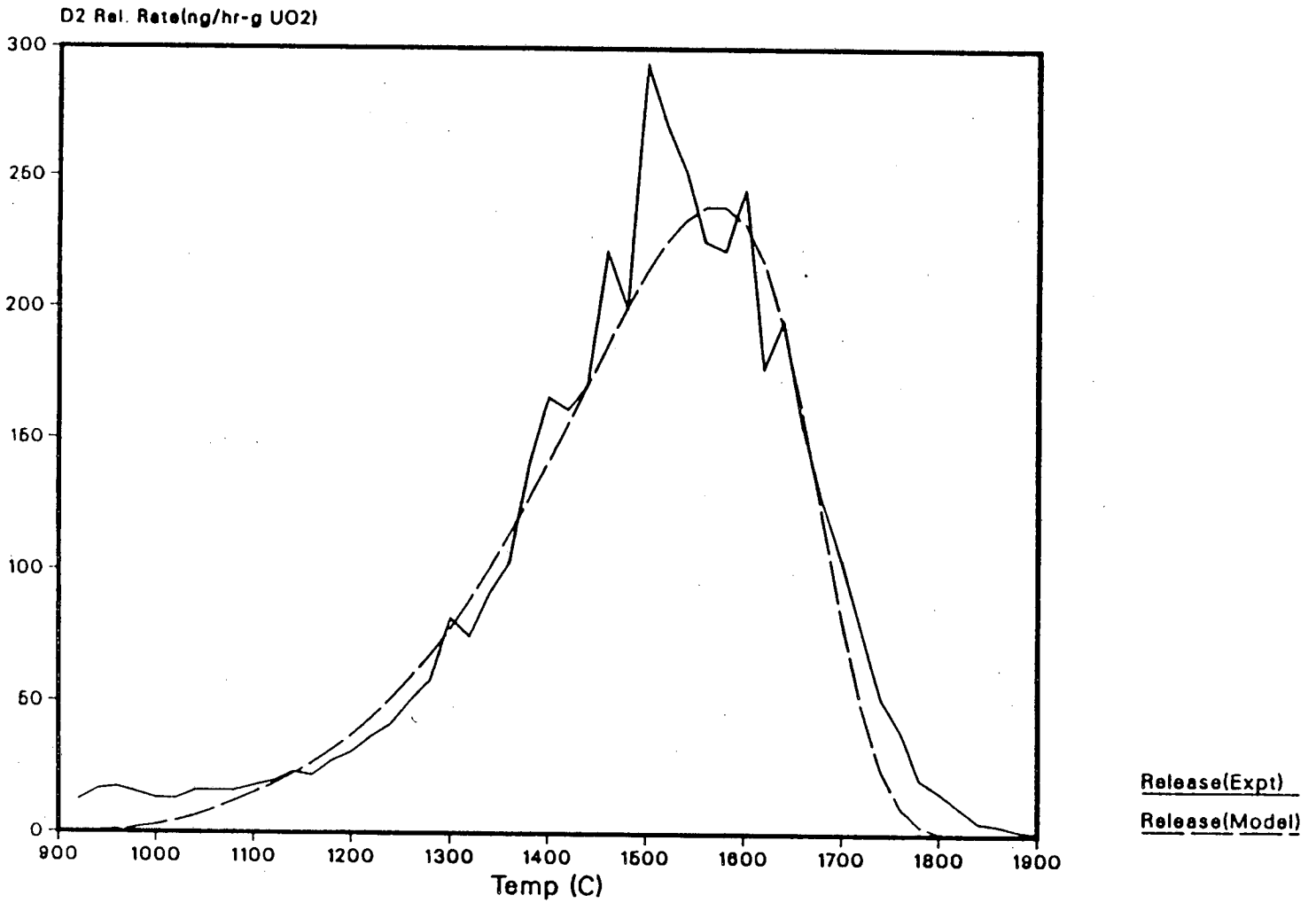

Fig. 30: Diffusion Model Best Fit to 2nd Peak of Expt 18
Best Fit Diffusivity Parameters:
D0= 1.77 E+4 cm2/sec; Ed= 319 kJ/Mol

from UO_2,[30] although in this earlier work this release was at a constant temperature in contrast to the temperature ramp used in this study.

The main feature of this model that distinguishes it from the simple diffusion model is that D atoms are distributed between mobile sites in the UO_2 lattice and trapping centers uniformly distributed in the UO_2 solid. These trapping centers can be natural defects in the solid that can significantly hinder the release rate. For simplicity it is assumed that there is only one type of trap. Mobile diffusing atoms are trapped and the trapped atoms are in turn detrapped. Atoms diffusing to the surface are released.

4.2.1. Solution of Diffusion Equation with Trapping and Resolution

With the above assumptions an additional variable, m, can be defined as the concentration of D atoms in traps. Traps are assumed to act as effective homogeneous sources or sinks with rates of trapping and detrapping given by:

$$gc = \text{trapping rate, ppm D/sec} \tag{32a}$$

and

$$bm = \text{detrapping rate, ppm D/sec} \tag{32b}$$

Where g is the trapping rate constant, and b is the resolution parameter, both having units of sec^{-1}. The two parameters are assumed to be independent of radius and time.

With the above definitions, an analogue of Eq (19) for this case of diffusion with trapping and resolution is given for the mobile D atoms as:

$$\frac{\partial c}{\partial t} = \frac{D(t)}{r^2}\frac{\partial}{\partial r}\left(r^2\frac{\partial c}{\partial r}\right) - gc + bm \tag{33a}$$

and for the trapped D atoms as:

$$\frac{\partial m}{\partial t} = gc - bm \tag{33b}$$

When the sample is outgassed with a linear temperature ramp described in Eq (22), Eqs. (33a) and (33b) can be simplified as was done in the simple diffusion

model. Expanding g and b as was done for D in Eqs. (23a) and (23b) gives for g:

$$g = g_0 \exp\left\{-\frac{E_g}{R}\left(\frac{1}{T} - \frac{1}{T_0}\right)\right\} = g_0\, f_g(t) \tag{34a}$$

Where E_g is the activation energy of trapping, g_0 is g at the temperature of infusion, T_0, and the function f_g can be determined using Eq (22). Expanding for b,

$$b = b_0 \exp\left\{-\frac{E_b}{R}\left(\frac{1}{T} - \frac{1}{T_0}\right)\right\} = b_0\, f_b(t) \tag{34b}$$

Where E_b is the activation energy of resolution, b_0 is b at the temperature of infusion, T_0, and the function f_b can be determined using Eq (22). Further simplification is obtained by defining a dimensionless time, τ, and dimensionless radius, ρ, and dimensionless mobile D atom concentration, C, as in Eqs. (23a-c) for the simple diffusion model. Additionally, a reduced trapped D atom concentration, M, can be defined as:

$$M = \frac{m}{C_0} \tag{35}$$

A dimensionless trapping rate constant G, and resolution parameter, B are defined as:

$$G = \frac{g_0 a^2}{D_0} \tag{36a}$$

and;

$$B = \frac{b_0 a^2}{D_0} \tag{36b}$$

Substituting these last 5 equations along with Eqs. (24a-c) for τ ρ, and C in Eqs. (33a) and (33b) gives:

$$\frac{\partial C}{\partial \tau} = f_D \frac{1}{\rho^2} \frac{\partial}{\partial R}\left(\rho^2 \frac{\partial C}{\partial \rho}\right) - G f_g\, C + B f_b\, M \tag{37a}$$

and

$$\frac{\partial M}{\partial \tau} = G f_g\, C - B f_b\, M \tag{37b}$$

For the initial conditions for C and M it is assumed that at the beginning of the outgas

the initial gas is partitioned between the lattice and the traps by the initial trapped fraction y. It is given by:

$$y = \text{fraction of gas in traps at } t=0 = \frac{g_0}{b_0 + g_0} \tag{38a}$$

The initial conditions for C and M are thus given by:

$$C = 1 - y \text{ at } \tau=0 \tag{38b}$$

$$M = y \text{ at } \tau=0 \tag{38c}$$

With the boundary conditions of Eqs. (27a) and (27b) for simple diffusion also applicable here.

The equations above can be solved numerically to give the reduced concentration of lattice atoms, C, as a function of position, and time. This solution can be related to a release rate using the analysis of Eqs. (29a-c) used for the simple diffusion model. To test the above model numerically, the case of $g_0 = 0$, and b_0 finite (giving y=0 and thus no trapping) was tested. This corresponds to simple diffusion and the numerical results obtained were identical to those obtained analytically. Other limiting cases were investigated, all giving the expected results.

4.2.2. Comparison of Solution with Results

After these initial tests of the model an attempt was made to reproduce the multiple peaks observed in this study with this model. In addition to the parameters D_0 and E_D present in the simple diffusion model, four additional parameters, g_0, b_0, E_g, and E_b, are produced to characterize trapping and resolution. These six parameters were allowed to vary (within reasonable bounds) and many release rate curves were obtained. Even by varying the three pre-exponential parameters through 10 orders of magnitude and the three activation energies by up to 400 kJ/mol, it was not possible to produce multiple peaks in the experimental temperature ranges. Thus this model of diffusion with trapping and resolution was not able to describe the results of this study.

4.3. Detrapping Model

The last model that was applied to the release of D_2 from UO_2 was that of detrapping. In this model the gas atoms are assumed to be trapped at specific sites in the solid. When thermally activated they are detrapped from these sites and rapidly diffuse to the surface where they are released. Detrapping from each site is considered to be independent of the detrapping from other sites, causing multiple peaks. This model is similar to one that has been proposed to describe the thermal desorption spectra of implanted tritium from stainless steel,[31] and deuterium from nickel.[32] In this model, the rate of release of trapped gas is governed by the following equation,

$$-\frac{dC}{dt} = k C^x \exp(-E_d/RT) \tag{39}$$

where x is the reaction order of detrapping; k is the pre-exponential factor of the detrapping rate constant; C is the concentration of trapped gas; and E_d is the activation energy for detrapping. The term dC/dt in units of (ppm atomic)/sec or (μg/g)/h is the release rate that is measured in this study. When the detrapping is operated at a linear heating rate (β) given in Eq (22), the release rate will reach a maximum value at a temperature of T_m, where $d^2N/dt^2 = 0$. From this condition and Eq (39) the relationship os T_m, β, and E_d is found to be,

$$\ln\left(\frac{T_m^{\,2}}{\beta}\right) = \frac{E_d}{RT_m} + \ln\left(\frac{E_d}{xRk\,C_m^{\,x-1}}\right) \tag{40}$$

where C_m is the concentration of trapped gas at T_m.

4.3.1. First and Second-Order Detrapping

In this study only first and second-order detrapping has been assumed. First order detrapping was observed by Erents[32]. For first-order detrapping, the analogs of Eqs (39) and (40) are,

$$-\frac{dC}{dt} = k C \exp(-E_d/RT) \tag{41}$$

and

$$\ln\left(\frac{T_m^{\,2}}{\beta}\right) = \frac{E_d}{RT_m} + \ln\left(\frac{E_d}{Rk}\right) \tag{42}$$

Eq (41) can be solved for the concentration as a function of time, C(t) giving

$$C(t) = C_0 \exp\left\{-k \int_0^t \exp(-E_d/RT)dt'\right\} \tag{43}$$

where C_0 is the initial concentration as defined in Eq (20), and t=0 is the start of the temperature ramp. With a known C_0 and assumed values of k and E_d for a particular temperature ramp, β, the concentration as a function of time, C(t) from Eq (43) is substituted in Eq (41) to give the release rate as a function of time.

In second-order detrapping Eq (39) becomes,

$$-\frac{dC}{dt} = k C^2 \exp(-E_d/RT) \tag{44}$$

The pre-exponential factor k has units of $sec^{-1}/(\mu g/g)$ or $sec^{-1}/(ppm\ atomic)$ depending on the units of concentration. Eq (44) can be solved as before for C(t) giving

$$C(t) = \left(\frac{1}{C_0} + k \int_0^t \exp(-E_d/RT)dt'\right)^{-1} \tag{45}$$

The release rate can be found by substituting C(t) into Eq (44). The form of Eq (40) for second-order detrapping is

$$\ln\left(\frac{T_m^{\,2}}{\beta}\right) = \frac{E_d}{RT_m} + \ln\left(\frac{E_d}{2Rk\,C_m}\right) \tag{46a}$$

From Eq (44), the concentration C_m at T_m is related to the maximum release rate R_{max} by

$$C_m = \left\{\frac{1}{k} R_{max} \exp(E_d/RT)\right\}^{1/2} \tag{46b}$$

4.3.2. Comparison of Solution with Results

As was shown in Sec. 3 the release rate curves exhibited multiple peaks, with sometimes up to four peaks present. The first peak present in many of these experiments was attributed to decomposition of uranium deuteride formed during the infusion process. This release of this deuteride was assumed to be governed by the decomposition of this species rather than detrapping; in those experiments where hydriding occurred the "deuteride" peak was removed before this analysis. In experiments where four peaks were observed, this removal of the first peak left three remaining peaks. As mentioned in Sec. 3.1 the fourth peak could actually be the tail of the third peak. With this additional assumption only two sites for trapping are present.

In this detrapping model there are only two adjustable parameters per peak; the pre-exponential factor of the detrapping rate constant, k, and the activation energy of detrapping, E_d. But, as was shown in Eq (43) for first-order detrapping, and Eqs. (46a,b) for second-order detrapping, these two parameters are related. This relation depends only on the temperature at the maximum of the release peak for first-order detrapping, and additionally, the release rate of this peak for second-order detrapping. Thus there is only one adjustable parameter per site, with two parameters (E_d and k) needed to characterize each site.

The temperature at the maximum of the release peaks, T_m, was obtained from the Gaussian fit analysis, with the initial concentration per site, C_0, being the areas under the individual peaks. The pre-exponential factor of the detrapping rate constant for each site was varied independently using a Monte Carlo method described previously. For each value of k so selected, a corresponding value of E_d was calculated from Eqs. (42), (46a), and (46b). After this initial fit, the values of T_m and C_0 of the peak were varied over a small interval to obtain a better fit. Thus the peak temperatures and areas vary slightly from the earlier Gaussian peak fit analysis. If necessary, the fit was re-optimized by again varying the rate constants for each site, but using the new T_m

and C_0 for each peak.

4.3.2.1. Fit for the Release of D_2 from Single Crystal UO_2

The single crystal outgassing experiments predominantly consisted of two peaks and required no removal of any peak owing to decomposition of uranium deuteride. An attempt was made to model the release curves with second-order detrapping from two sites but the fits obtained were unsatisfactory. A first-order detrapping from two independent sites was determined to give the best fit to the results. The fit for the release rate curve of Expt. 19 is shown in Fig. 31. The D_2 release in (ng/hr)/g UO_2 is shown for both the experimental and calculated release versus the temperature of the sample in degrees C. For this experiment values of 3.98 sec^{-1} for k, and 79 kJ/mol for E_d for the first site and 2.75 x 10^3 for k, and 208 kJ/mol for E_d for the second site were obtained.

This model was applied to all the D_2 release rate curves from single crystal UO_2. A summary of these results is shown in Table 5. Although it would have been desirable to have a single pre-exponential factor and activation energy for each site fit all experiments, this was not possible. Instead a best fit was obtained for each experiment independently.

For experiments 18 and 19, having similar infusion conditions, similar pre-exponential factors and activation energies were obtained.

For the second peak, which occurred at a temperature of 1410 to 1665 °C, for 6 of the 8 experiments in Table 5 a pre-exponential factor, k of $.4 \times 10^3$ to 84×10^3 sec^{-1} was obtained with a corresponding activation energy, E_d of 200 to 270 kJ/mol.

The behavior of the rate constants and activation energies for the first peak was more erratic. For 5 of the 8 experiments with first peak temperatures between 850 and 1110 °C the k's varied between .2 and 10 sec^{-1} and the E_d's between 58 and 108 kJ/Mol.

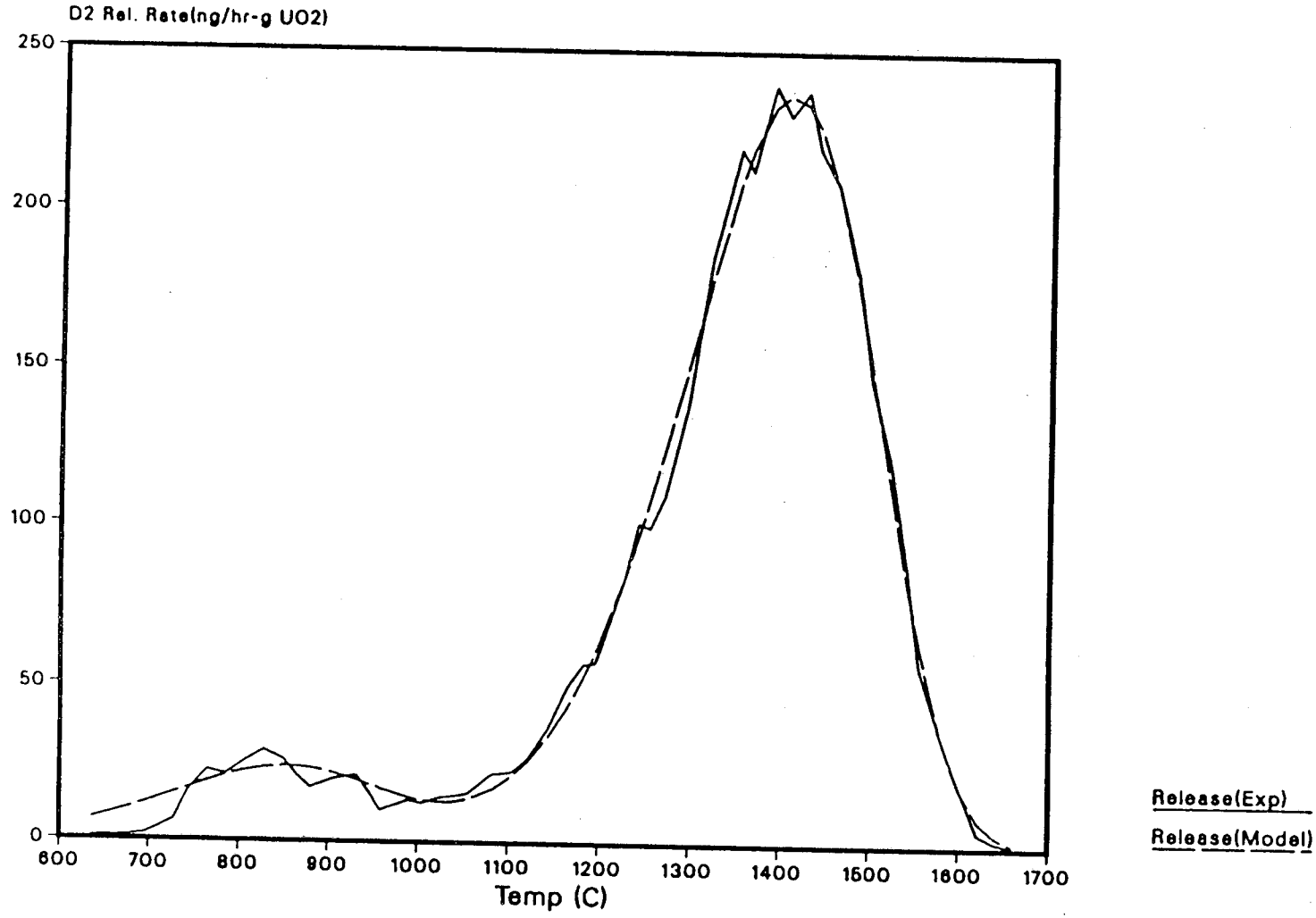

Fig. 31: Detrapping Model Best Fit to Expt. 19
1st Site: 1st-Order Detrapping; k= 3.98 sec-1, Ed= 79 kJ/Mol
2nd Site: 1st-Order Detrapping; k= 2.75 E+3 sec-1, Ed= 208 kJ/Mol

Table 5

SINGLE CRYSTAL UO_2 SUMMARY DETRAPPING MODEL FITTED PEAKS										
EXPT #	INFUSION T (C)	INFUSION P (atm)	PK TEMPS (C) 1	PK TEMPS (C) 2	D_2 DISSOLVED Per PK(ng/g) 1	D_2 DISSOLVED Per PK(ng/g) 2	DETRAP CONSTANTS* K(sec-1) 1	DETRAP CONSTANTS* K(sec-1) 2	DETRAP CONSTANTS* E_d(kJ/mol) 1	DETRAP CONSTANTS* E_d(kJ/mol) 2
18	1600	10	882	1544	17	211	0.25	438.	58	199
19	1600	10	850	1410	15	163	3.98	2.7E+3	79	208
20	1500	10	1239	1419	56	17	1.2E+3	2.2E+5	176	267
21	1400	10	1112	1497	23	10	3.23	1.6E+4	98	212
23	1300	10	1104	1420	0.5	9.2	9.5	8.4E+4	108	254
24	1600	5.42	984	1609	26	107	0.74	3.7E+4	74	272
26	1600	20	908	1665	20	219	1.7E+5	4.1E+3	181	247
27	1600	26.8	860	1602	67	263	535	0.71	122	115

* First-order detrapping

The temperature and pressure dependence of the total deuterium released from the second site was similar to that obtained earlier for the total release from both sites. Because of the erratic behavior of the first site, no temperature and pressure dependence could be determined for this site.

4.3.2.2. Fit for the Release of D_2 from Polycrystalline UO_2

For polycrystalline degassing experiments with infusion temperatures of 1400 °C or greater, the peak arising from decomposition of uranium deuteride was removed prior to analysis. When possible, the last two peaks were combined into one, giving a maximum of two sites for these experiments. No fit was attempted for experiments where it had been determined that the sample had not reached saturation.

The fit for a typical release rate curve (experiment 2) is shown in Fig. 32. The first peak was fitted with a first-order detrapping model, and the second peak with second-order detrapping. Other possibilities were examined but produced unsatisfactory fits. An examination of the first peak seems to suggest a linear pressure dependence, implying solution of hydrogen in molecular form. As no recombination is necessary in detrapping a dissolved molecule, a first-order process would result.

A fit for Expt 3, which was characterized by a large activation energy of detrapping of the first peak, is shown in Fig. 33. The large pre-exponential factor is necessary for this sharp peak. For experiments with infusion temperatures less than 1400 °C it was found that a one-site, second-order detrapping model was appropriate, as shown for Expt 11 in Fig. 34.

A summary of the fits achieved using this model for the other D_2 release rate curves from polycrystalline crystal UO_2 is shown in Table 6. All the experiments with infusion temperatures of 1400 °C or greater have a first peak with first-order detrapping and a second site with second-order detrapping. The first peak temperatures used with this model in all but two of the experiments, are between 750 and 890 °C. For

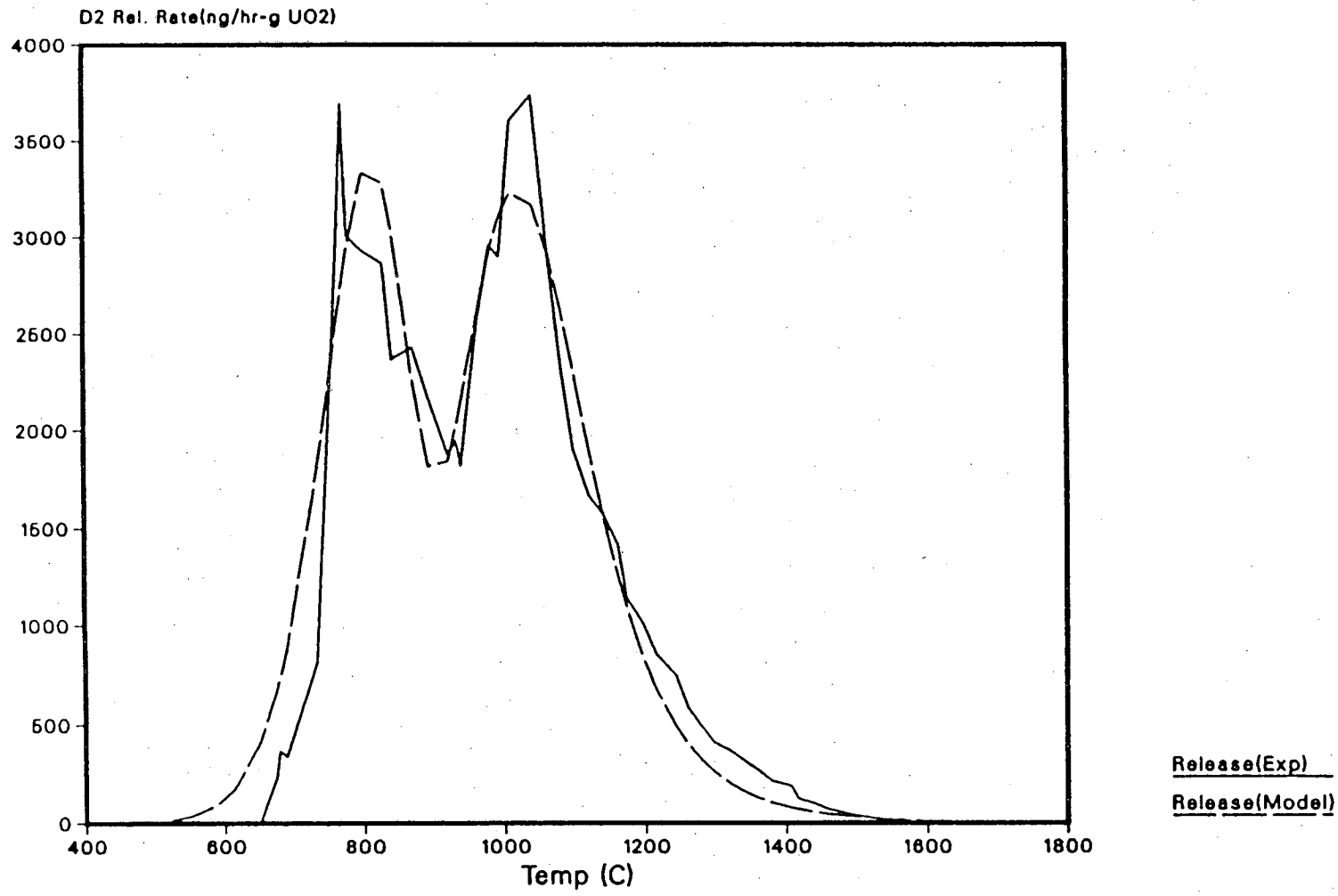

Fig. 32: Detrapping Model Best Fit to Expt. 2
1st Site: 1st-Order Detrapping; k= 6.0 E+4 sec-1, Ed= 156 kJ/Mol
2nd Site: 2nd-Order Detrapping; k= 89. sec-1/ng/g, Ed= 201 kJ/Mol

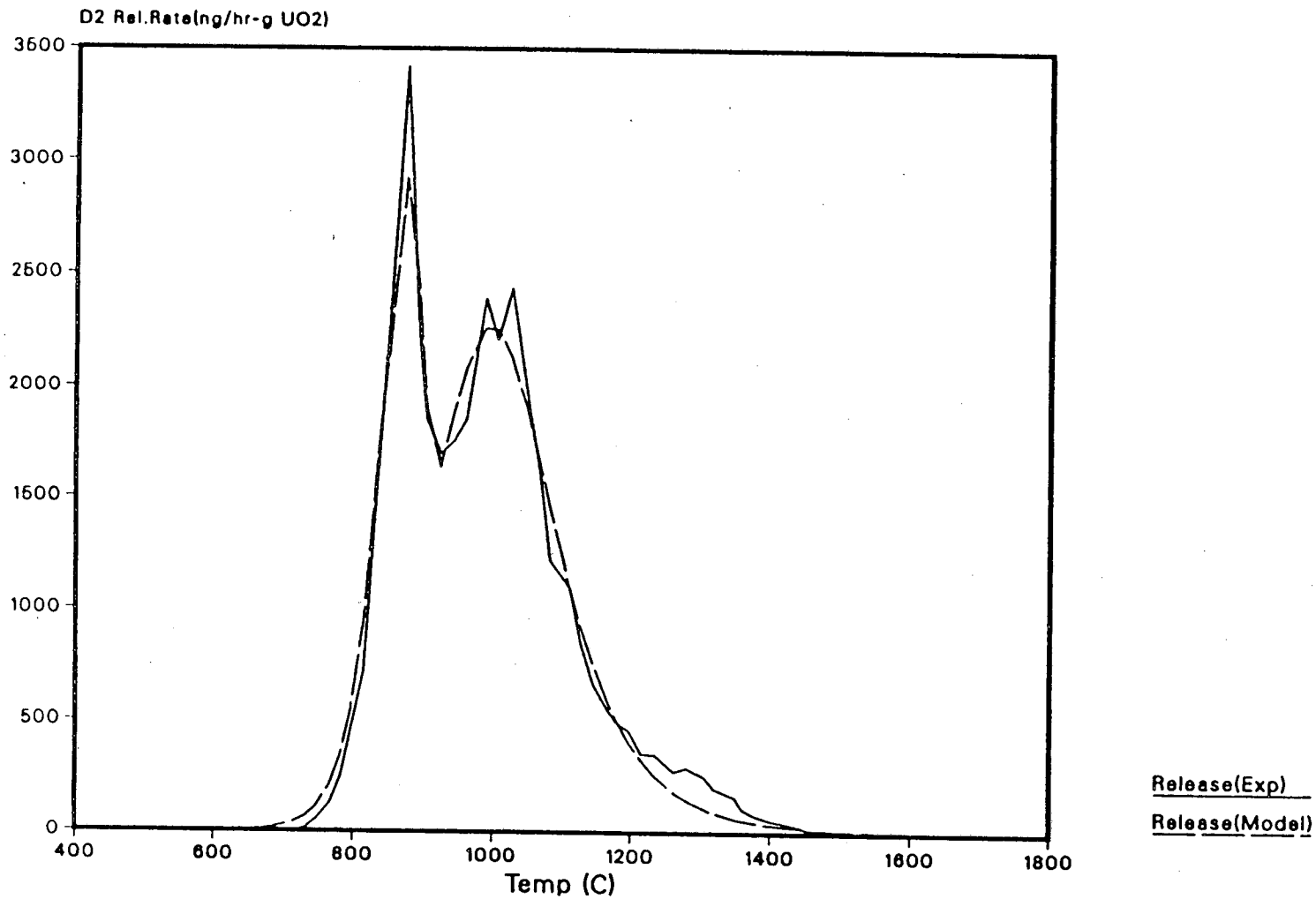

Fig. 33: Detrapping Model Best Fit to Expt. 3
1st Site: 1st-Order Detrapping; k= 1.0 E+15 sec-1, Ed= 381 kJ/Mol
2nd Site: 2nd-Order Detrapping; k= 212. sec-1/ng/g, Ed= 201 kJ/Mol

the first group of experiments with an infusion pressure of 10 atm of D_2 the range of temperature is even narrower. For the second peak the range of temperatures for all but two of the experiments is 890 to 1100 °C. For the first group of experiments, all save one exhibited peaks in a range of 930 to 1050 °C.

The pre-exponential factors, *k*, and energies of activation, E_d, are shown in Table 6. The second peak appears to be more consistent than the first peak. For the top two sections of the table all but one experiment have *k* values between 0.1 and 577 $sec^{-1}/(ng/g)$ and an E_d between 140 and 205 kJ/mol. For experiments with similar infusion temperatures and pressures there is an even greater similarity as evidenced in the detrap parameters for Expts 17 and 30, or 6 and 16, or even for the hypo-toichiometric urania specimens of Expts. 32 and 33. Unfortunately the first peak is less consistent, particularly for some of the experiments at infusion temperatures of 1600 °C. For some of these experiments the first peak at 800 to 900 °C was sharp requiring a combination of a large *k* and large E_d(i.e., the desorption rate constant).

To obtain a consistent set of parameters for the first peak an additional analysis was performed. If the product of *k* and $\exp(-E_d/RT)$ are plotted for 9 of the 11 of the experiments of the top two sections of Table 6(as in Fig. 35), the extreme variability of the individual parameters is removed. It is possible to obtain an "average" line representing the first-order detrapping from this site. The detrapping parameters for this "average" line are 6×10^7 sec^{-1} for *k*, and 220 kJ/mol for E_d.

The temperature dependence of the total deuterium released from each site as determined with this model was examined. An Arrhenius plot of the total D_2 released from the first site for 10 atm infusion pressure is shown in Fig. 36. A linear fit to these six points gives a heat of solution, ΔH_s of 101±35 kJ/mol. An Arrhenius plot for the total D_2 released from the second site is shown in Fig. 37. A linear fit to all nine of these points gives a resultant ΔH_s of 82±10 kJ/mol. The point representing the lowest infusion temperature (1000 °C) experiment was excluded in the fitting

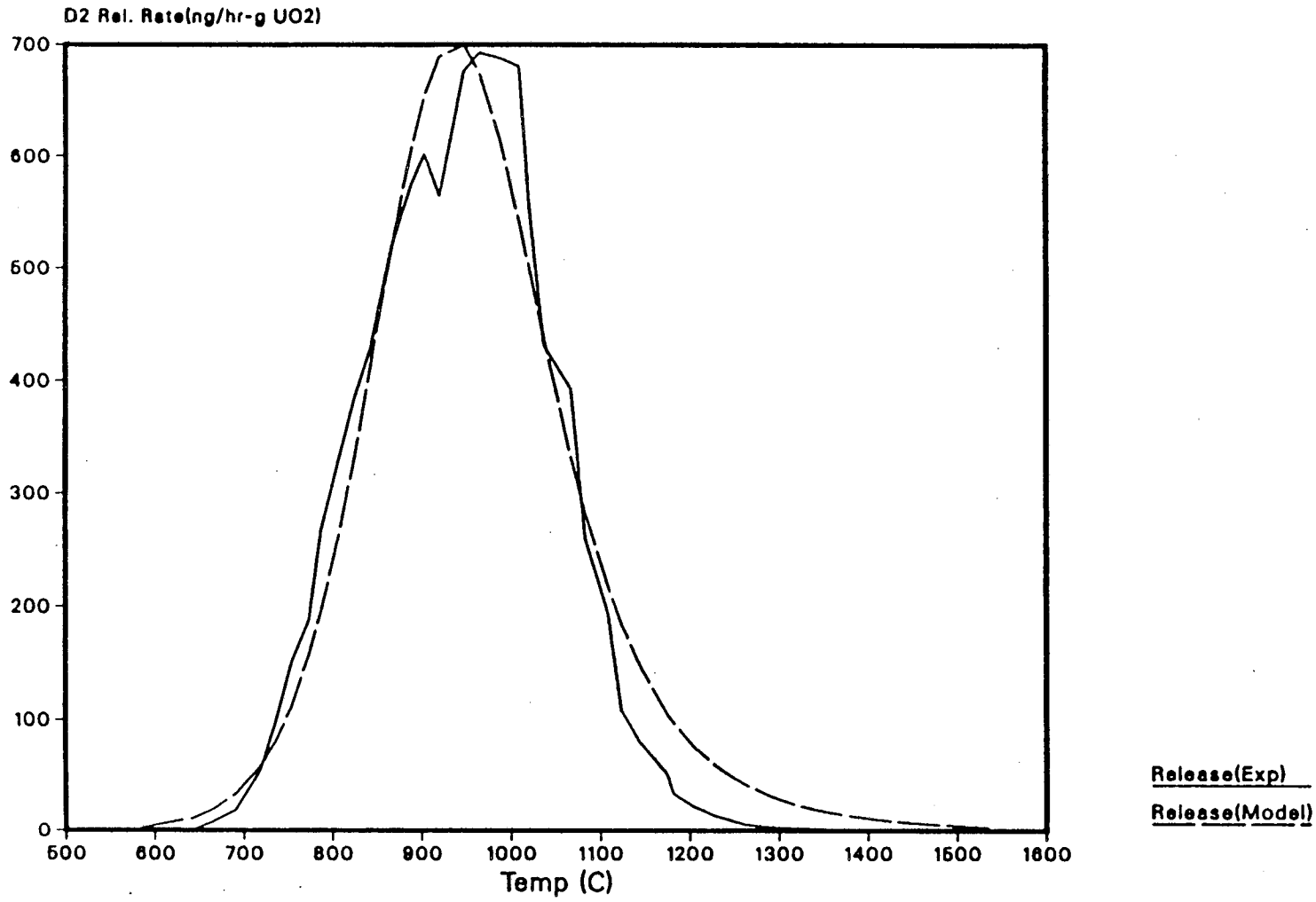

Fig. 34: Detrapping Model Best Fit to Expt. 11
2nd-Order Detrapping from one Site:
k= 43.5 sec-1/ng/g, Ed= 166 kJ/Mol

Table 6

POLYCRYSTALLINE UO_2 SUMMARY
DETRAPPING MODEL FITTED PEAKS

EXPT #	EXPT Specimen	INFUSION T (C)	INFUSION P (atm)	PK TEMPS (C) 1	PK TEMPS (C) 2	D_2 DISSOLVED Per Pk(ng/g) 1	D_2 DISSOLVED Per Pk(ng/g) 2	DETRAP CONSTANTS K(sec-1) 1*	DETRAP CONSTANTS K(sec-1/ng/g) 2*1	E_d(kJ/mol) 1	E_d(kJ/mol) 2
1	UO_2	1600	10	846	1051	522	1366	3.2E+5	9.1	176	178
2		1600	10	806	1019	1170	2113	6.0E+4	89.	155	201
3		1600	10	870	997	343	1387	1.0E+15	211.	381	201
4*2		1600	10	800	957	397	1545	1.1E+15	0.16	364	155
17		1400	10	792	949	195	713	1.3E+5	21.2	160	164
30		1400	10	891	1200	312	546	4.8E+4	3.3	166	177
6		1200	10		929		369		68.		167
16		1200	10		943		423		577		190
11		1000	10		940		468		43.5		167
12	UO_2	1600	5.4	794	986	278	1740	1.2E+17	0.31	377	138
28		1600	16.5	921	1152	2100	1349	37.1	27.0	105	204
13		1600	20	693	894	1277	7282	1.5E+17	5.60	360	166
29		1600	25	804	905	707	2774	8.3E+14	1.8E+3	357	213
14		1600	32	856	1072	1095	3502	4.1E+8	0.10	242	144
9*3,4	UO_2	1200	10		935		699		4.1		147
31*4		1600	10	878	1113	454	1000	62.9	0.21	105	143
15*5		1600	10	747	889	848	6186	1.0E+17	434	377	204
35*4	$UO_{2.065}$	1600	10	762	947	1098	322	555	6.1E+6	111	277
32	$UO_{1.976}$	1600	10	868	1090	3.38E4	7470	743	1.0E+4	126	275
33*6	$UO_{1.90}$	1600	10	853	971	5.11E4	1.72E4	3.8E+3	2.1E+6	138	316

* First-order detrapping
*1 Second-order detrapping
*2 Outgassed at 200 K/h instead of 400 K/h
*3 Infusion conditions. 1/2 hr at 1600, 1/2 hr at 1200
*4 Specimen cooled down in the crucible
*5 Specimen preheated to 1800 C for 3 hrs
*6 Powdering of specimen during infusion

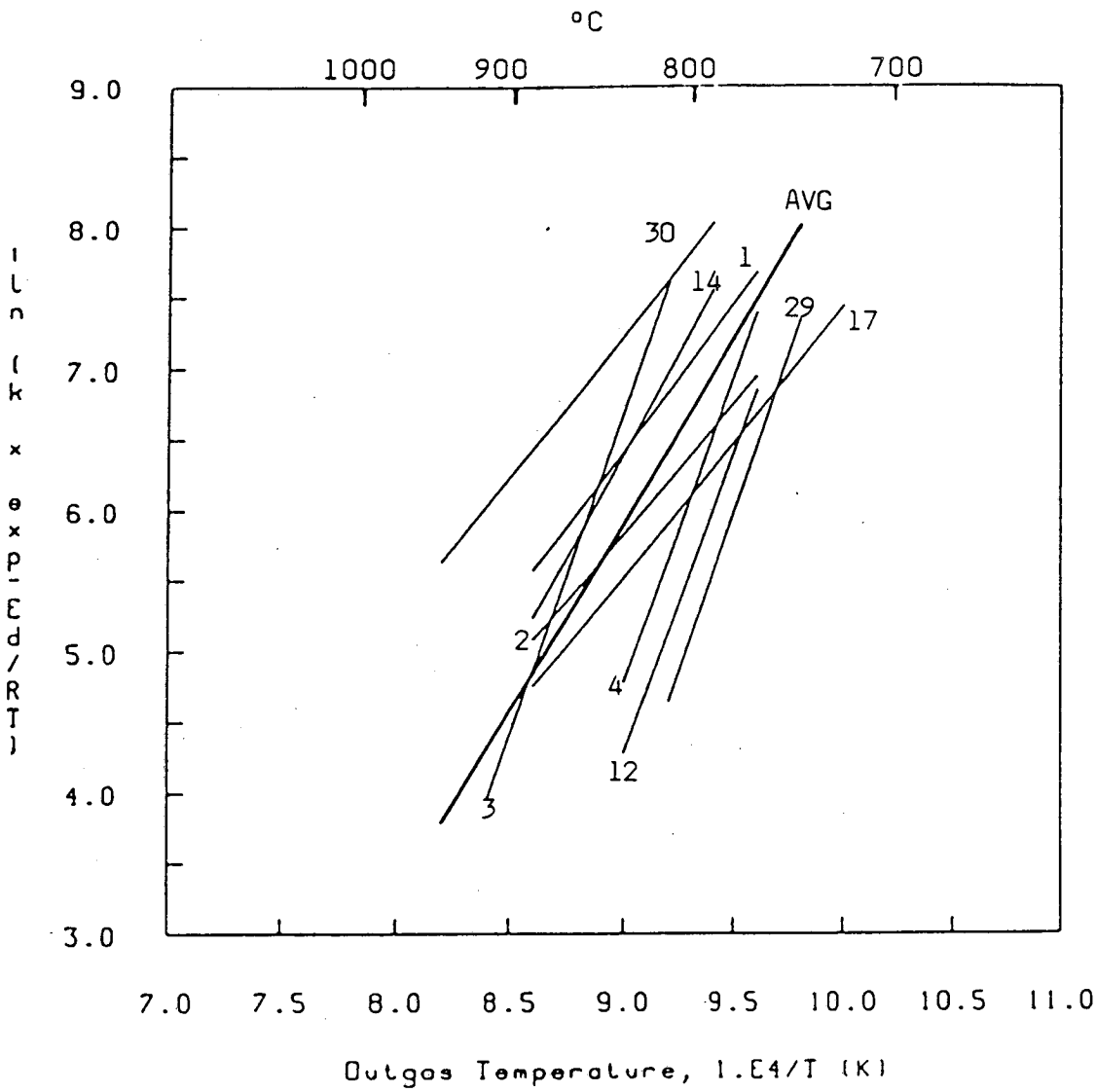

Fig. 35 Arrhenius Plot of the detrapping rate constant for the first site of the polycrystalline UO_2 samples (Expt. # is indicated)

procedure.

An analysis of the pressure dependence of the total D_2 released from each site did not give as good a fit as above, partially because of the uncertainty in the partitioning of the total release between the two sites for the high pressure infusion experiments. In Fig. 38 a plot of the log of the total D_2 released from the first site as a function of the log of the infusion pressure at 1600°C is shown. The nine points have been fit to a straight line giving a slope of ~ 0.8±.2. This slope is closer to 1.0 than to 0.5, implying molecular binding of hydrogen in this site. In Fig. 39 a similar plot of the log of the total D_2 released from the second site as a function of the log of the infusion pressure is shown. A linear fit to eight of these nine points (the point representing the 20 atm infusion pressure experiment was excluded) has a slope of ~ 0.42±.20. This slope of nearly ½ implies trapping of hydrogen in atomic form in this second site.

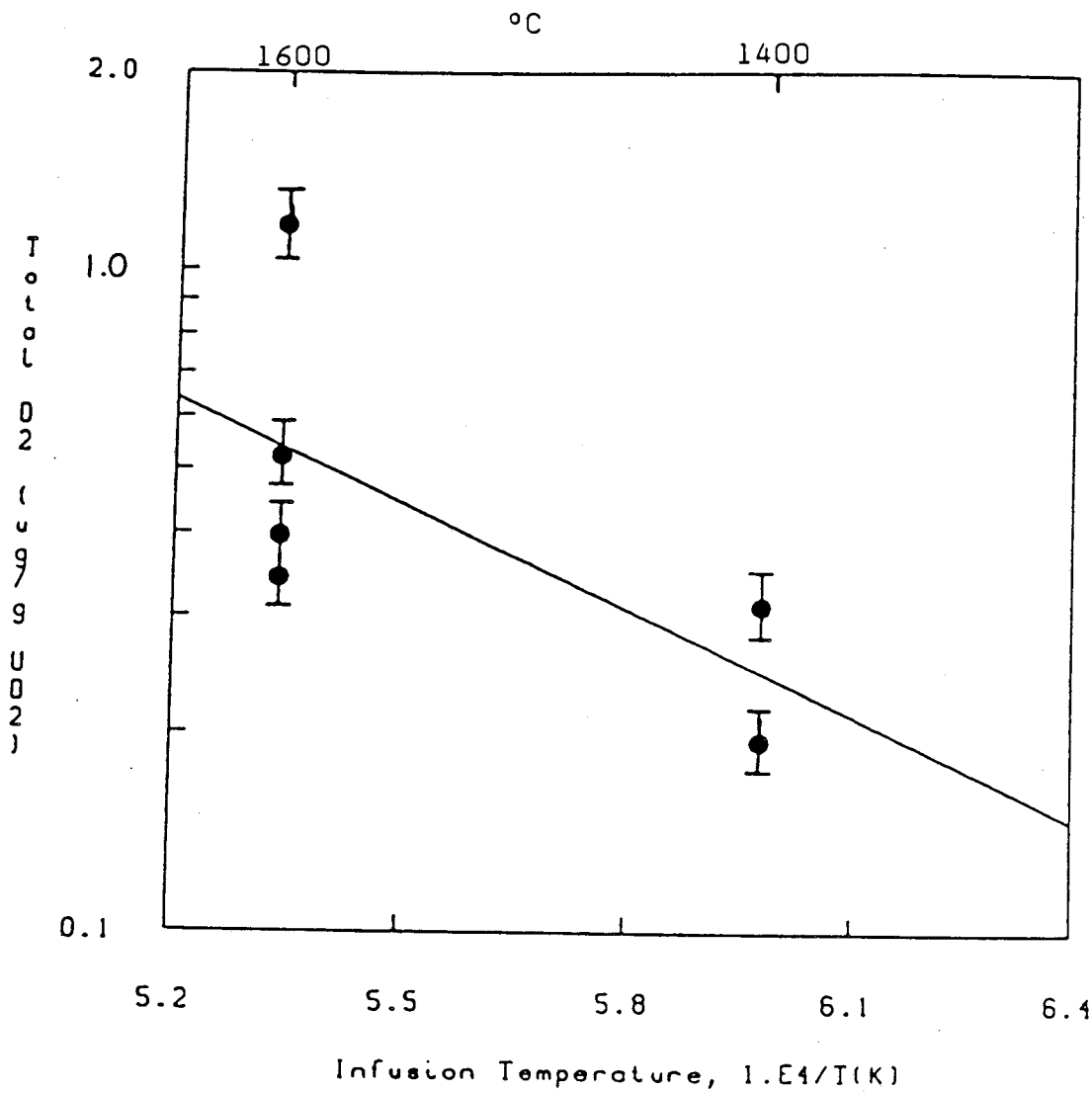

Fig. 36 Arrhenius plot of total D_2 release from first trapping site in polycrystalline UO_2 for a 10 atm D_2 infusion pressure; $\Delta Hs = +101$ kJ/Mol

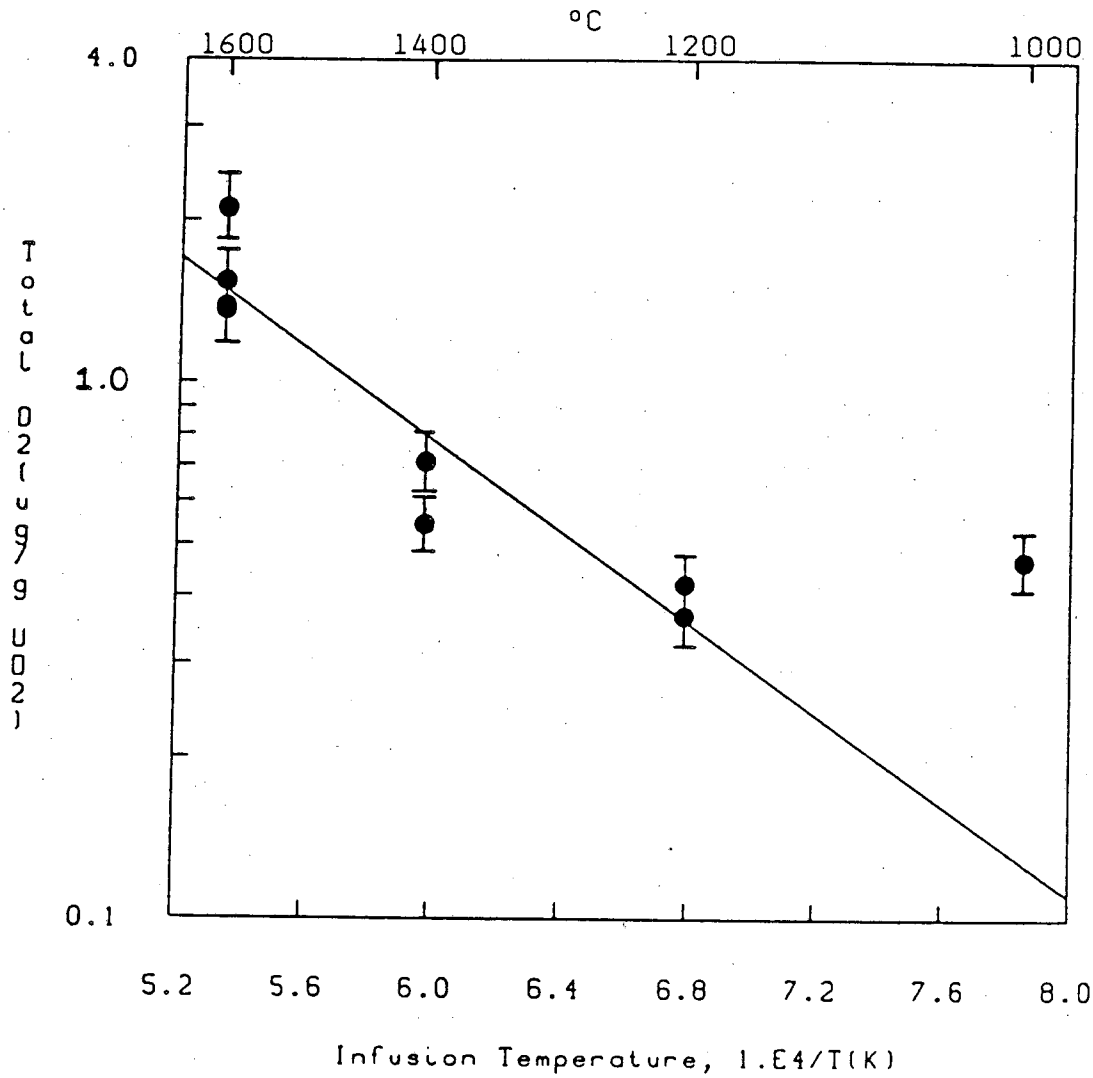

Fig. 37 Arrhenius plot of total D_2 release from second trapping site in polycrystalline UO_2 for a 10 atm D_2 infusion pressure; $\Delta Hs = +82$ kJ/Mol

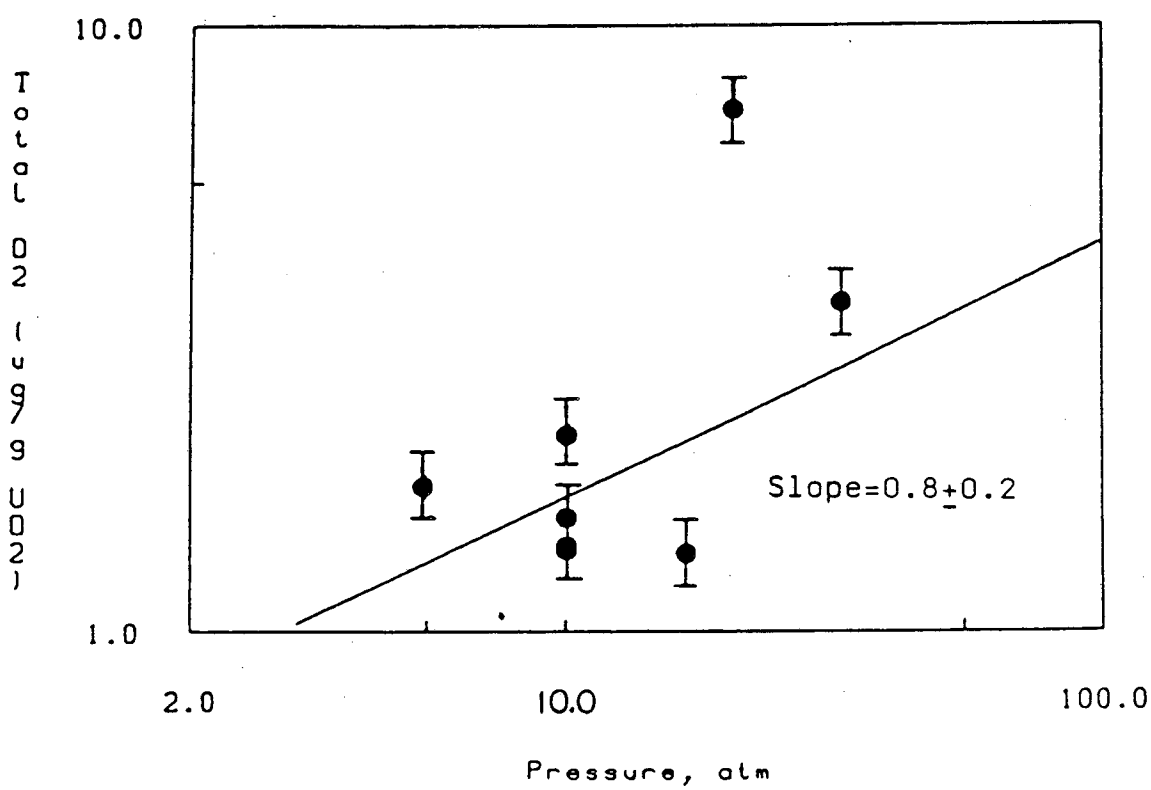

Fig. 38 Log of total D_2 release vs log of D_2 infusion pressure for first trapping site in polycrystalline UO_2 for an infusion temperature of 1600 °C.

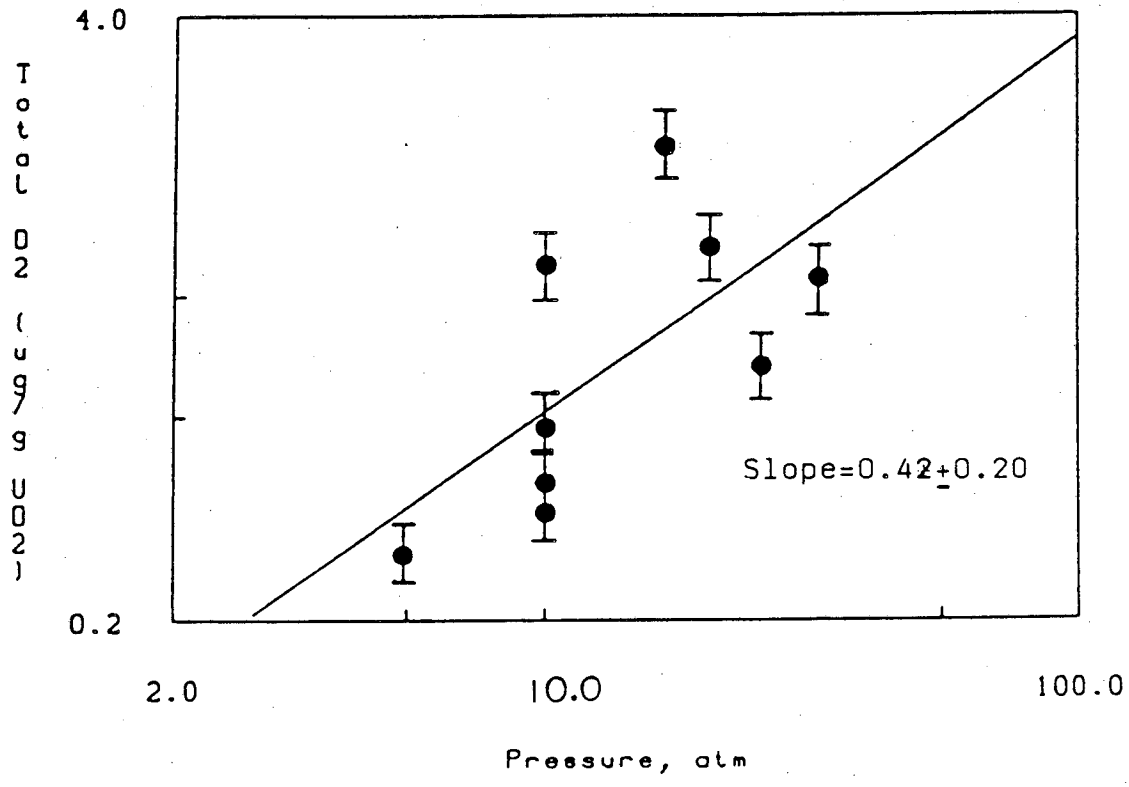

Fig. 39 Log of total D_2 release vs log of D_2 infusion pressure for second trapping site in polycrystalline UO_2 for an infusion temperature of 1600 °C

5. DISCUSSION OF TRAPPING

5.1. Trapping in Uranium Dioxide

The model discussed in Sec. 4.3 assumes that deuterium gas atoms are trapped at specific sites in the uranium dioxide solid. In single crystal UO_2 specimens there are few possible trapping sites. These trapping sites can be either dislocation lines or possible impurity atoms. A certain amount of thermally produced vacancies are also present and can serve as trapping sites in these specimens.

In polycrystalline UO_2 specimens many more possible trapping sites are present than in the single crystal specimens. For these sintered specimens, trapping sites such as grain boundaries are present as well as a greater amount of impurity atoms and dislocations than for the single crystal specimens. Additionally, these samples have a closed porosity of 7%, and these closed pores can act as possible trapping sites. If it is assumed that during infusion these pores act as gas bubbles containing D_2 at a pressure of $P_e + 2\gamma/R$ where P_e is the infusion pressure, γ, the surface tension, and R, the pore radius, a "solubility" can be calculated. Assuming an infusion pressure of 10 atm of D_2, a γ of 0.6 Pa-m[30] for UO_2, and from Fig. 3 an average pore radius of 2 μm, the above relation gives a pressure of 1613 kPa. Assuming ideal gas behavior, for a UO_2 sample of 7% closed porosity at 1600 deg °C, the deuterium solubility is determined to be 2.64 μg/g. For the hypostoichiometric specimens, the many vacancies present act as additional trapping sites.

5.2. Trapping of Hydrogen in Metals and other Refractory Materials

As mentioned in Sec. 4.3 trapping of hydrogen was observed in stainless steel by Hirabayashi[31] and in nickel by Erents[32]. In the former study the main emphasis was on the surface trapping of tritium on stainless steel, but detrapping of "residual hydrogen" that had diffused into the bulk was observed. This tritium originating from the bulk was evolved at 750 and 970 K and was assumed to be held in the microstructure

of the steel. Otsubo[33] also observed evolution of hydrogen from traps in steel at similar temperatures, with additional trapping in the ferrite grain-boundary, micro-voids, and other micro-structure of the steel. Wilson and Baskes[34] also observed trapping of hydrogen as deuterium in stainless steel, although detrapping occurred at only 330 K.

In addition to trapping of deuterium in nickel, Erents[35] has also observed trapping of deuterium in tungsten and molybdenum. He also observed that desorption from these traps was the rate-controlling step in release of deuterium from the solid. In the release of deuterium from tungsten, vacancies were assumed to act as traps giving a temperature peak at 850 K. These vacancies had been produced by deuterium bombardment. The release of deuterium from molybdenum was observed at lower temperatures than from tungsten.

A series of papers by Brice and Doyle[36,37,38] have dealt with hydrogen trapping in refractory materials including ones suitable to act as fusion reactor components. Additionally a model was developed to explain this retention. In silicon, this model suggests that the hydrogen traps are multiple-vacancy complexes. In stainless steel the hydrogen traps were also assumed to be multiple-vacancy complexes. Holland and Merrill[39] also observed trapping of hydrogen as tritium in fusion reactor materials. They assumed that the trapping sites resulted from dislocations and impurities in the materials.

Buters and Van den Beukel[40] have studied trapping of helium in various materials, as well as helium desorption from molybdenum. They showed that dislocations and point defects such as vacancies could act as traps in the bulk lattice. They determined that during outgassing, the trapped helium is released at temperatures characteristic of the binding state of the trap.

5.3. Trapping in This Experiment

From the above observations it is possible to attempt to identify the trapping sites

found in this experiment. For the polycrystalline UO_2 specimens two trapping sites were shown in Sec. 4.3.2.2. The first site that was only present in experiments with infusion temperatures of 1400 °C or greater may be vacancies that are produced at those temperatures. As was shown in Sec. 3.3.2 only in these experiments was the UO_2 reduced to hypostoichiometric urania, precipitating uranium metal that reacted with the D_2 gas to form UD_3. In the two experiments using initially hypostoichiometric urania samples the solubility was observed to be up to 3 orders of magnitude greater than for the stoichiometric samples. For Expt. 32 where the oxygen-to-uranium ratio was 1.976 it is possible to calculate the fraction of anion vacancies occupied if it is assumed that the deuterium which is detrapped from the first site is coming entirely from vacancies. If every vacancy was to contain one deuterium atom, a stoichiometry of 1.976 would give a total D solubility of 24,000 ppm. For Expt. 32 the total D_2 observed to be detrapped from the first site was 33.8 μg/g or 4560 ppm implying that 19% of the vacancies is occupied with deuterium. Additionally, the temperature at which this site was detrapped, (i.e. 750 to 890 °C) is similar to that observed above for detrapping of hydrogen from vacancies in stainless steel. (i.e. ~ 600 °C) The second trapping site could be owing to any of the microstructural defects present in the polycrystalline solid; the grain boundaries, the closed pores, or impurity atoms in the solid. Assuming that the second trapping site is the closed pores, the observed 1 to 2 μg/g of D_2 released from these sites is comparable to the 2.64 μg/g solubility in these pores calculated in Sec. 5.1 for the same infusion conditions.

The identity of the trapping sites in the single crystal specimens is more difficult to determine. The first trapping site could also possibly be owing to vacancies, but its detrapping rate constants and even its order of detrapping is different from the first polycrystalline trapping site. The second trapping site in the single crystal specimens differs considerably from the polycrystalline specimens, being more strongly bound, with release temperatures in the 1400 to 1650 °C range, rather than the 900 to 1100 °C

observed in the latter specimens. As their are less trapping sites available in the single crystal specimens, the identity of this site is unclear. In addition, the very different fabrication histories of the single crystal and polycrystalline UO_2 specimens could explain the considerable difference in the nature of the trapping sites.

6. CONCLUSIONS

6.1. Thermodynamic Solubility of Hydrogen in UO_2

The solubility of hydrogen in the lattice of single crystal and in polycrystalline UO_2 was determined. The dissolution of hydrogen in both single crystal and polycrystalline UO_2 was found to be a two step process, implying that hydrogen is present in atomic form in UO_2, corresponding to Sievert's law. The heat of solution of hydrogen in both single crystal and polycrystalline UO_2 was found to be positive, which shows that solution is endothermic with respect to the hydrogen molecule.

The Sievert's law constant of D in single crystal UO_2 was determined to be:

$$S = 3.0\text{x}10^7 \exp\left(\frac{-235\ \text{kJ}}{\text{RT}}\right) \frac{\text{ppm atomic}}{\sqrt{\text{atm}}}$$

and for D in polycrystalline UO_2 was determined to be:

$$S = 5.5\text{x}10^4 \exp\left(\frac{-100\ \text{kJ}}{\text{RT}}\right) \frac{\text{ppm atomic}}{\sqrt{\text{atm}}}$$

6.2. Chemical Nature and Location of Hydrogen in UO_2

The solubility of hydrogen in polycrystalline UO_2 was found to be ~ 10 times that of hydrogen in single crystal UO_2, implying that 90% of the dissolved hydrogen in polycrystalline UO_2 is present in the grain boundaries and other microstructural defects not present in single crystal UO_2.

The hydrogen solubility in hypostoichiometric urania was found to be up to 3 orders of magnitude greater than in stoichiometric UO_2, depending on the oxygen-to-uranium ratio of the specimen. This difference was due partially to formation of UD_3 during quenching of the infused sample, but was also because of the increased number of extrinsic anion vacancies present in the hypostoichiometric urania. This implies that the primary solution site of hydrogen in the UO_2 lattice is the anion vacancy. In

hyperstoichiometric urania the added oxygen had no appreciable effect on the observed hydrogen solubility.

6.3. Release Kinetics of Hydrogen from UO_2

It was found that the released deuterium was observed to be in the molecular state rather than combined with oxygen as D_2O.

The release rate curves for the single-crystal and polycrystalline UO_2 specimens exhibited multiple peaks. These multiple peaks were inconsistent with release governed by diffusion or by diffusion with trapping and resolution. Attempts to fit the peaks individually with a diffusion model produced abnormal diffusivity parameters suggesting the unsuitability of diffusion to describe the release kinetics.

It was determined that the release kinetics of hydrogen from UO_2 is governed by thermally-activated release from traps or specific binding sites in both the polycrystalline and single-crystal UO_2 specimens. A maximum of two trapping sites were observed for each type of UO_2.

For single-crystal UO_2 first-order detrapping from both sites was observed. The first site with a peak release occurring at temperatures of 850 to 1100 °C was fit with a pre-exponential factor, k, of 0.2 to 10 sec^{-1}, and a corresponding activation energy, E_d of 58 to 108 kJ/Mol. The second site with a peak release occurring at temperatures of 1410 to 1665 °C was fit with a k of 0.4×10^3 to 84×10^3 sec^{-1}, and a corresponding E_d of 200 to 270 kJ/Mol.

For polycrystalline UO_2 first-order detrapping was observed for the first site, but second-order detrapping was observed for the second. The first site with a peak release occurring at temperatures of 800 to 900 °C was fit with one average k of 6×10^7 sec^{-1}, and a corresponding E_d of 220 kJ/Mol. The second site with a peak release occurring at temperatures of 890 to 1100 °C was fit with a second-order k of 0.1 to 577 $sec^{-1}/(ng/g)$ and a corresponding E_d of 140 to 205 kJ/Mol.

APPENDIX A

Estimate of D_2 loss during Quenching

It was assumed in Sec. 3.4 that the D_2 loss during quenching was insignificant. Since hydrogen solution in UO_2 is endothermic, specimens saturated at high temperature have a thermodynamic tendency to reject hydrogen as the temperature drops. Using the temperature behavior of the sample during a quench determined in Sec. 2.2.3, the fraction of initial saturated D_2 retained in the quench can be estimated by two models. The first model assumes that D_2 release is controlled by bulk diffusion, with the diffusivity of hydrogen in UO_2 determined by Wheeler[2]. In the second model, the rate of release is assumed to be controlled by detrapping from traps in the solid with rates that were determined in Sec. 4.3.

A.1 Release Via Simple Diffusion

The diffusion equation for mobile deuterium atoms in a sphere was given in Eq (19) in Sec. 4.1. In this equation the diffusivity, D, is given as a function of T, the temperature of the solid at a particular position and time. The dependence of temperature on r and t during the quench converts D into a function of r and t during the quench. The initial condition of Eq (20) and boundary condition of Eq (21b) still hold for this analysis but the surface boundary condition is now given by:

$$c(a,t) = C_{Sat}(T_s) \tag{A-1}$$

The time dependence of the surface temperature, T_s, converts $C_{Sat}(T_s)$, the saturation concentration at the surface, to a known function of t, via the usual temperature dependence of the Sievert's law constant. The temperature dependence of the Sievert's law constant for single crystal and polycrystalline UO_2 was given in Sec. 3.4.1 and 3.4.2 respectively. The values of the radius, a, for the single crystal and polycrystalline specimens used in this calculation are 0.4 and 0.45 cm respectively. These values are

½ the average equivalent sphere diameters shown previously in Sec. 2.1. Eqs. (19-21) with the new boundary condition (A-1) were solved numerically giving the concentration, c, as a function of the position, r and time, t. This concentration distribution was then integrated over the sphere and then divided by the initial saturation concentration to give the fraction of the initial infused D_2 retained as a function of time. The results of this analysis for both the polycrystalline and single crystal samples that have been quenched from 1600 °C at 10 atm of D_2 are shown in Figs. A-1 and A-2 respectively. A resultant loss of about 20% for the polycrystalline sample and 25% for the single crystal sample is determined using this model of release via simple diffusion.

A.2 Release via Detrapping

This model assumes that release of D_2 during the quench is governed by detrapping from the two sites present in the solid. The rate of release from the sites of type it in a unit volume at radius r at time t is given by:

$$\frac{dc_i}{dt} = -k_i\, c_i^{\,x} \exp\left(-\frac{E_{di}}{RT(r,t)}\right) \tag{A-2}$$

where c_i is the concentration on the site i at the radius, r, and k_i, x, and E_{di} are the pre-exponential factor of the detrapping rate constant, the reaction order and the detrapping activation energy for site i. To find the total deuterium lost from the unit volume at the radius r it is necessary to integrate Eq (A-2)

$$\int_{c_{i_f}}^{c_{i_0}} \frac{dc_i}{c_i^{\,x}} = k_i \int_0^{\infty} \exp\left(\frac{-E_{di}}{RT(r,t)}\right) dt \tag{A-3}$$

where c_{i_0} is the radially uniform concentration of deuterium on site i at saturation, and c_{i_f} is the radially dependent final deuterium concentration on site i. This calculation gives the fraction retained, $\frac{c_{i_f}}{c_{i_0}}$, as a function of r, which is then integrated over the sphere to give the total retained on a particular site.

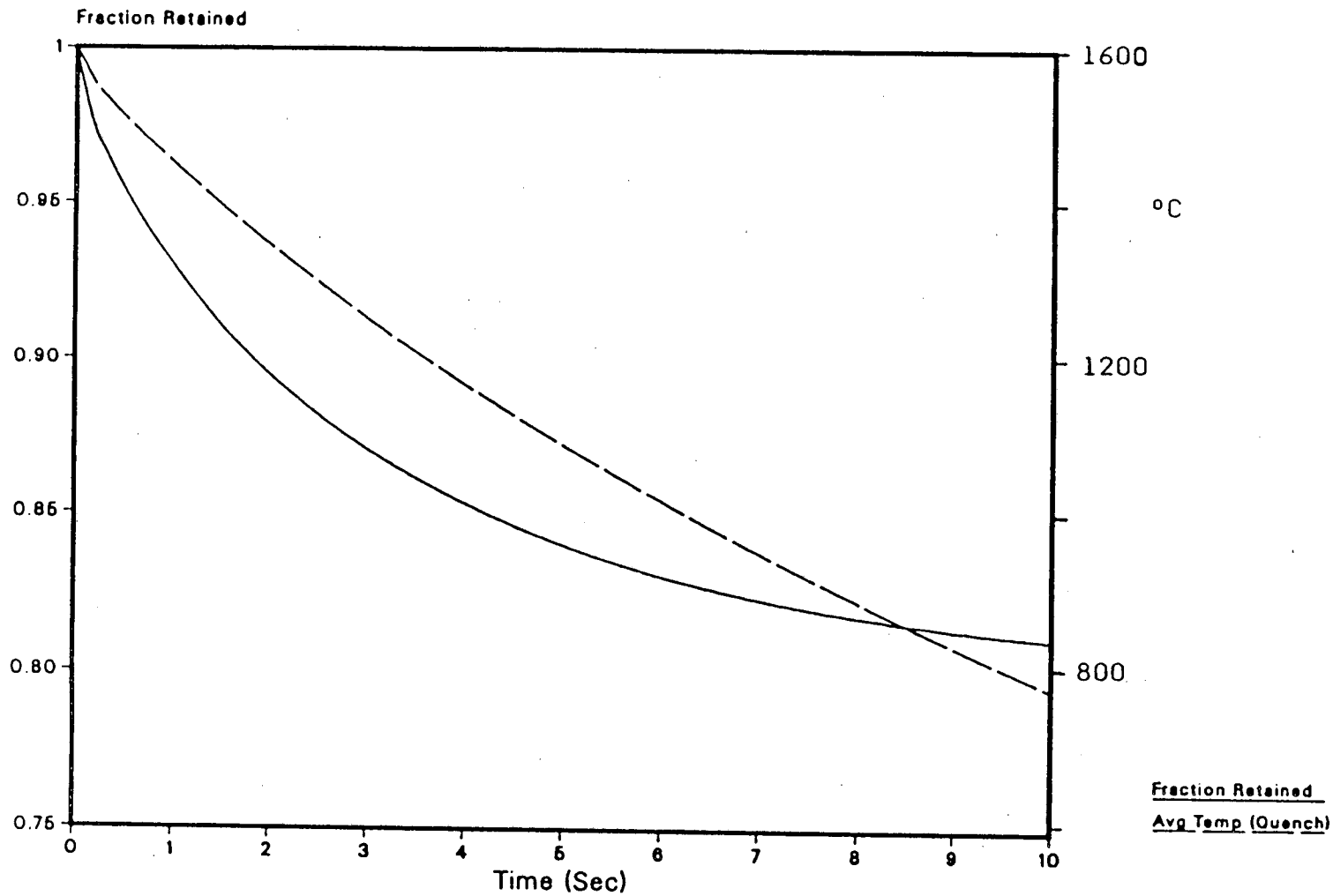

Fig. A-1: Fraction of Total Infused D2 Retained After Quench of Polycrystalline UO2 Assuming Loss by Diffusion
Total Retained= 81%

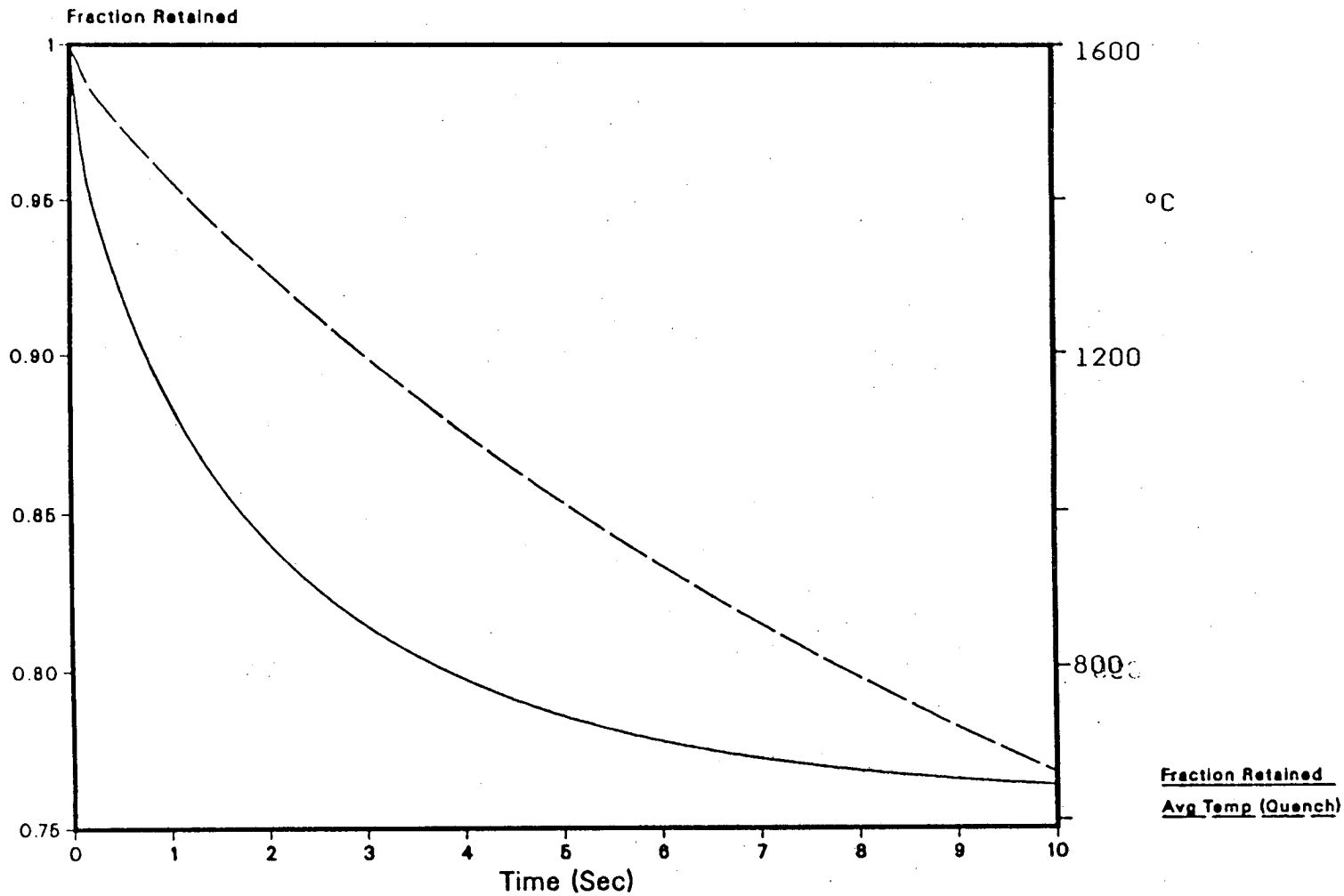

Fig. A-2: Fraction of Total Infused D2 Retained After Quench
of Single Crystal UO2 Assuming Loss by Diffusion
Total Retained= 76%

The above analysis was applied to the polycrystalline and single crystal results from Sec. 4.3. For the polycrystalline samples, a first order detrapping with a k of $6x10^7$ sec^{-1} and E_d of 220 kJ/mol was used for the first site. The second site was characterized by second order detrapping with a k of 100 sec^{-1}/ng/g, and E_d of 200 kJ/mol was used in the analysis. For the first polycrystalline site the above analysis predicts that none of the initial D_2 is retained in the quench, while for the second site, 100% retention is predicted. For the single crystal UO_2 samples only the second peak was examined with this model, as the first peak was too small and erratic to study. A first order detrapping with a k of $5x10^3$ sec^{-1} and E_d of 210 kJ/mol was used. Nearly 100% retention of D_2 in the quench is predicted.

A.3 Uniform Release Model

The preceding two models represent opposite limiting cases. In the second, it was assumed that release of D_2 was determined by detrapping from traps in the solid, and that diffusion was assumed to be infinitely rapid. But the above analysis shows that under these conditions the first site would be completely depleted, which is contrary to experiment. Most likely both processes are occurring. As suggested by Erents[32] the release of deuterium from traps is a two stage process with first a detrapping from a trapping site, and then diffusion of deuterium out of the lattice. For the second site in the polycrystalline and single crystal sample this would imply that since the detrapping did not occur during the quench, diffusion kinetics are moot. For the first site in the polycrystalline sample, release during quenching is probably governed by diffusion, since detrapping appears to be rapid. At the much lower temperatures of the release experiment, however, the more highly-activated detrapping kinetics controls the release rate. However, as much as 20% of the saturation concentration could have been lost during the quench.

There is experimental evidence that even the 20% loss is too high. In Expt 31

the sample was allowed to cool in place with a slower cooling rate compared with the normal procedure. (i.e. requiring 18 s to cool to 1000 °C vs 6 s. in the drop quench) If bulk diffusion was rate-controlling the above model predicts that the first site should be completely depleted. However Table 6 shows that this is not correct; the amount retained in this peak is only slightly less than in the experiments with the same infusion conditions and a normal quench. This observation suggests that for a normal quench the amount lost in the first peak will even be less than the 20% predicted by diffusion, using Wheeler's[2] diffusivity, where extrapolation to temperatures as high as 1600 °C overpredicts hydrogen mobility in UO_2.

APPENDIX B

Experimental Release Rate Curves

The experimental release rate curves for the experiments summarized in Tables 3 and 4 are shown in Figs. B-1 to B-31. In these figures, the release rate in ng/hr-g UO_2(in Figs. B-22,23 the release rate is given in μg/hr-g UO_2), and temperature of the outgas in deg °C are given as a function of the time in hours. The figures are numbered in the order in which they appear in the tables, with the polycrystalline UO_2 experiments summarized in Table 4 first, followed by the single crystal UO_2 experiments summarized in Table 3. The release rate curve for experiment 34, the dissolution of UD_3, not shown here, was shown previously in Fig. 8.

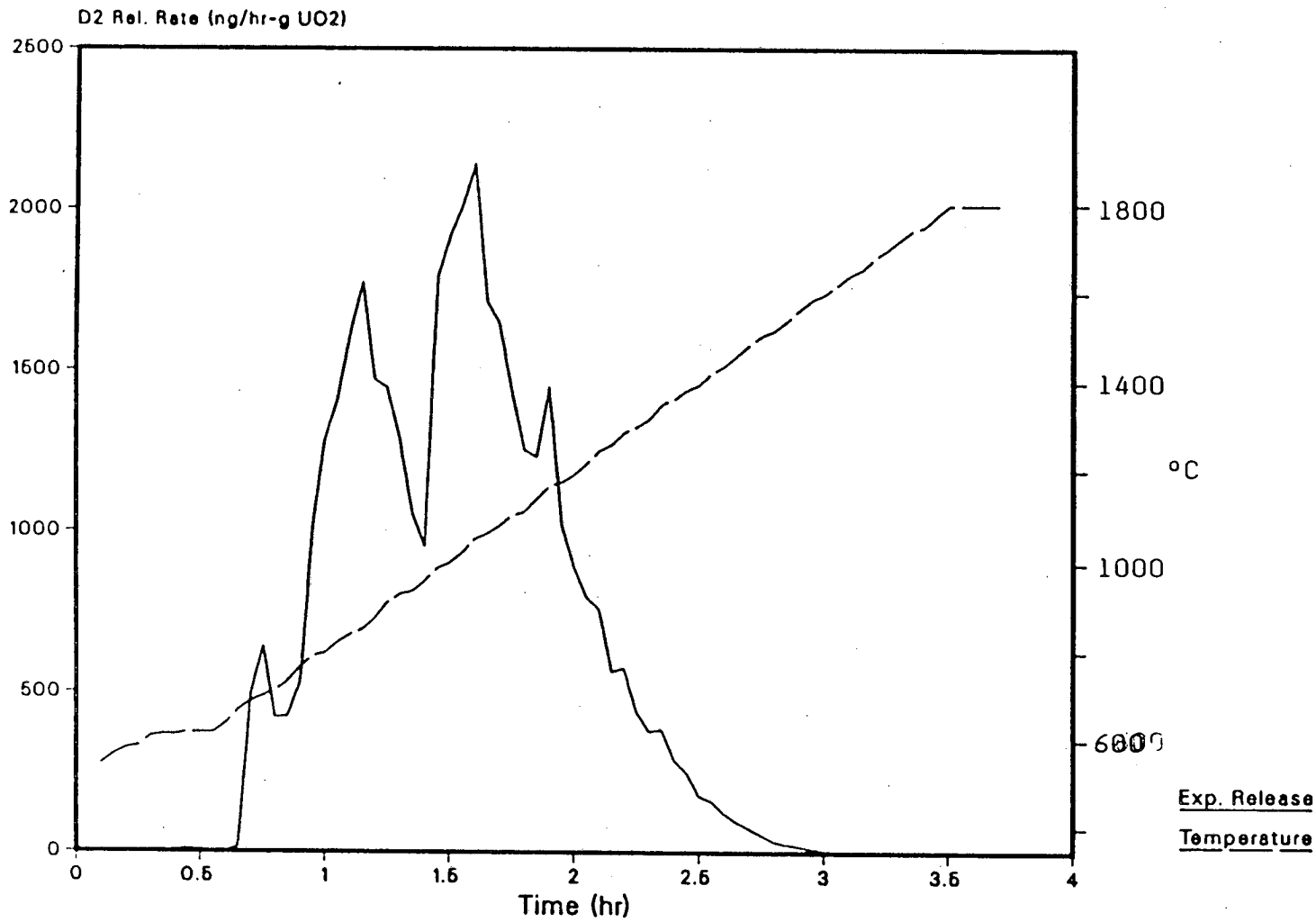

Fig. B-1 EXPT 1 Polycrystalline UO2
Infusion Conditions:
t= 1 hr T= 1600 C P= 10 atm D2

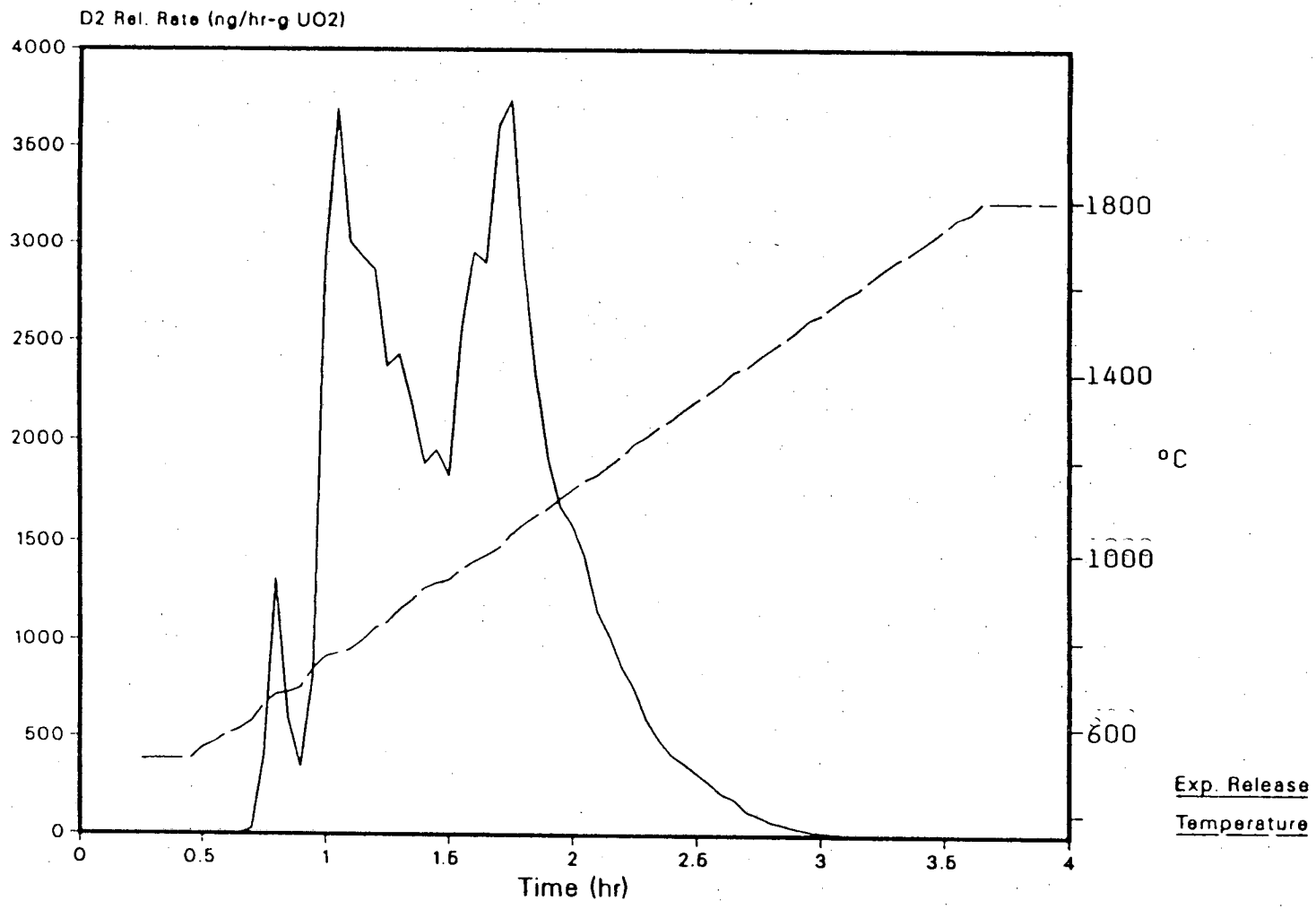

Fig. B-2 EXPT 2 Polycrystalline UO2
Infusion Conditions:
t= 1 hr T= 1600 C P= 10 atm D2

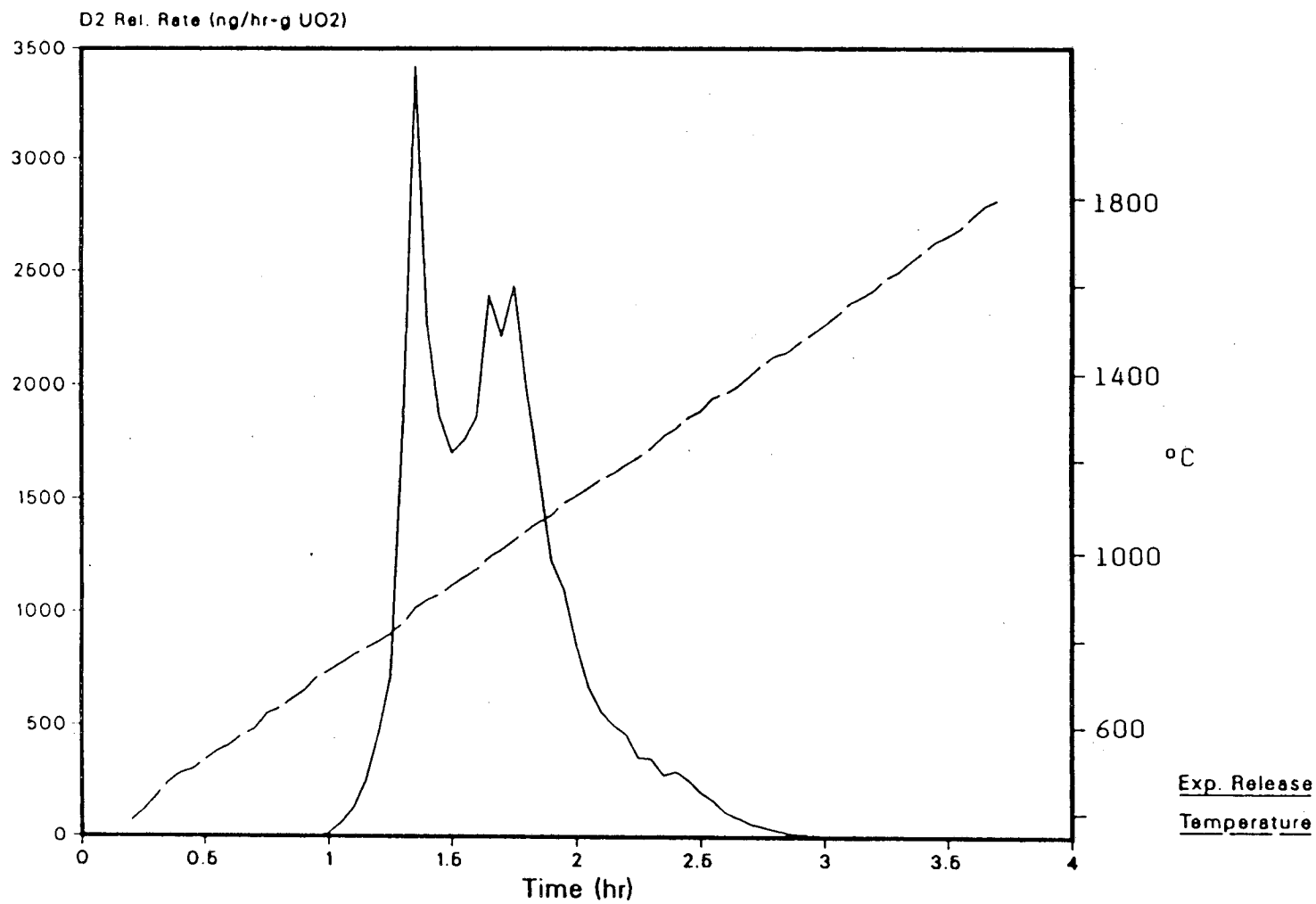

Fig. B-3 EXPT 3 Polycrystalline UO2
Infusion Conditions:
T= 2 hr T= 1600 C P= 10 atm D2

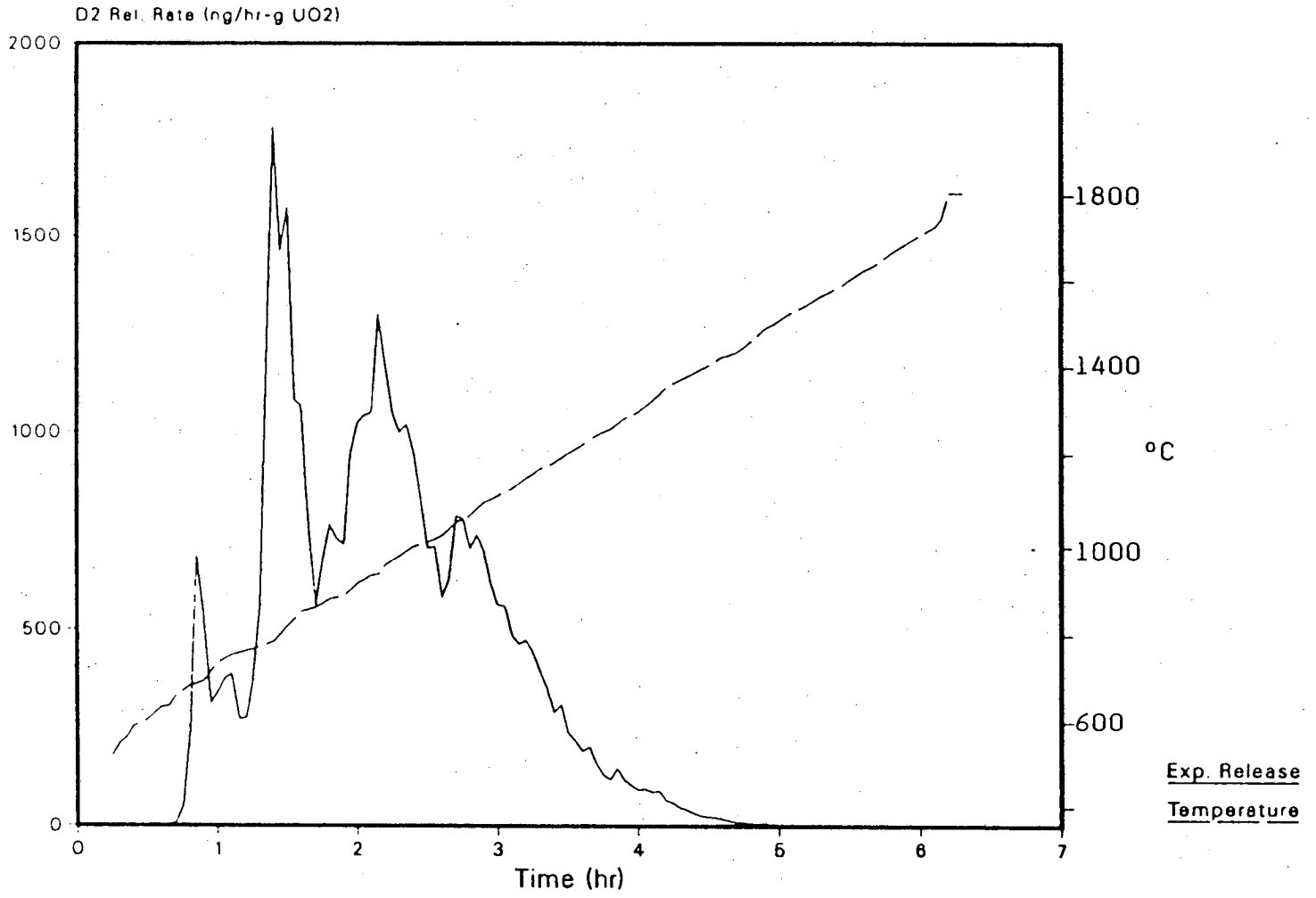

Fig. B-4 EXPT 4 Polycrystalline UO2
Infusion Conditions:
T= 1 hr T= 1600 C P= 10 atm D2

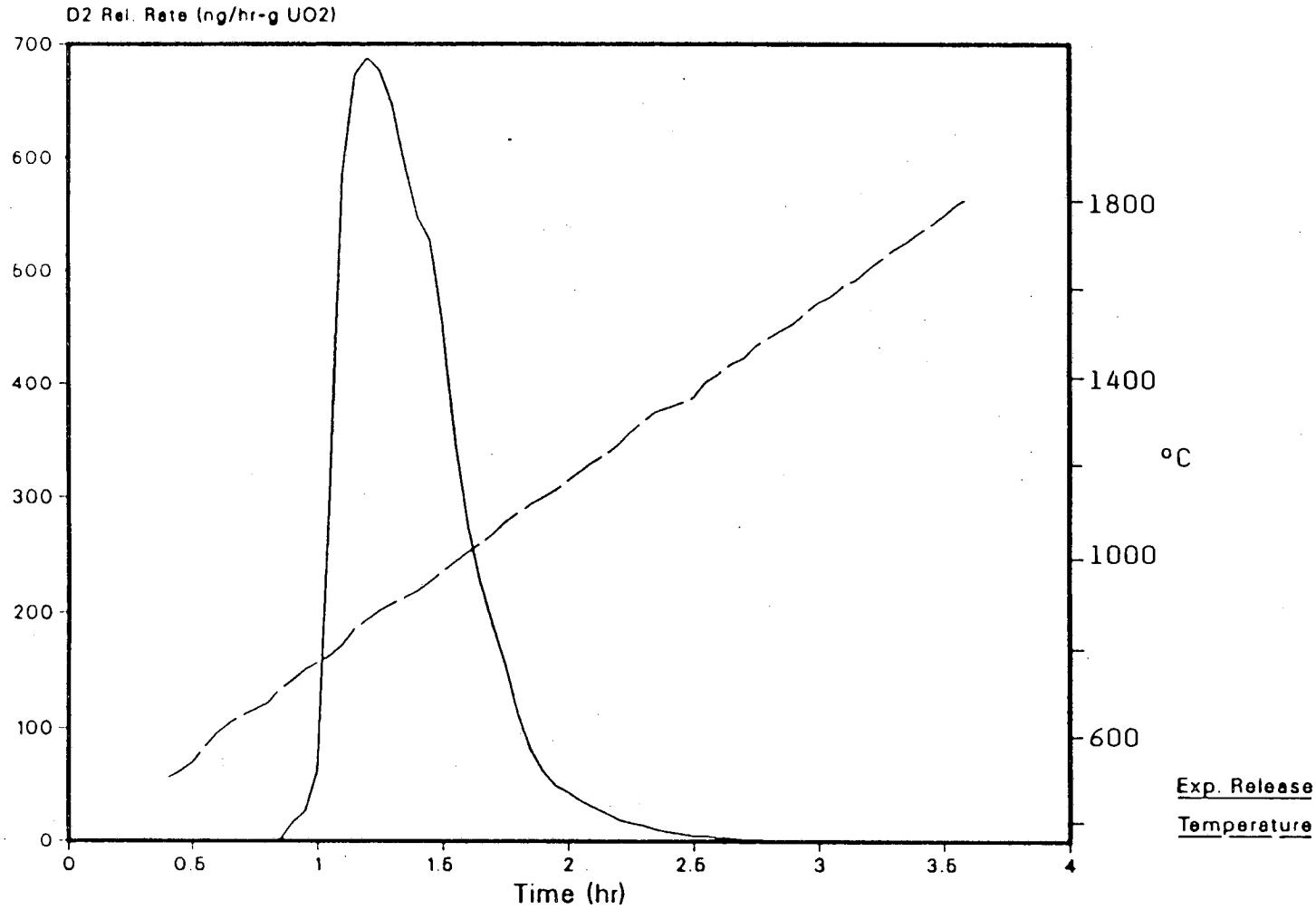

Fig. B-5 EXPT 5 Polycrystalline UO2
Infusion Conditions:
T= 1 hr T= 1400 C P= 10 atm D2

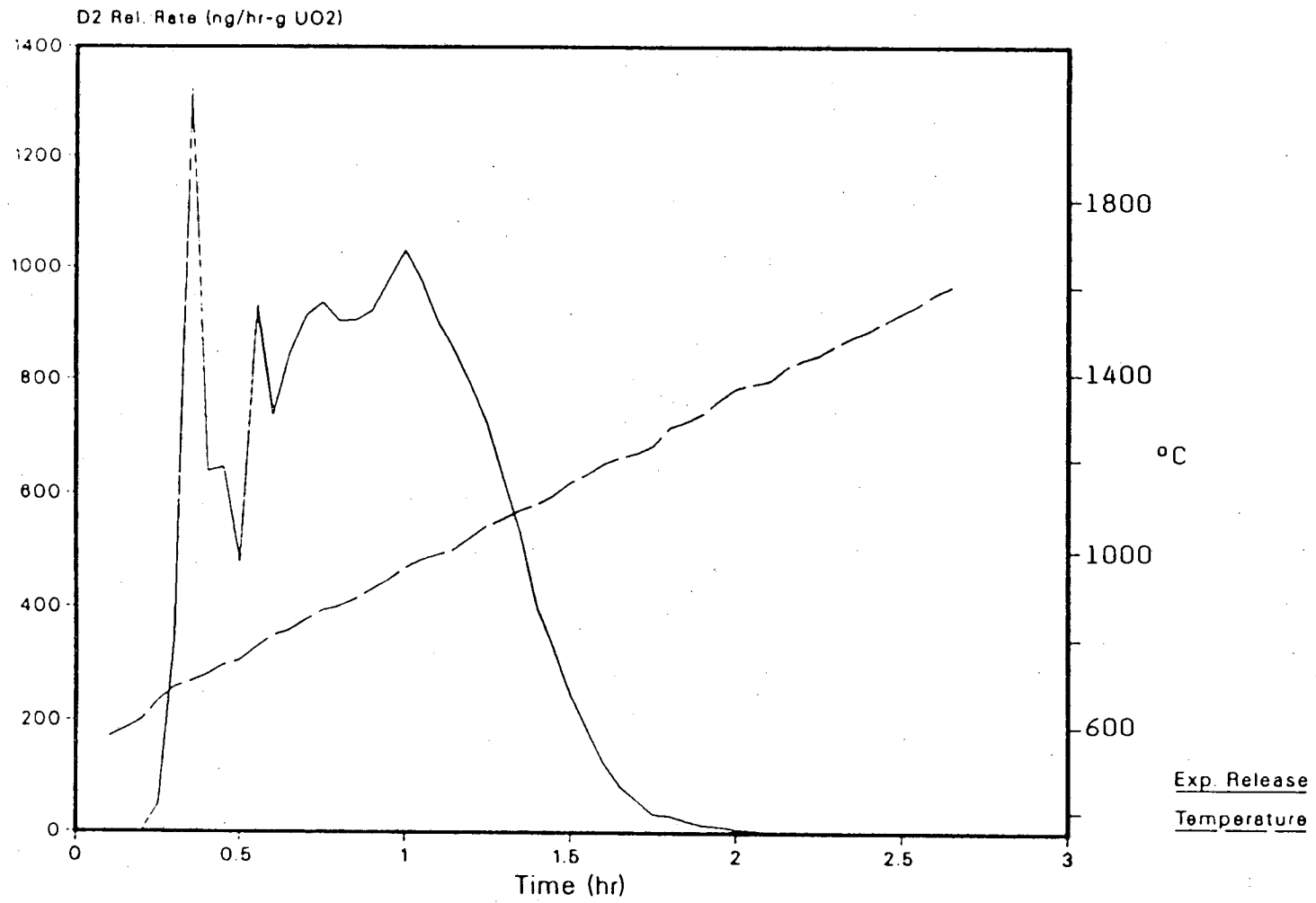

Fig. B-6 EXPT 17 Polycrystalline UO2
Infusion Conditions:
t= 2 hr T= 1400 C P= 10 atm D2

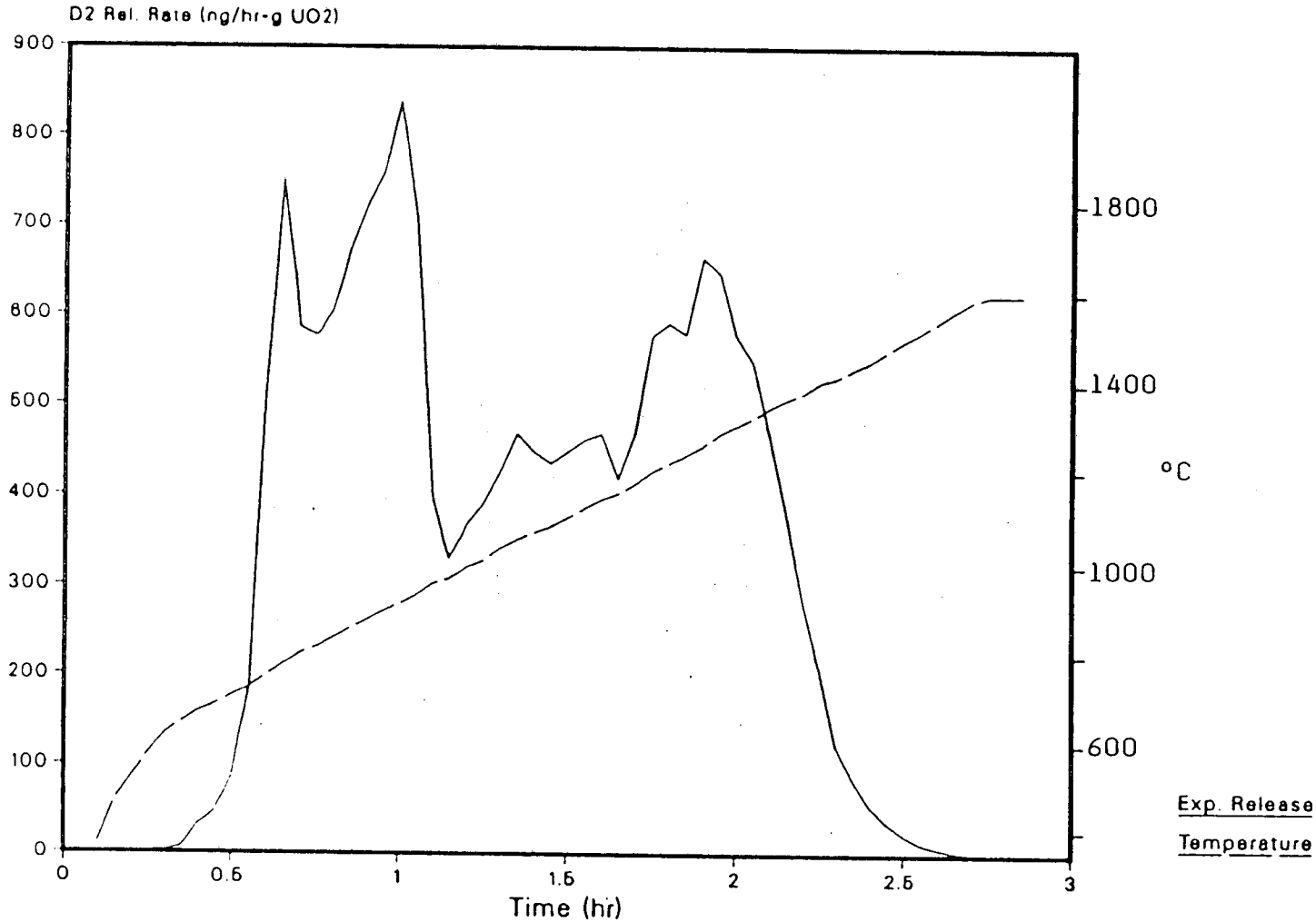

Fig. B-7 EXPT 30 Polycrystalline UO2
Infusion Conditions:
t= 3 hr T= 1400 C P= 10 atm D2

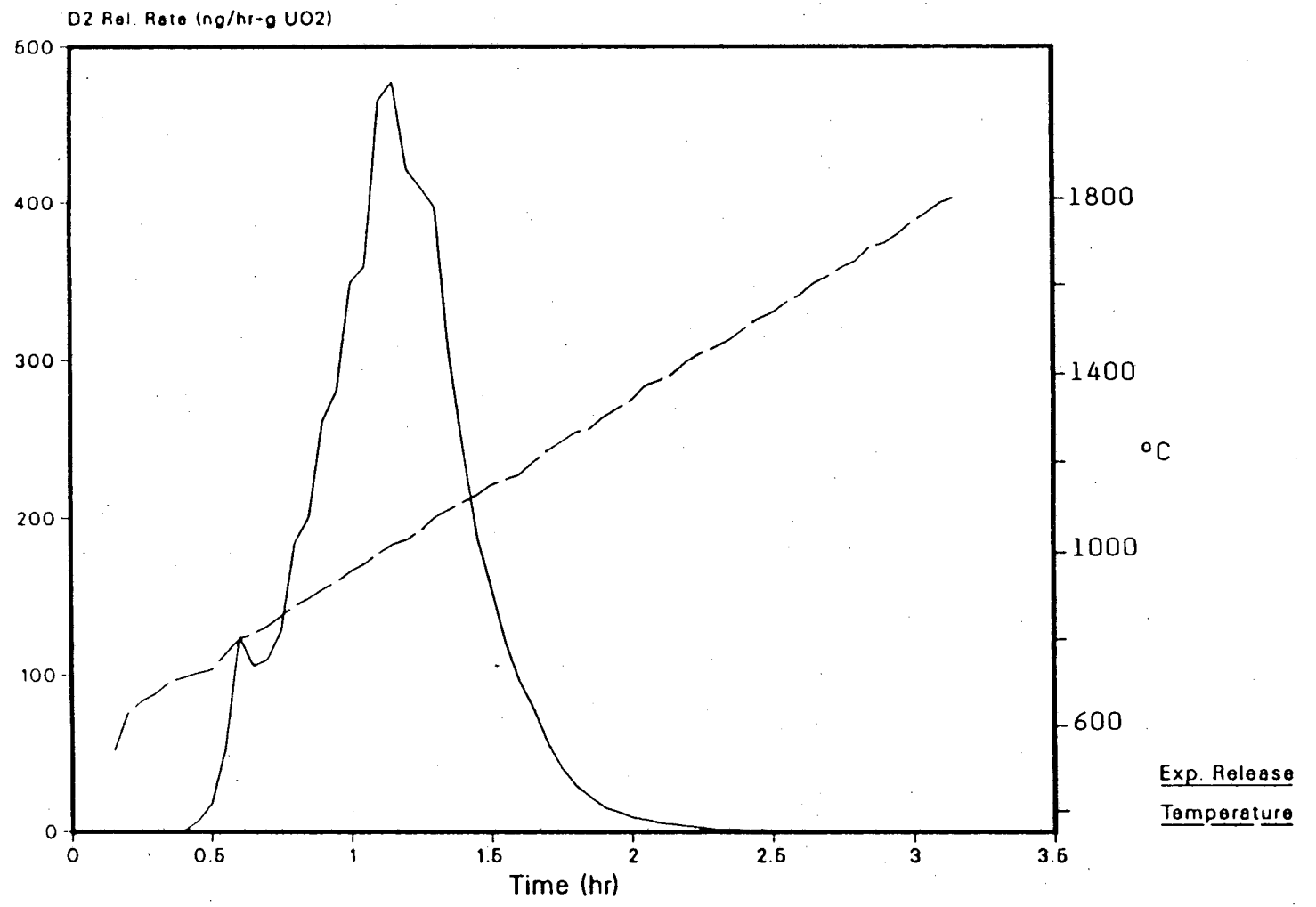

Fig. B-8 EXPT 8 Polycrystalline UO2
Infusion Conditions:
t= 1 hr T= 1300 C P= 10 atm D2

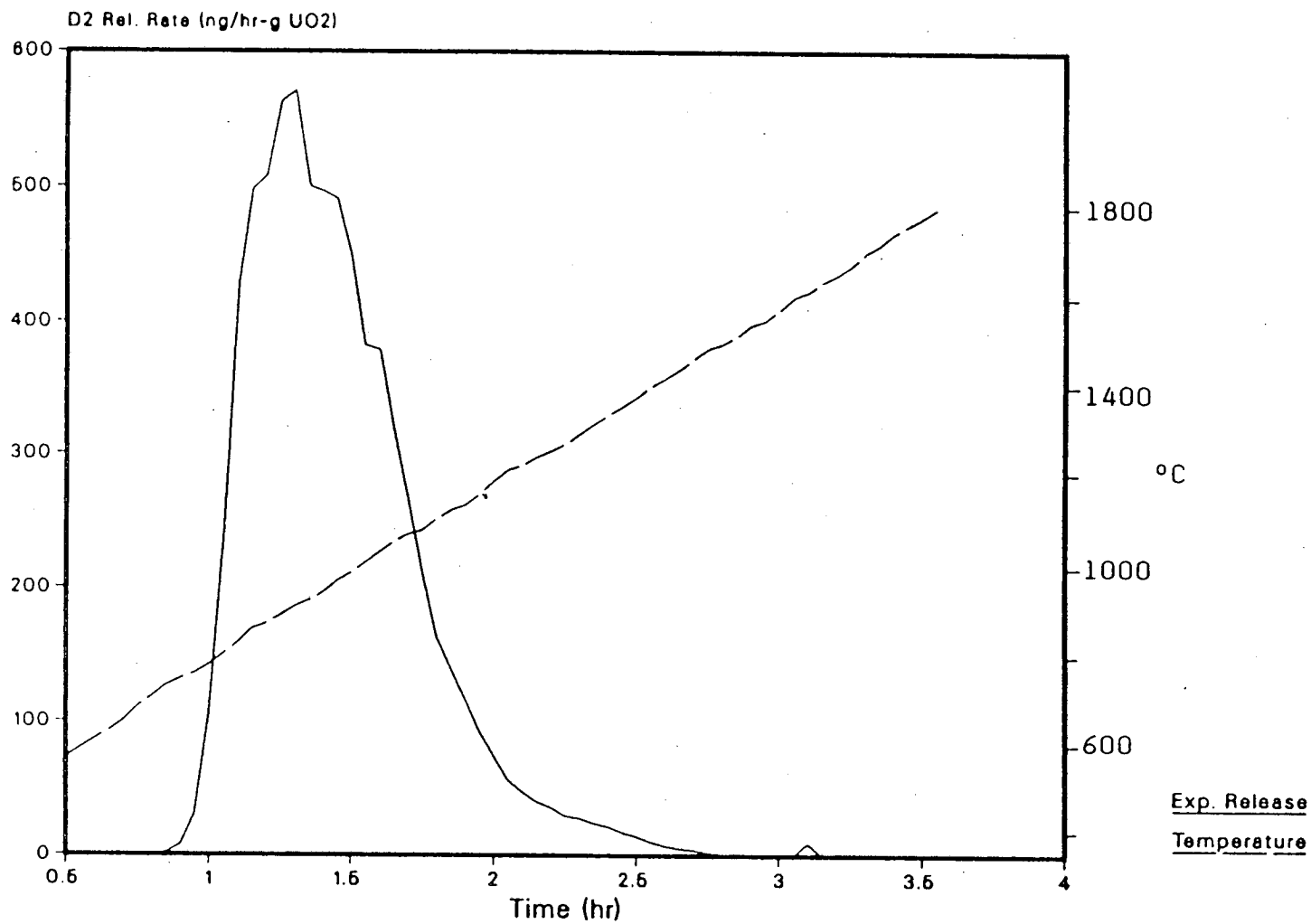

Fig. B-9 EXPT 6 Polycrystalline UO2
Infusion Conditions:
t= 1 hr T= 1200 C P= 10 atm D2

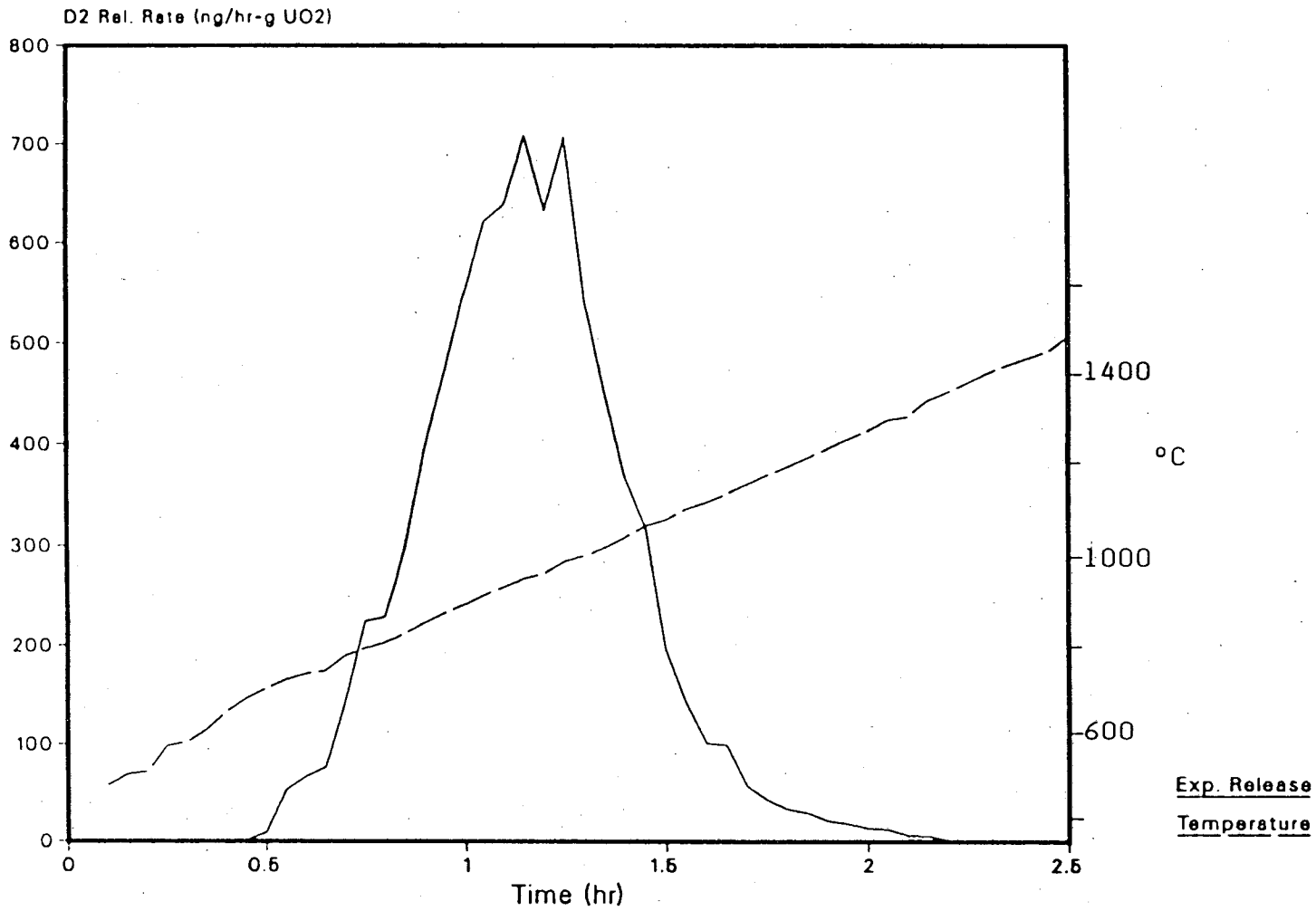

Fig. B-10 EXPT 16 Polycrystalline UO2
Infusion Conditions:
t= 2 hr T= 1200 C P= 10 atm D2

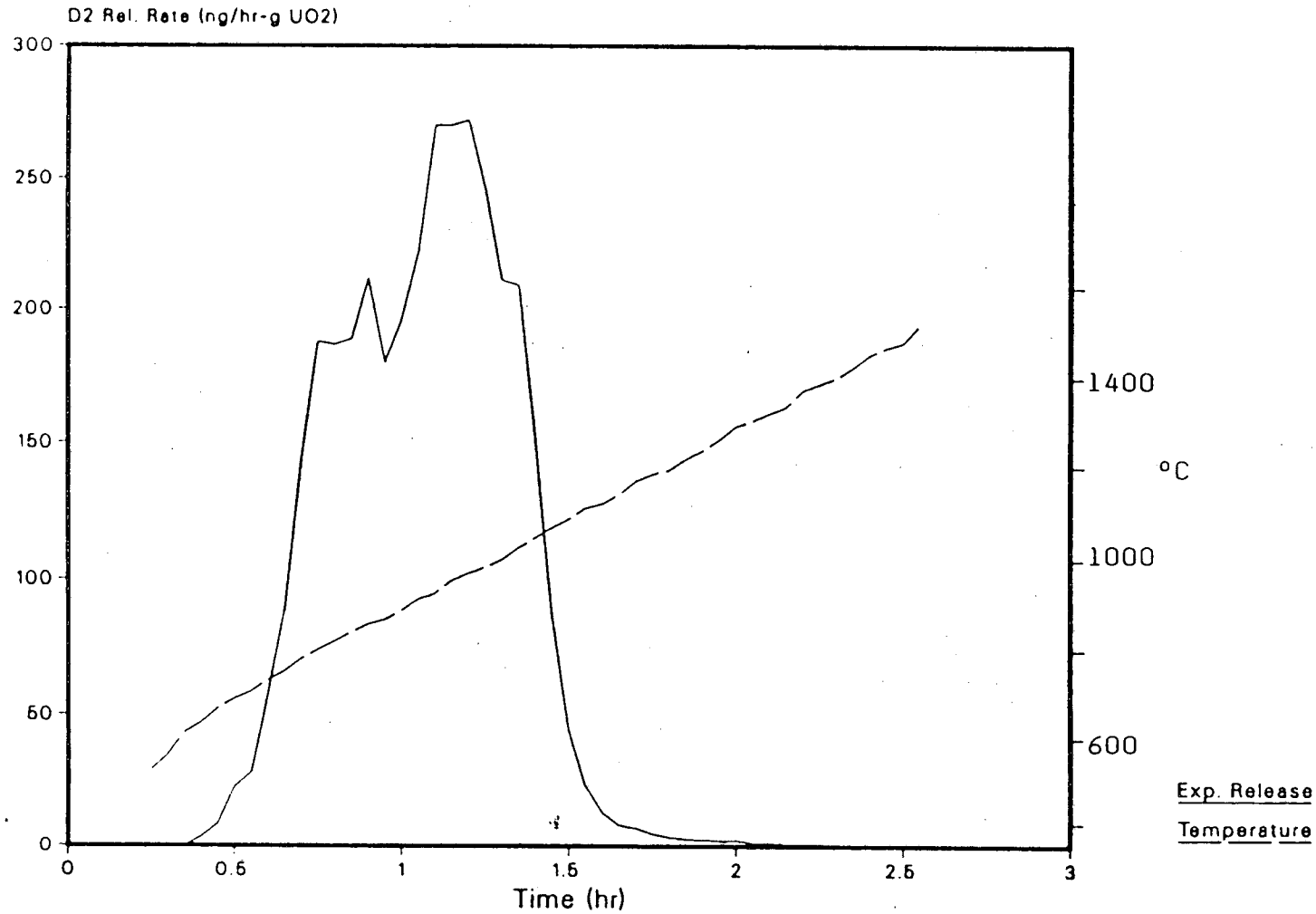

Fig. B-11 EXPT 10 Polycrystalline UO2
Infusion Conditions:
t= 1 hr T= 1000 C P= 10 atm D2

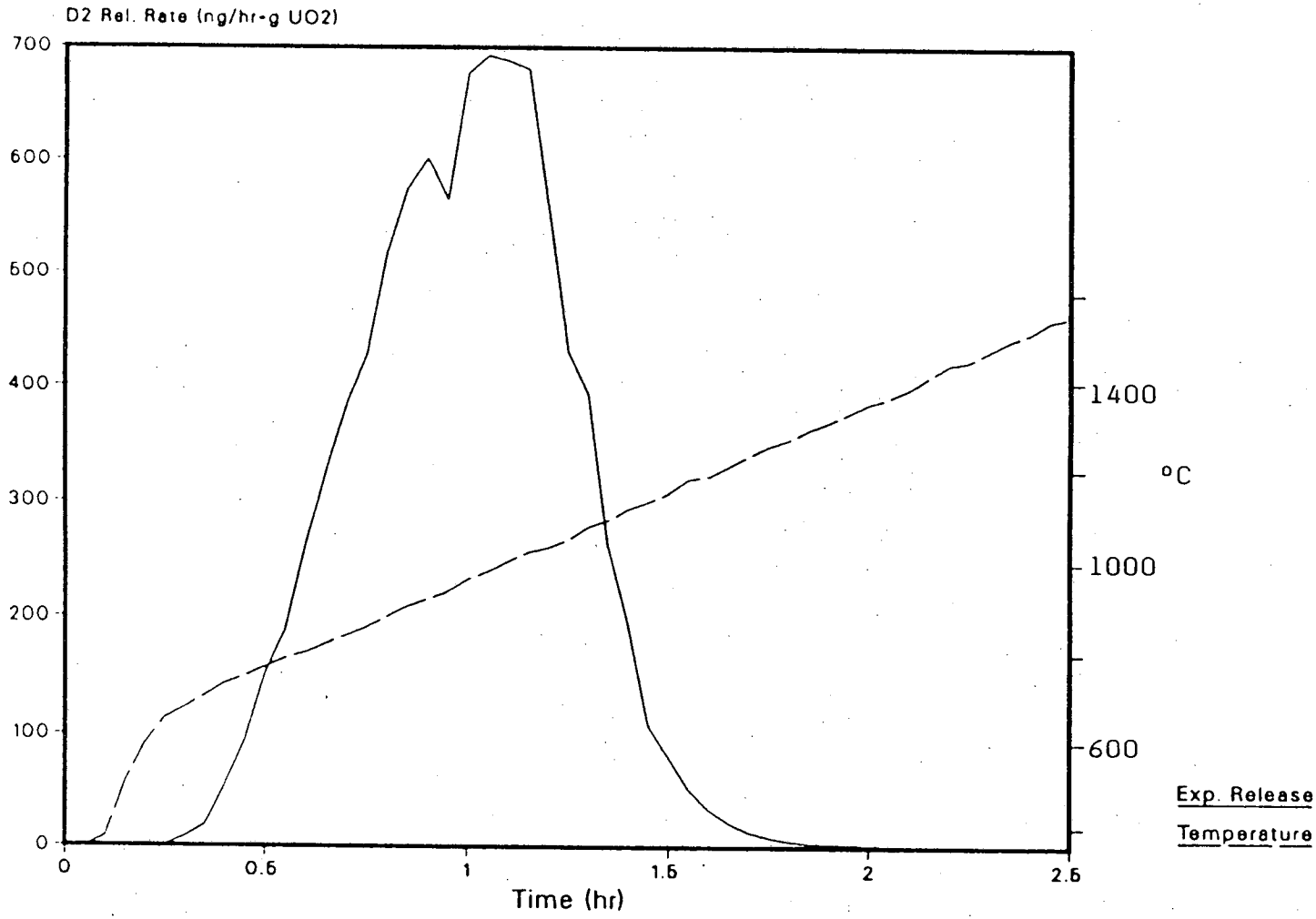

Fig. B-12 EXPT 11 Polycrystalline UO2
Infusion Conditions:
t= 2 hr T= 1000 C P= 10 atm D2

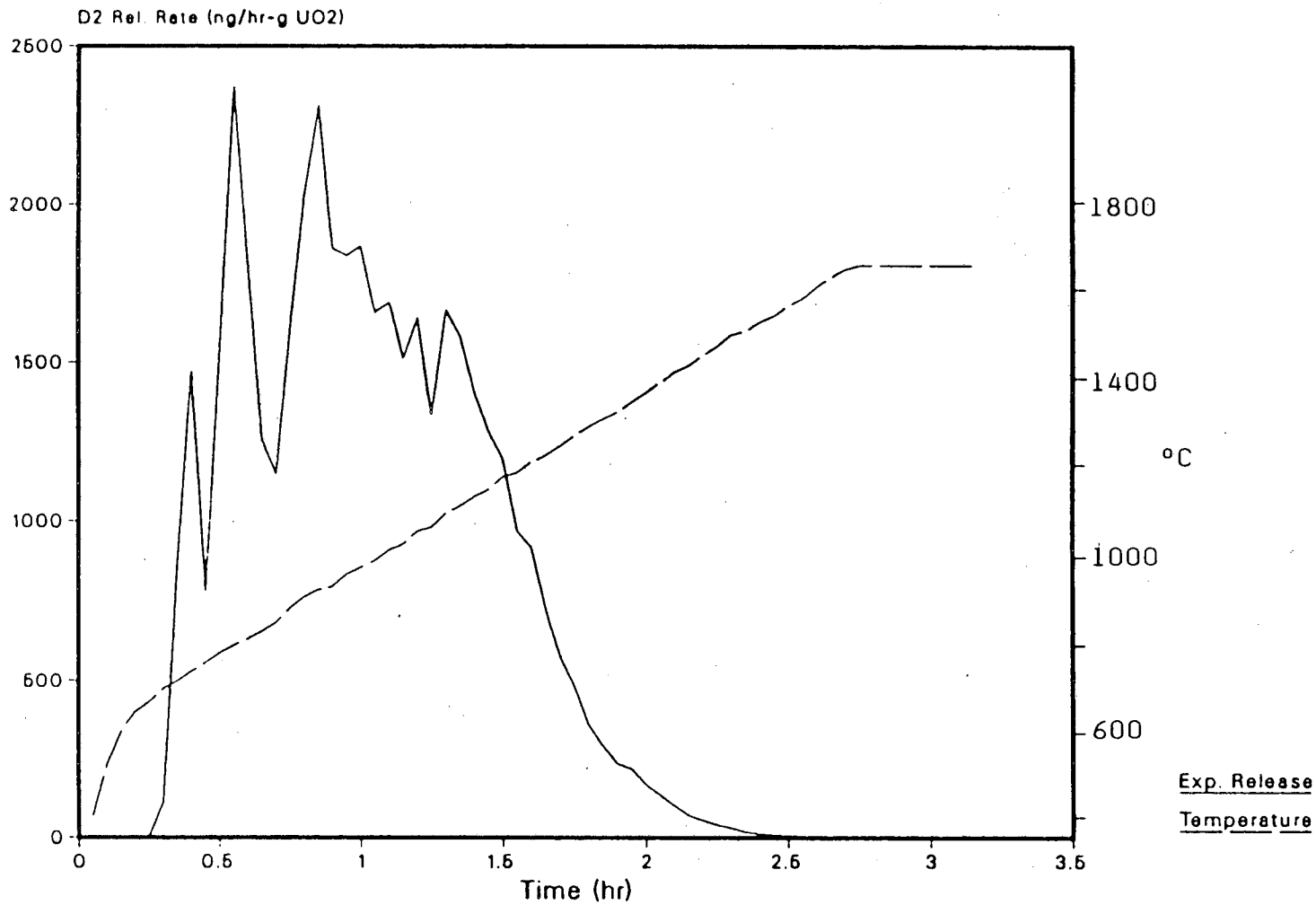

Fig. B-13 EXPT 12 Polycrystalline UO2
Infusion Conditions:
t= 1 hr T= 1600 C P= 5.4 atm D2

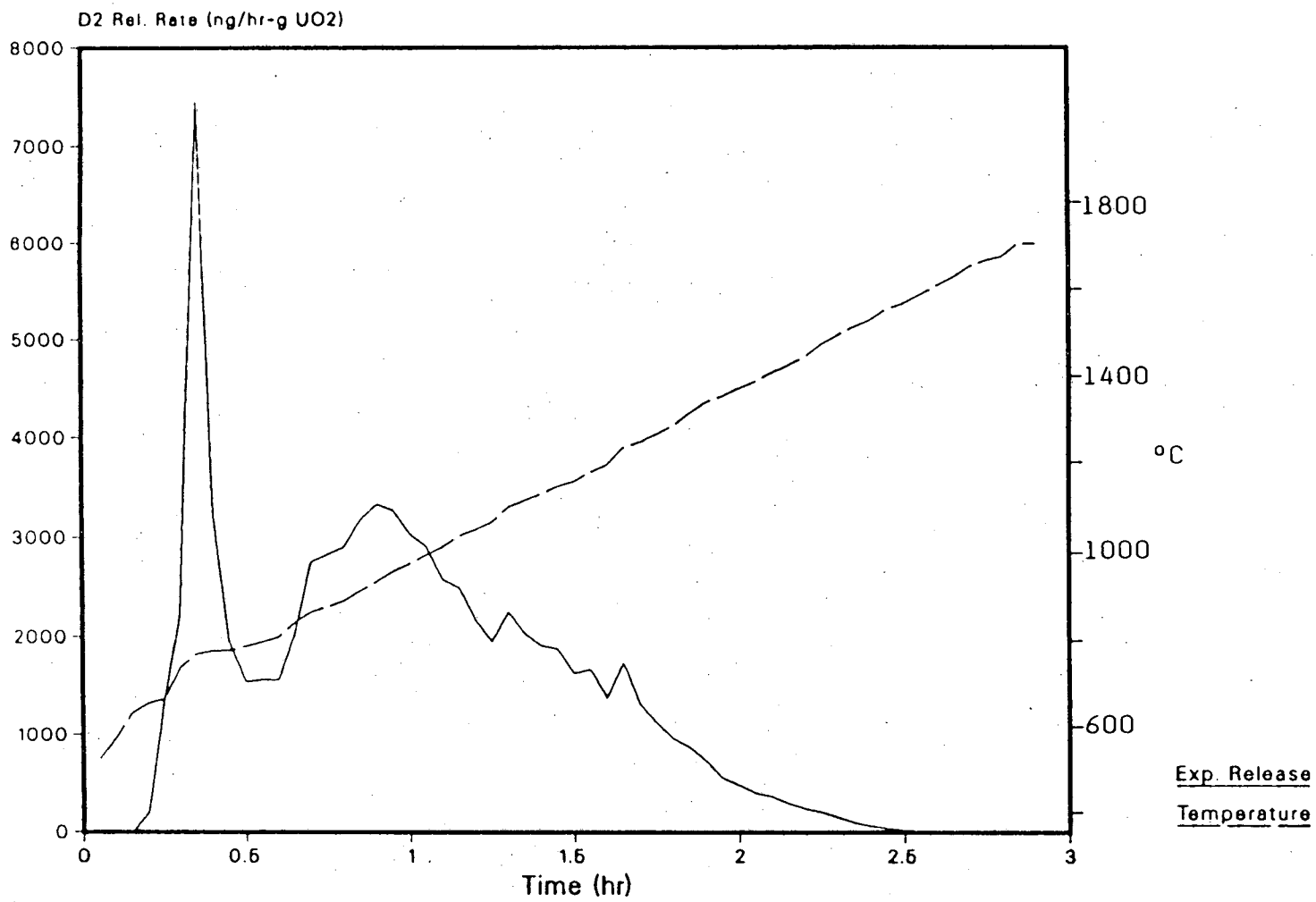

Fig. B-14 EXPT 28 Polycrystalline UO2
Infusion Conditions:
t= 1 hr T= 1600 C P= 16.5 atm D2

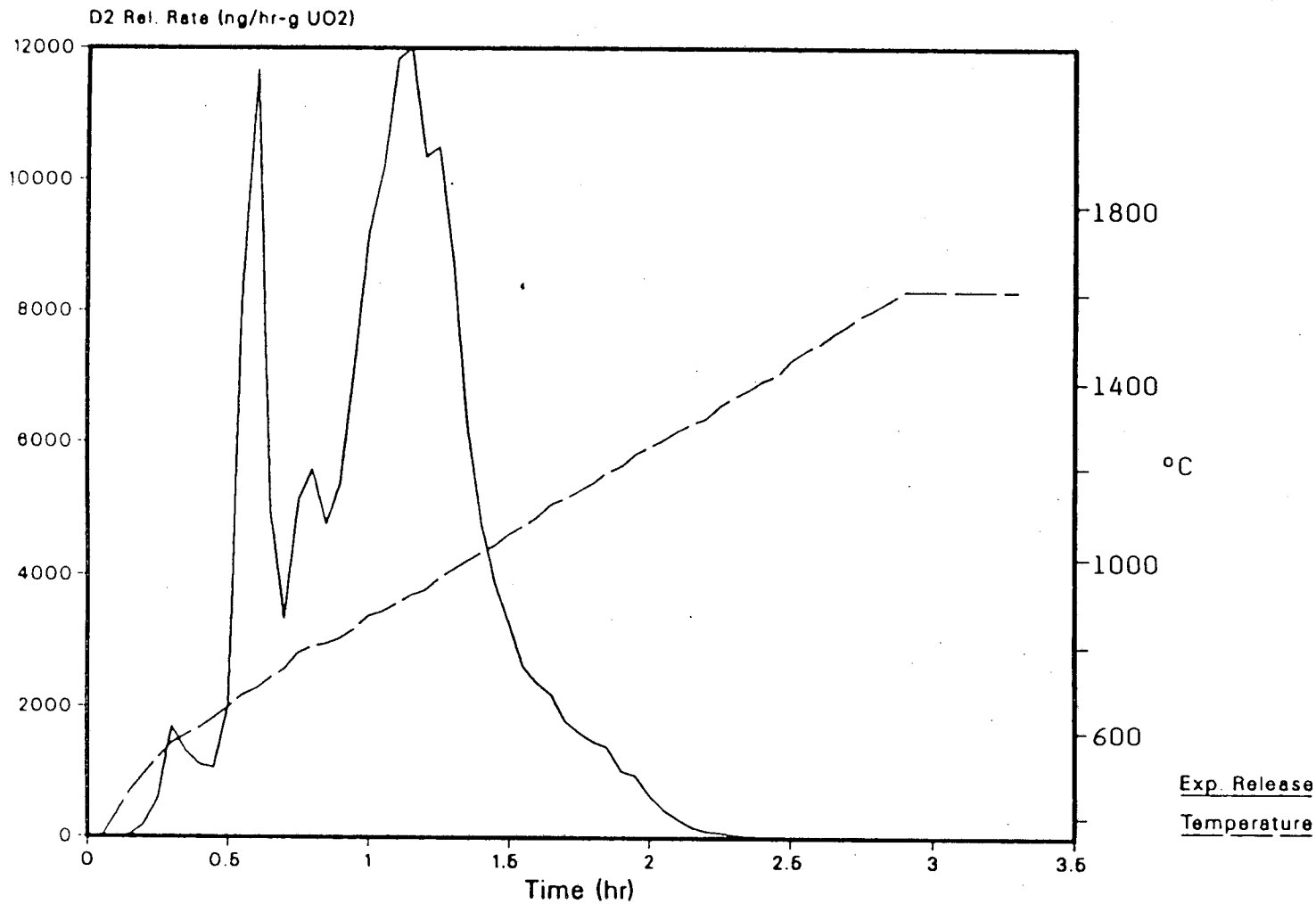

Fig. B-15 EXPT 13 Polycrystalline UO2
Infusion Conditions:
t= 1 hr T= 1600 C P= 20 atm D2

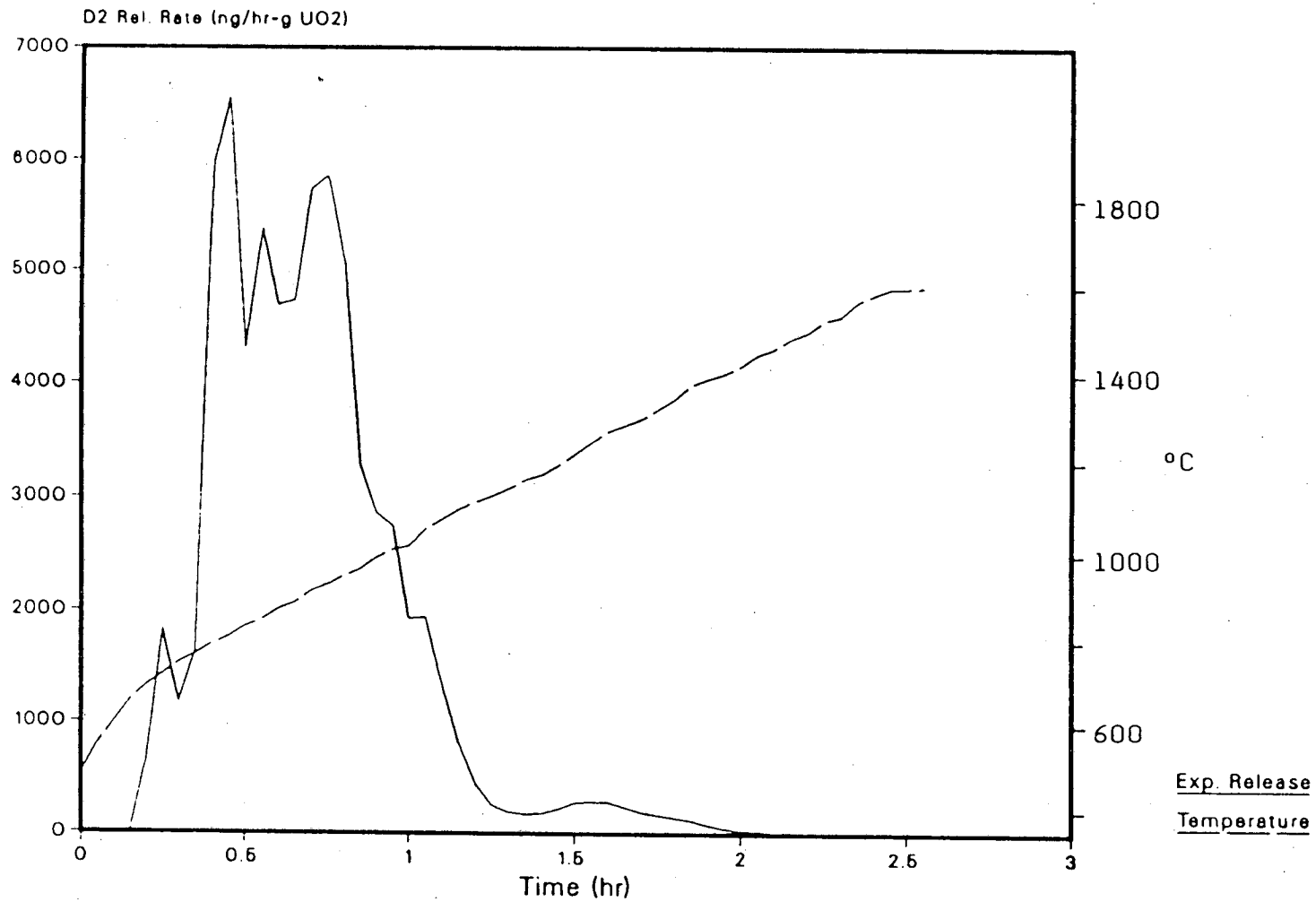

Fig. B-16 EXPT 29 Polycrystalline UO2
Infusion Conditions:
t= 1 hr T= 1600 C P= 25 atm D2

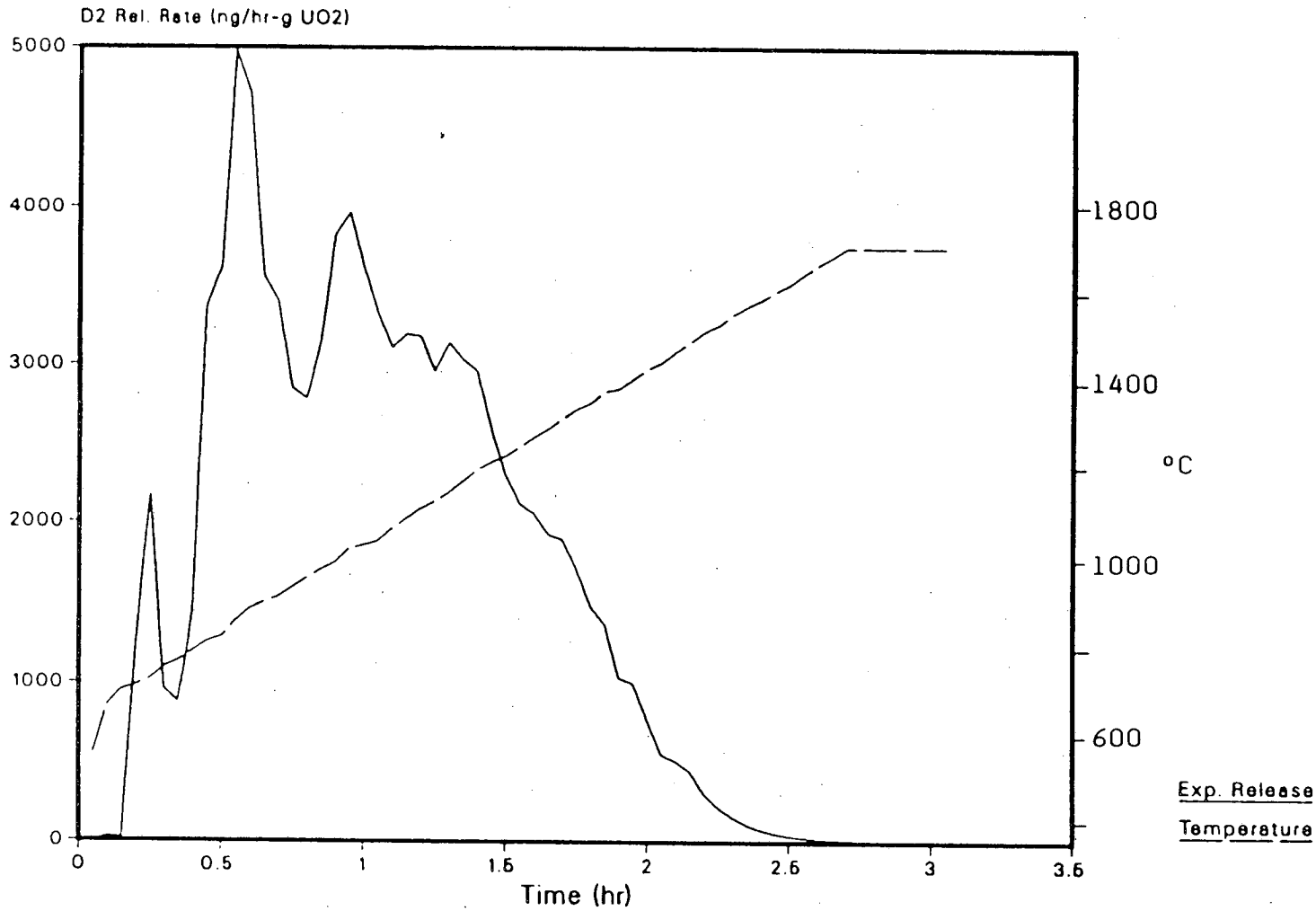

Fig. B-17 EXPT 14 Polycrystalline UO2
Infusion Conditions:
t= 1 hr T= 1600 C P= 32 atm D2

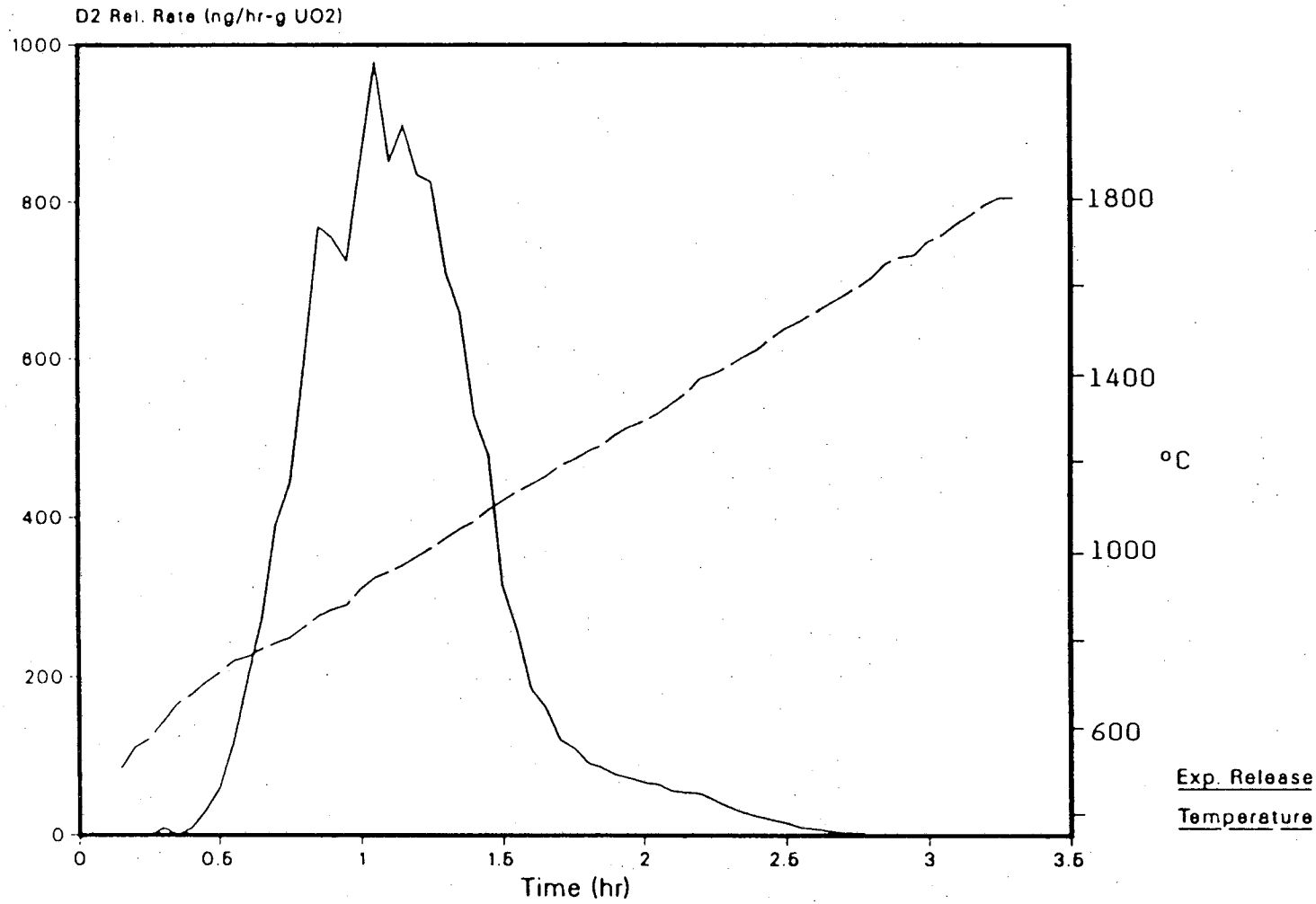

Fig. B-18 EXPT 9 Polycrystalline UO2
Infusion Conditions:
t= 1/2 hr at T= 1600 C; 1/2 hr at T= 1200 C, P = 10 atm D2

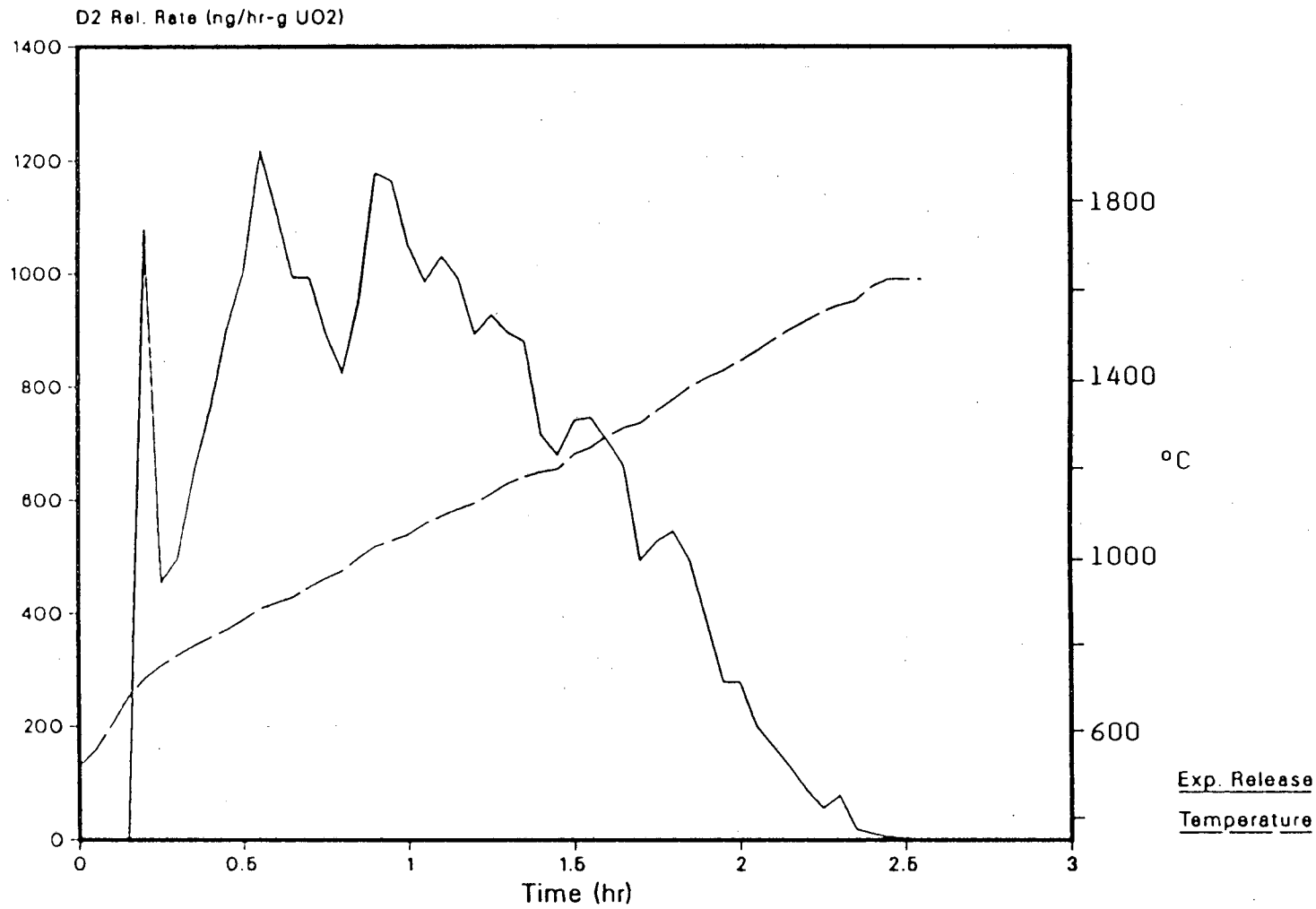

Fig. B-19 EXPT 31 Polycrystalline UO2
Infusion Conditions:
t= 1 hr T= 1600 C P= 10 atm D_2; slow quench

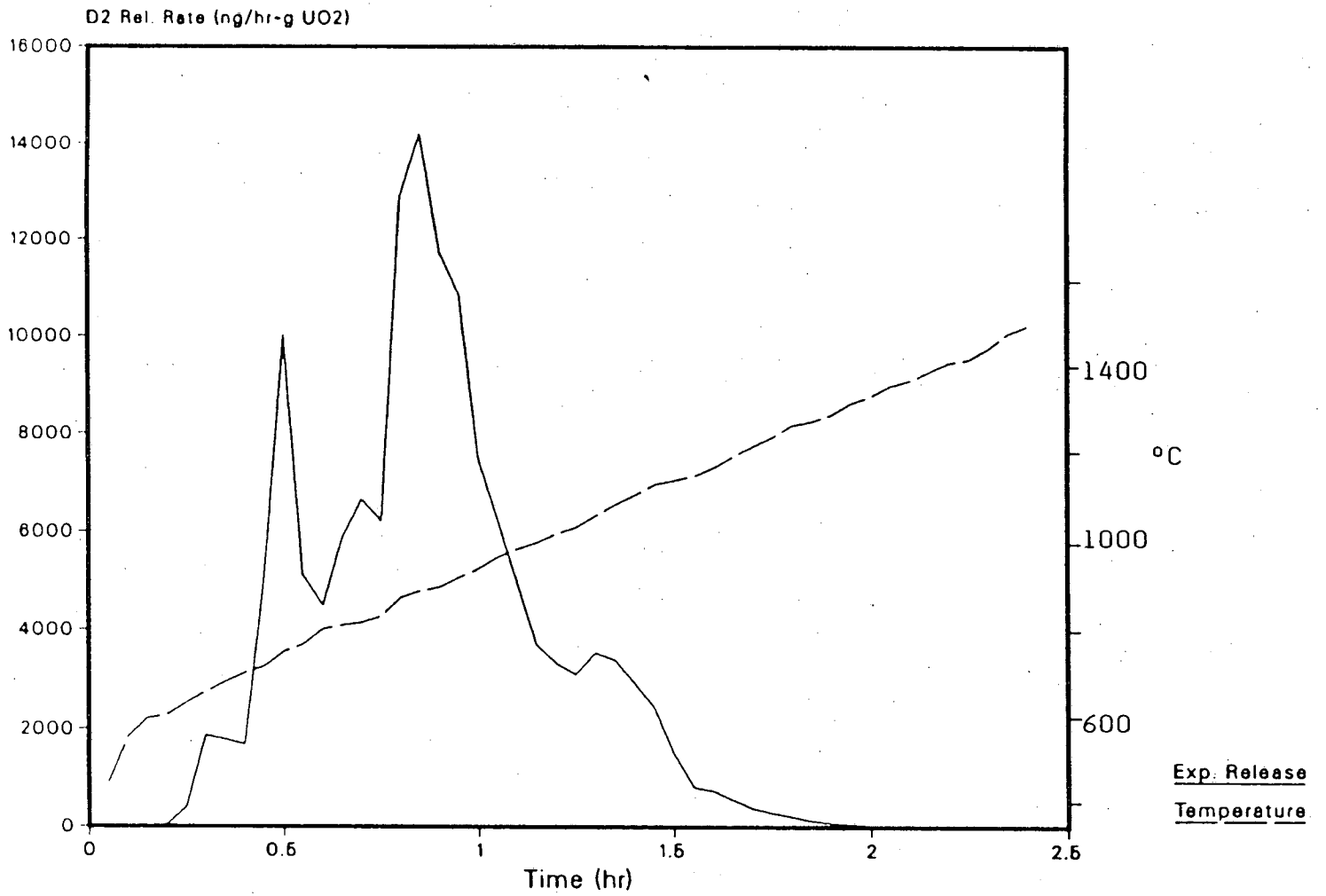

Fig. B-20 EXPT 15 Preheated Polycrystalline UO2
Infusion Conditions:
t= 1 hr T= 1600 C P= 10 atm D_2

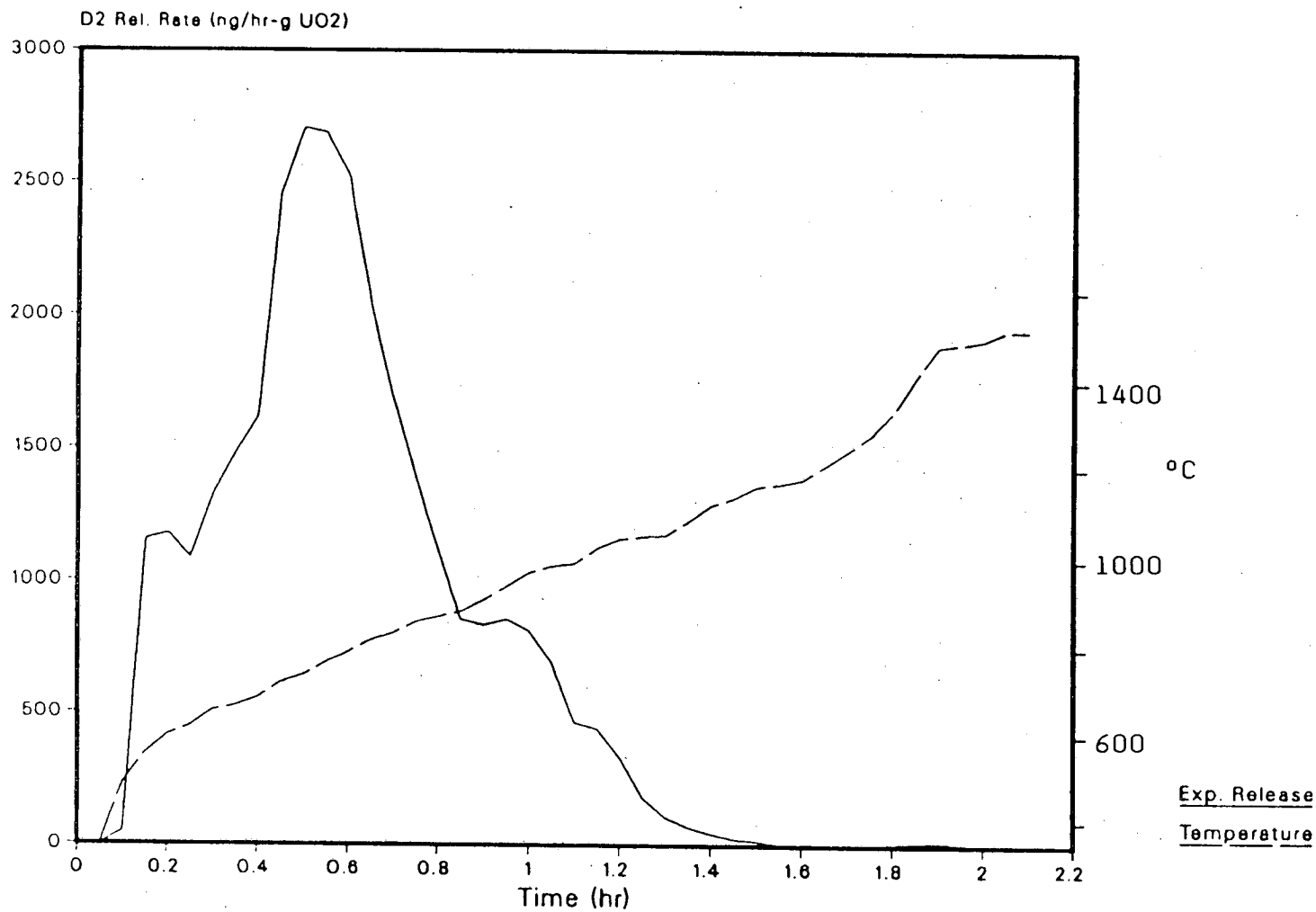

Fig. B-21 EXPT 35 Polycrystalline UO2.065
Infusion Conditions:
t= 1 hr T= 1600 C P= 10 atm D_2; slow quench

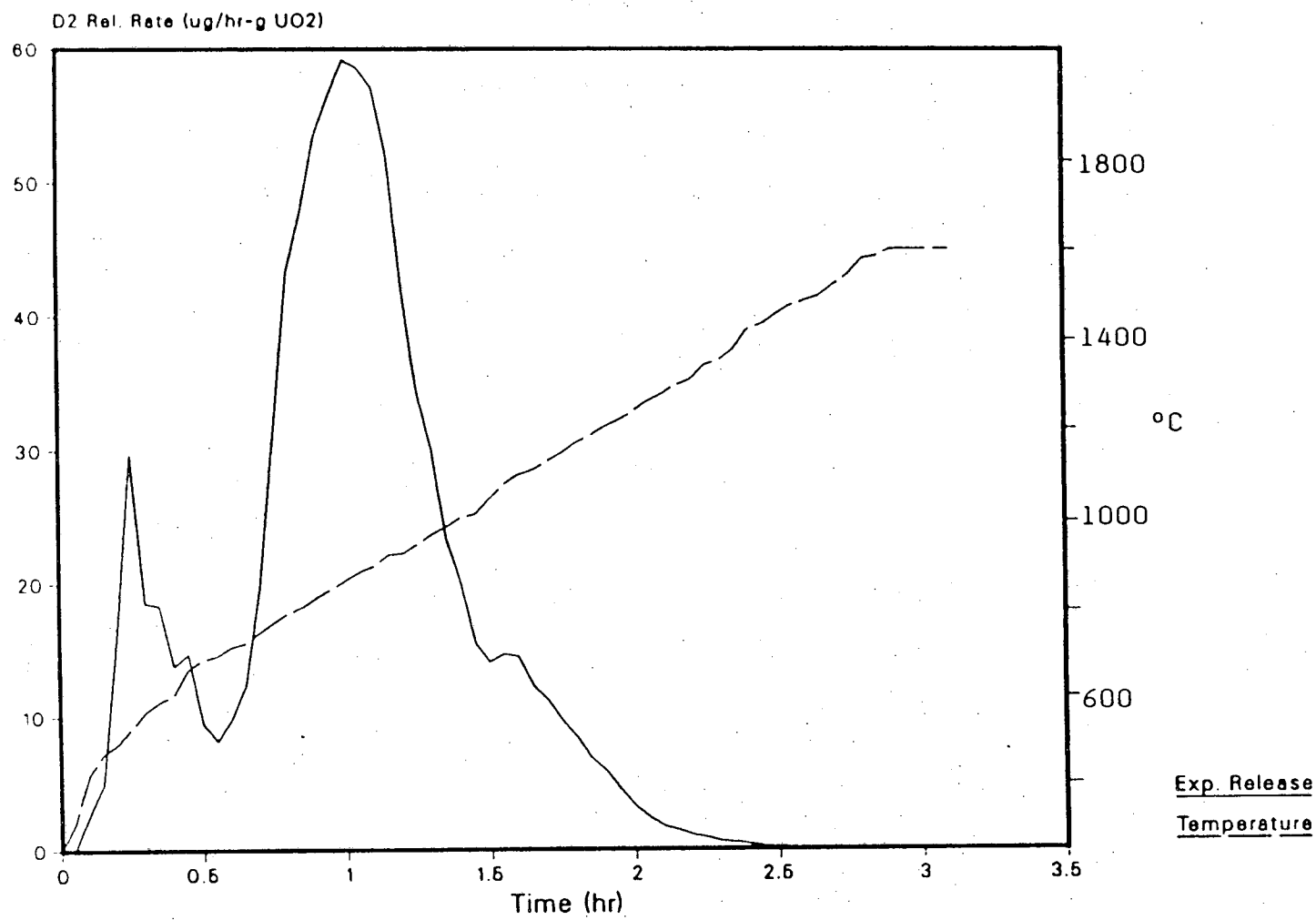

Fig. B-22 EXPT 32 Polycrystalline UO1.976
Infusion Conditions:
t= 1 hr T= 1600 C P= 10 atm D_2

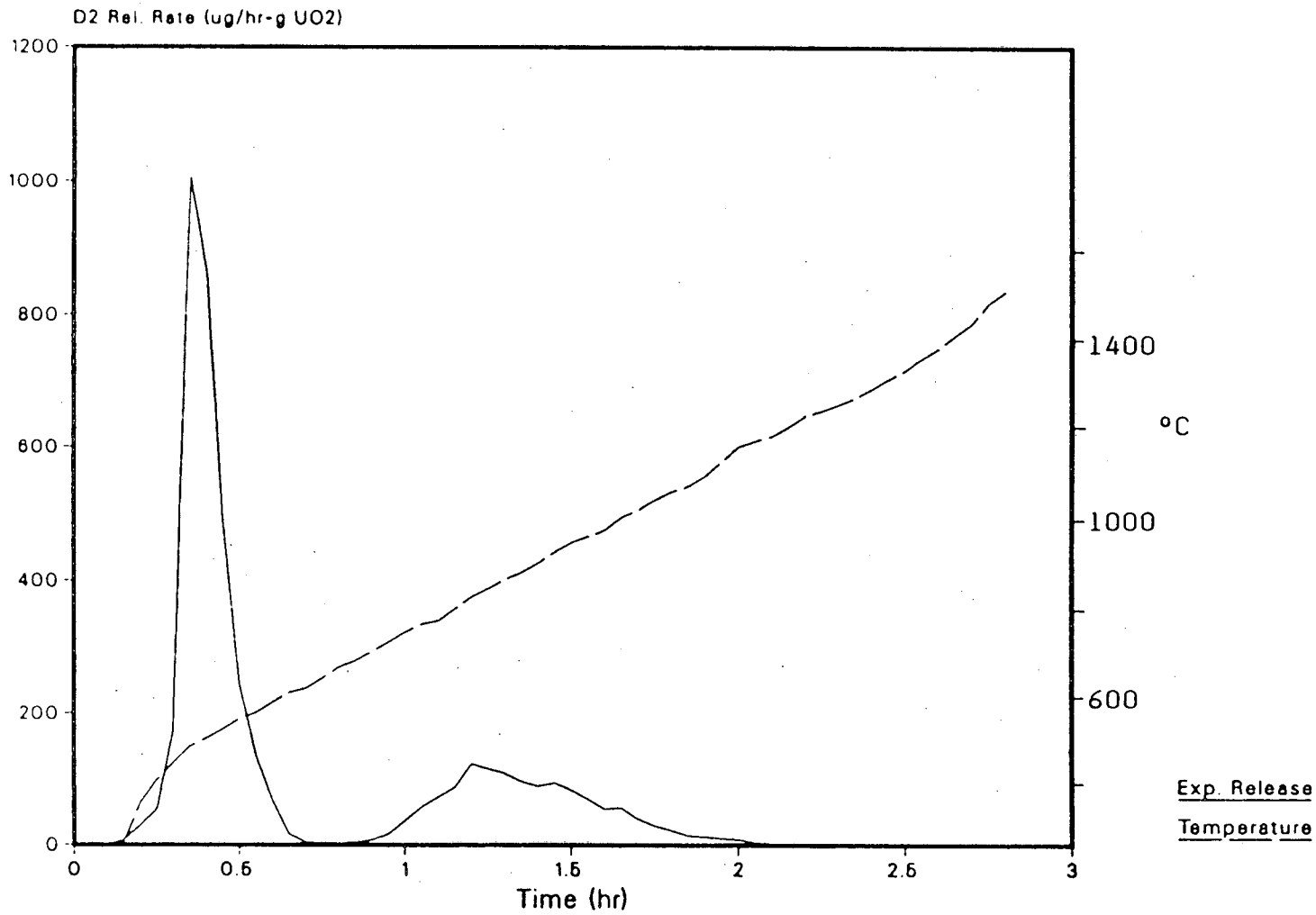

Fig. B-23 EXPT 33 Polycrystalline UO1.90
Infusion Conditions:
t= 1 hr T= 1600 C P= 10 atm D_2

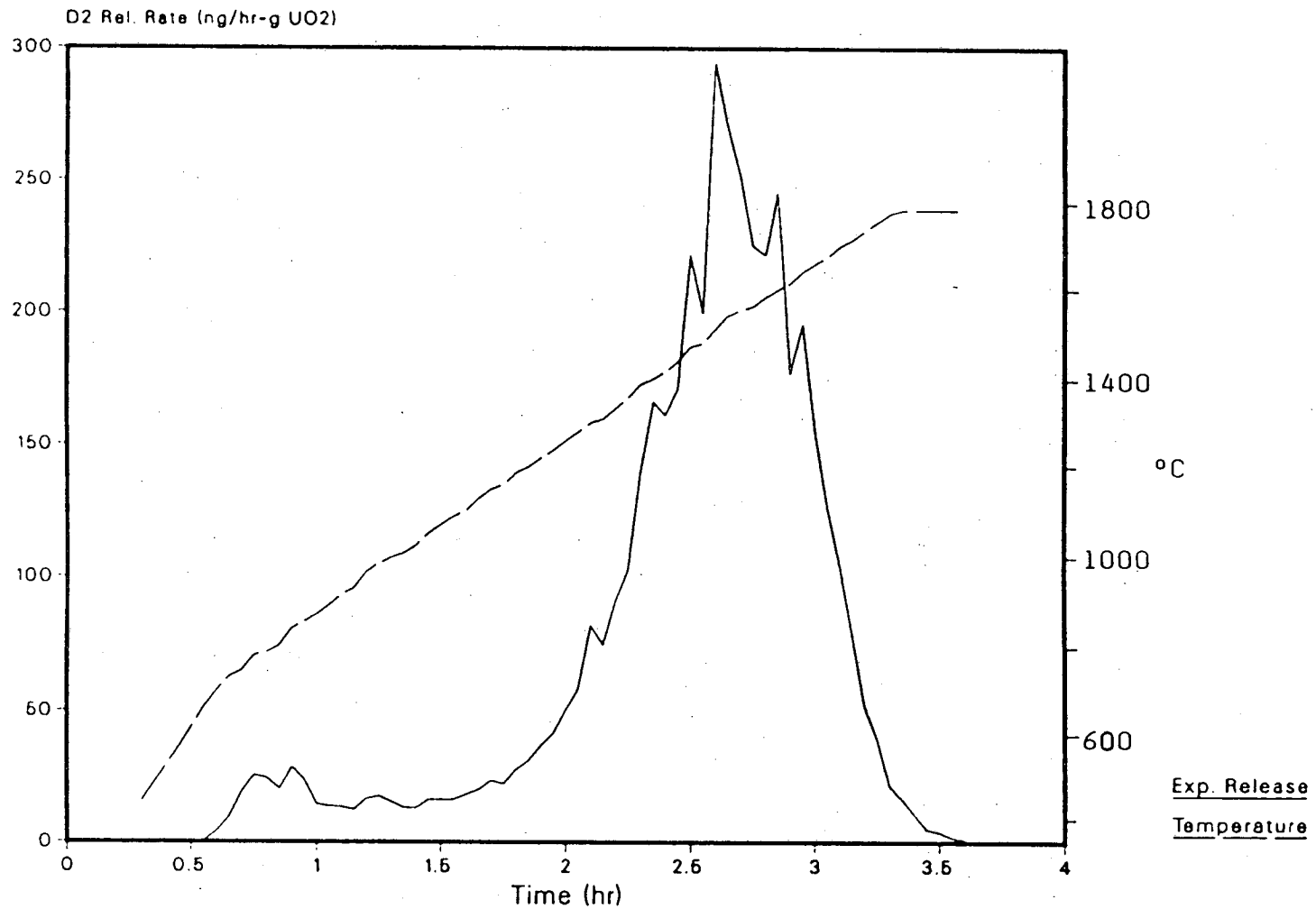

Fig. B-24 EXPT 18 Single Crystal UO2
Infusion Conditions:
t= 1 1/4 hr T= 1600 C P= 10 atm D2

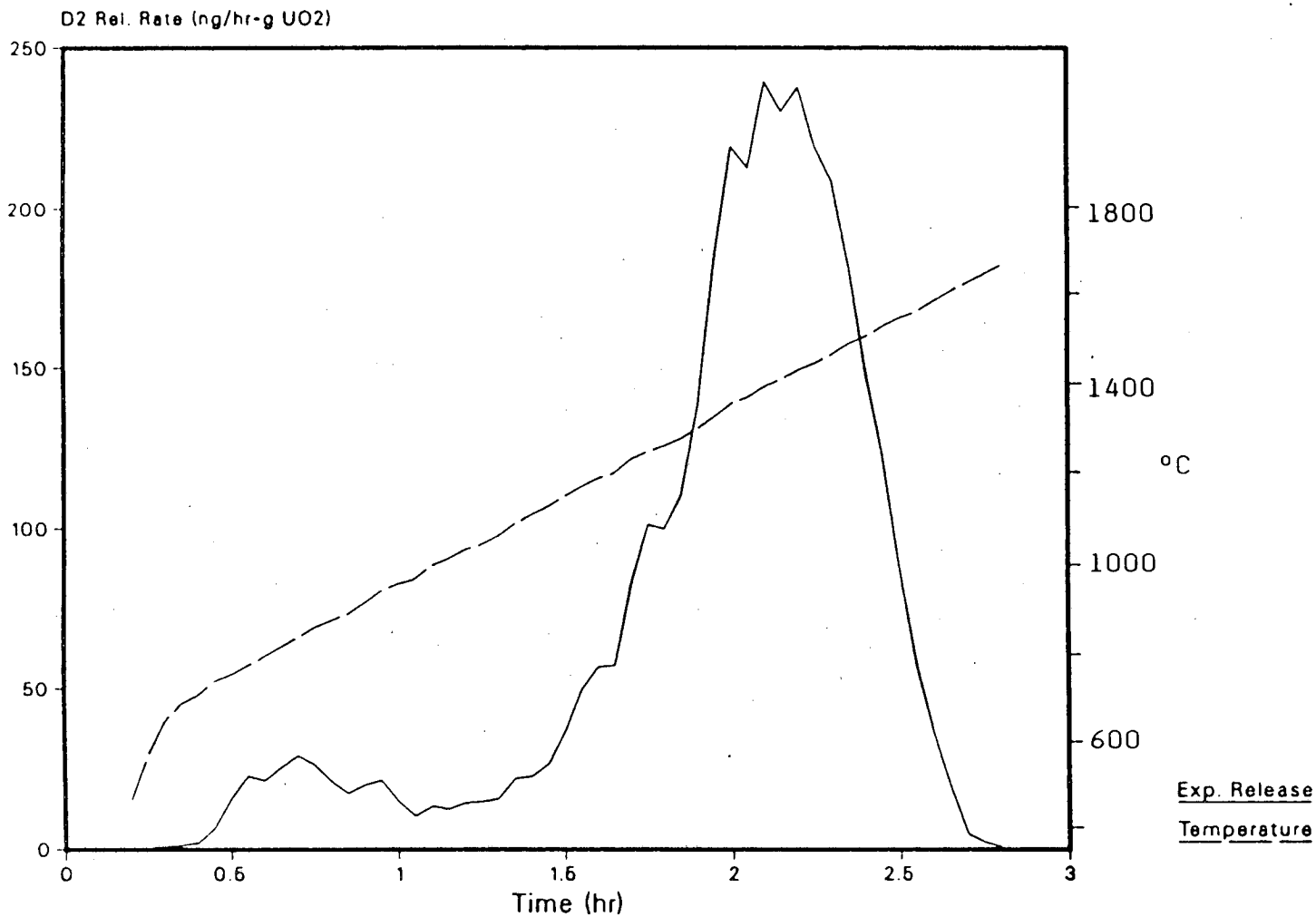

Fig. B-25 EXPT 19 Single Crystal UO2
Infusion Conditions:
t= 1 1/4 hr T= 1600 C P= 10 atm D2

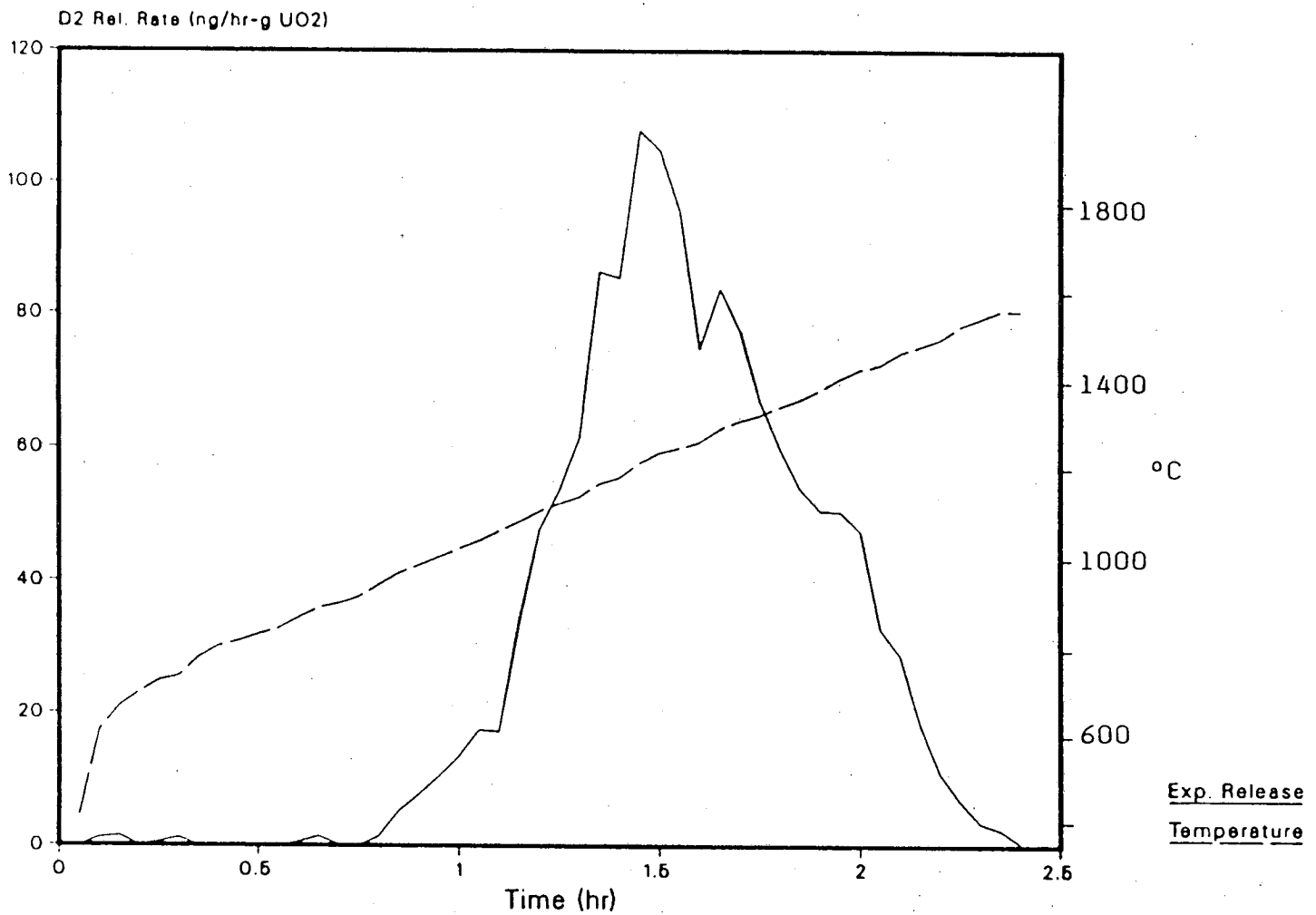

Fig. B-26 EXPT 20 Single Crystal UO2
Infusion Conditions:
t= 1 1/4 hr T= 1500 C P= 10 atm D2

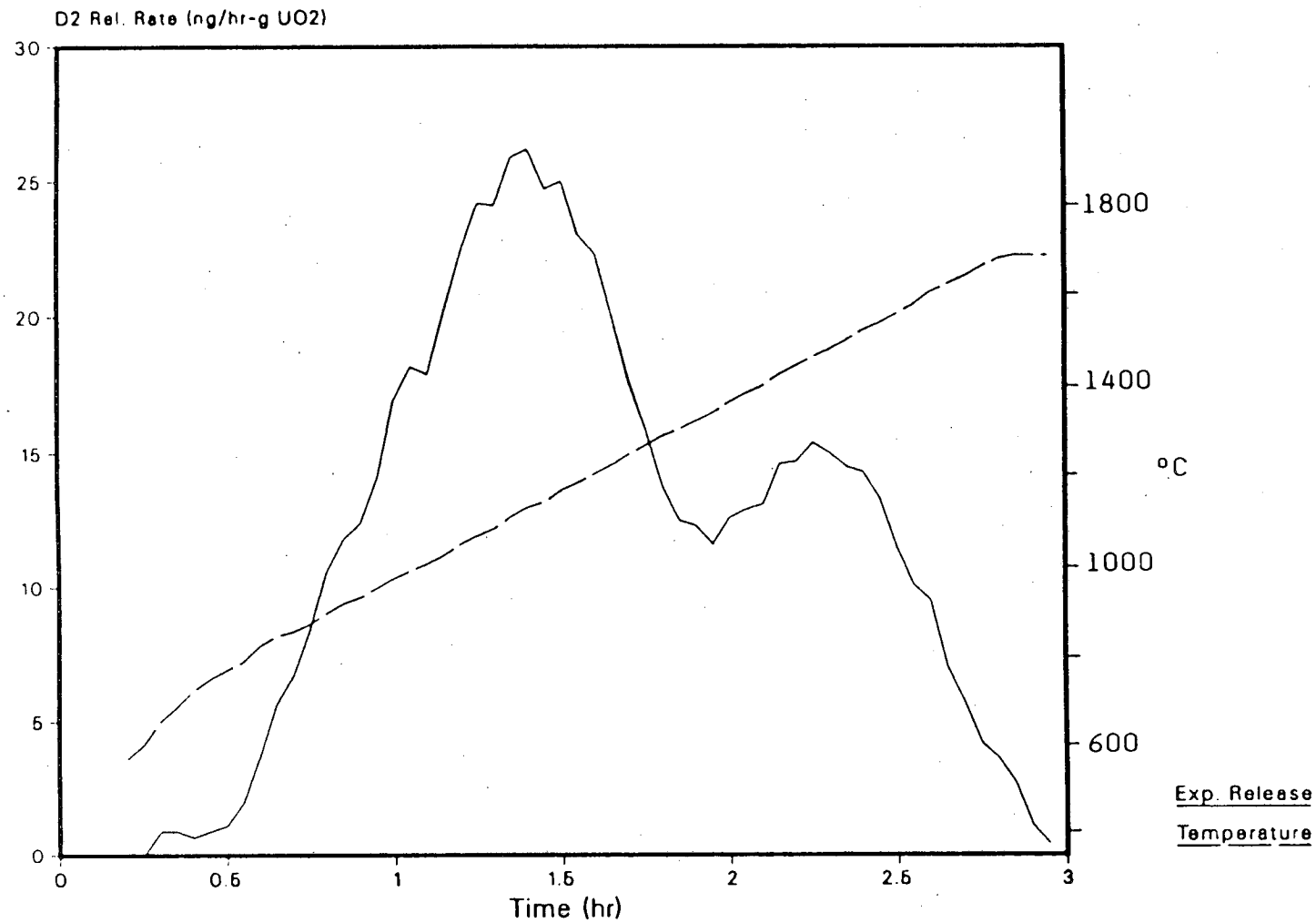

Fig. B-27 EXPT 21 Single Crystal UO2
Infusion Conditions:
t= 2 hr T= 1400 C P= 10 atm D2

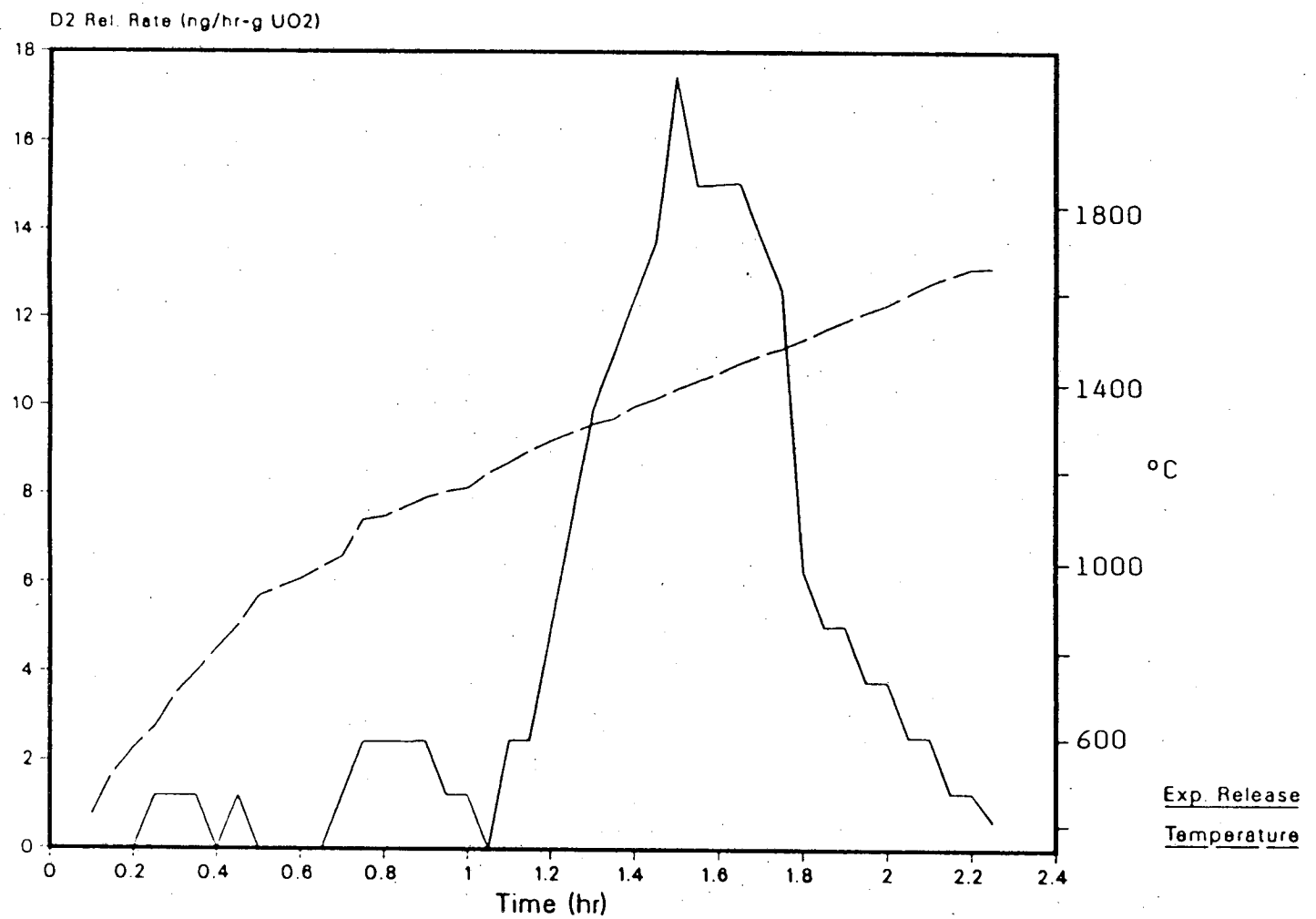

Fig. B-28 EXPT 23 Single Crystal UO2
Infusion Conditions:
t= 2 hr T= 1300 C P= 10 atm D2

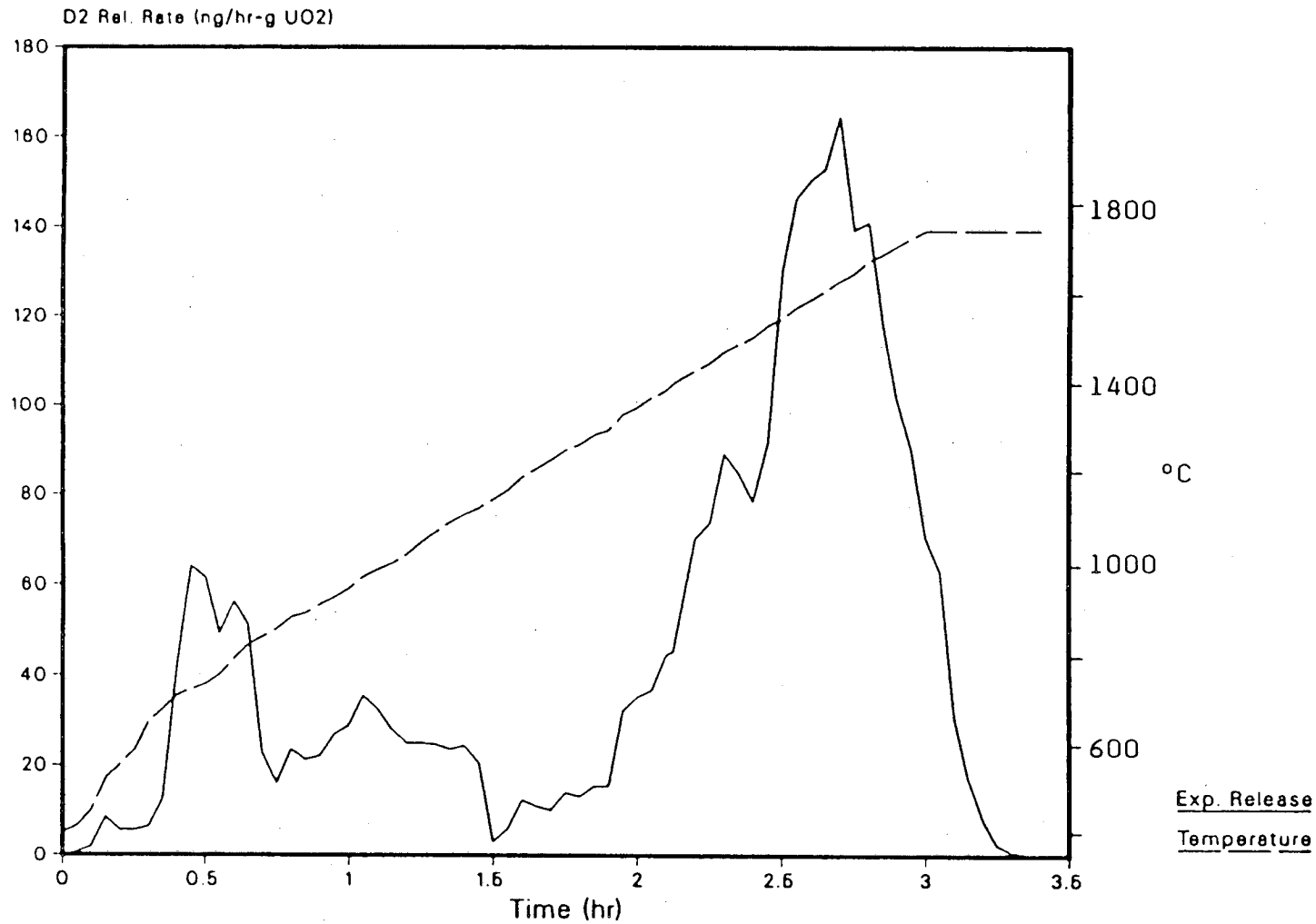

Fig. B-29 EXPT 24 Single Crystal UO2
Infusion Conditions:
t= 1 1/4 hr T= 1600 C P= 5.4 atm D2

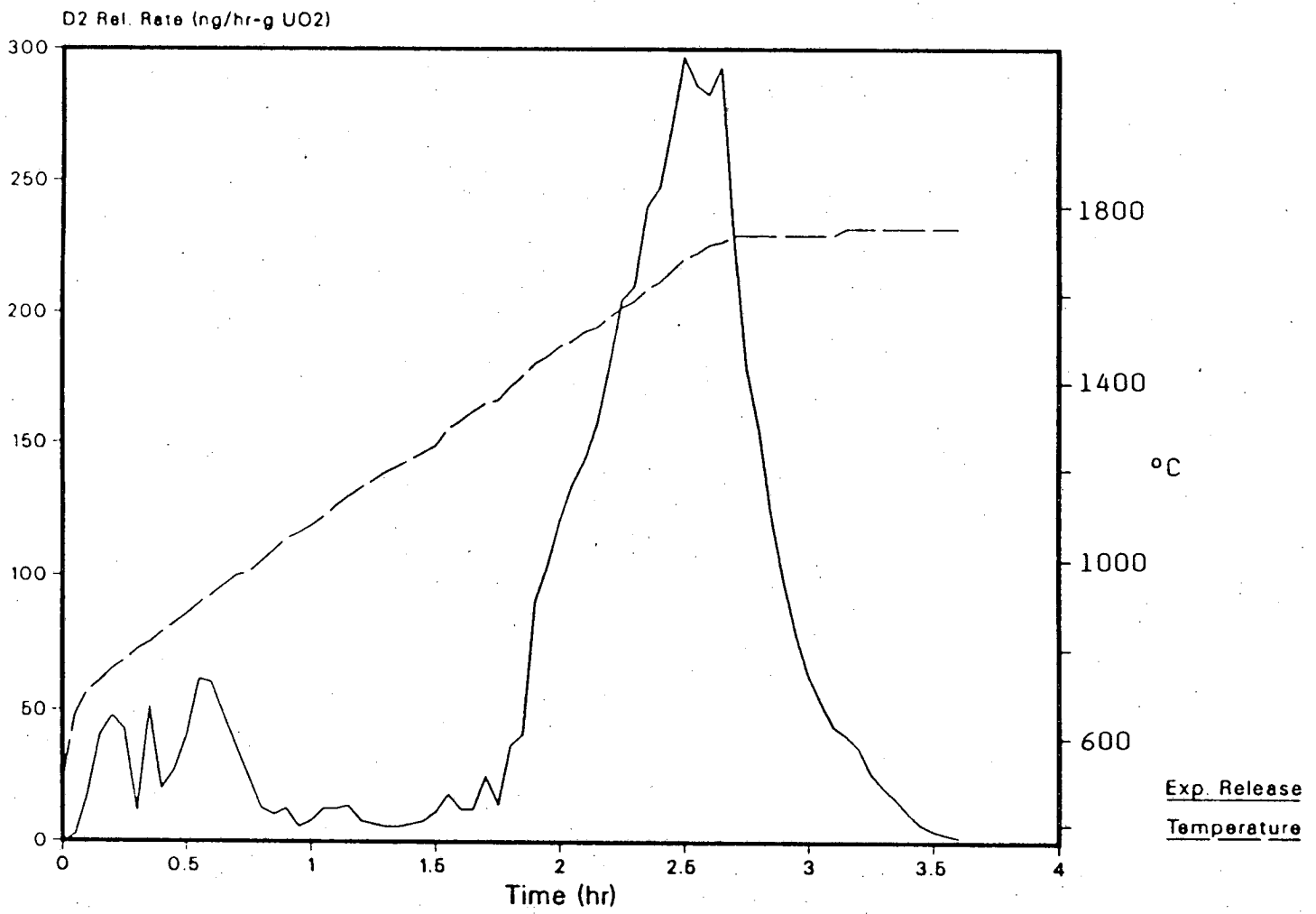

Fig. B-30 EXPT 26 Single Crystal UO2
Infusion Conditions:
t= 1 1/4 hr T= 1600 C P= 20 atm D2

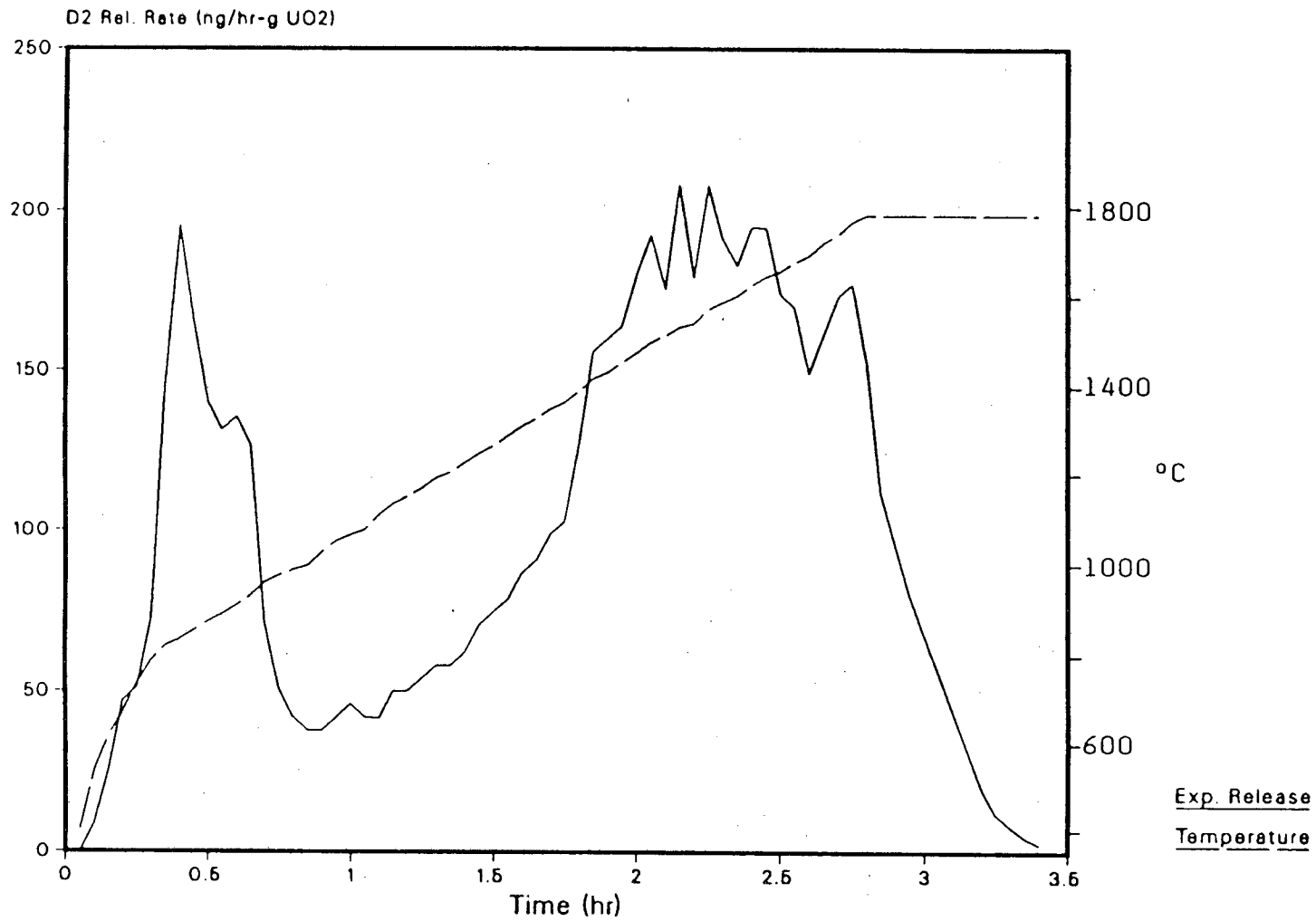

Fig. B-31 EXPT 27 Single Crystal UO2
Infusion Conditions:
t= 1 1/4 hr T= 1600 C P= 26.8 atm D2

References

1. D. R. Olander, D. F. Sherman, and M. B. Balooch, "Retention and Release of Water by Sintered Uranium Dioxide," *J. Nucl. Mat.*, vol. 107, pp. 31-45, 1982.

2. V. J. Wheeler, "The Diffusion and Solubility of Hydrogen in Uranium Dioxide Single-Crystals," *J. Nucl. Mat.*, vol. 40, pp. 189-194, 1971.

3. J. H. Goode and V. C. A. Vaughan, "Voloxidation-Removal of Volatile Fission Products from Spent LMFBR fuels," ORNL-TM-3723, 1973.

4. T. S. Elleman, L. R. Zumwalt, and K. Verghese, "Hydrogen Transport and Solubility in Nonmetallic Solids," Proceedings, ANS Topical Meeting, Conf. on the Technology of Controlled Nuclear Fusion, Santa Fe, May 9-11, 1978.

5. D. L. Smith, "Blanket Materials for DT Fusion Reactors," *J. Nucl. Mat.*, vol. 103/104, p. 19, 1981.

6. M. Abdou and et al., "Blanket Comparison and Selection Study- Interim Report," ANL/FPP/TM-177, Sept. 1983.

7. P. G. Groner and W. Seifritz, "Ceramic Lithium Components for Solid Breeder Concepts for Fusion Reactors," *Nucl. Technology/Fusion*, vol. 5, pp. 109-177, March, 1984.

8. D. R. Olander, "Theory of Helium Dissolution in Uranium Dioxide. II. Helium Solubility," *J. of Chem. Phys.*, vol. 43: No. 3, pp. 785-788, 1965.

9. Y. Aratono, M. Nakashima, M. Saeki, and E. Tachikawa, "The Diffusivities of Fission-Created or Thermally-Doped Tritium in Uranium Dioxide," *J. Nucl. Mat.*, vol. 110, pp. 201-207, 1982.

10. D. Scargill, "Diffusion of Fission Product Tritium in Irradiated UO_2," *J. Nucl. Mat.*, vol. 74, pp. 62-67, 1978.

11. Y. Aratono and E. Tachikawa, "Release-Behavior of Tritium and its Chemical Forms in Heating Irradiated UO_2(Li)-Pellet"," *J. Inorg. Nucl. Chem.*, vol. 39, pp.

2125-2130, 1977.

12. Y. Aratono, M. Nakashima, M. Saeki, and E. Tachikawa, ''Release Behaviors of Tritium from Uranium Dioxide During Reactor Operation,'' *J. Nucl. Mat.*, vol. 114, pp. 234-241, 1983.

13. C. S. Alexander, T. S. Elleman, and et al., ''Tritium Diffusion in Nonmetallic Solids of Interest for Fusion Reactors, Final Report,'' DOE/ET/52022-5, 1979.

14. T. S. Elleman, D. Rao, K. Verghese, and L. Zumwalt, ''Hydrogen Diffusion, Dissolution and Permeation of Non-Metallic Solids,'' ORO-4721-t1, 1979.

15. S. K. Roy and R. S. Coble, ''Solubility of Hydrogen in Porous Polycrystalline Aluminum Oxide,'' *J. Am. Ceram. Soc.*, vol. 50: No. 8, pp. 435-436, 1967.

16. T. Iwaki and M. Muira, ''Studies of the Surface of Titanium Dioxide, III. The Electrical Conduction and the Hydrogen Uptake,'' *Bull. Chem. Soc. Japan*, vol. 49, pp. 2321-2, 1976.

17. D. G. Thomas and J. J. Lander, ''Hydrogen as a Donor in Zinc Oxide,'' *J. Chem Physics*, vol. 25, pp. 1136-1142, 1956.

18. H. Katsuta, S. Konishi, and H. Yoshida, ''Solubility and Diffusivity of Hydrogen in Li_2O,'' *J. Nucl. Mat.*, vol. 116, pp. 244-248, 1983.

19. T. Smith, ''Kinetics and Mechanism of Hydrogen Permeation of Oxide Films on Zirconium,'' *J. Nucl. Mat.*, vol. 18, pp. 323-336, 1966.

20. H. R. Ihle and C. H. Wu, ''The Solubility of Hydrogen Isotopes in Solid Lithium Oxide,'' Presented at the 3rd Topical Meeting on Fusion Reactor Materials, Albuquerque, NM, Sept 22-23, 1983.

21. ''Standard Test Method for Water Absorption, Bulk Density, Apparent Porosity, and Apparent Specific Gravity of Fired Whiteware Products,'' ASTM G373-72.

22. J. Crank, *The Mathematics of Diffusion, 1st ed.*, p. 90, Clarendon Press, Oxford, 1964.

23. Oak Ridge National Laboratory, ''Risk Peripheral Shielding Rouine Collection--HEATING 6,'' PSR-199, 1983.

24. A. K. Srivastava and D. R. Olander, ''Retention and Release of Water Vapor by Uranium Dioxide,'' *Trans. Amer. Nucl. Soc.*, vol. 28, p. 216, 1978.

25. R. E. Stickney, ''Diffusion and Permeation of Hydrogen Isotopes in Fusion Reactors: A Survey,'' in *The Chemistry of Fusion Technology*, ed. by D. M. Gruen, Plenum Press, New York, N. Y., 1972.

26. R. Frauenfelder, *J. Chem. Phys.*, vol. 48, p. 3955, 1968.

27. Joseph J. Katz and Eugene Rabinowitch, *The Chemistry of Uranium*, pp. 208-210, Dover Publications, Inc., N.Y., N.Y., 1951.

28. R. K. Edwards and A. E. Martin, *Thermodynamics of Nuclear Materials*, 2, p. 423, IAEA, Vienna, 1965.

29. H.S. Carslaw and J.C. Jaeger, *Conduction of Heat in Solids, 2nd Ed.*, p. 235, Oxford University Press, London, 1959.

30. D. R. Olander, *Fundamental Aspects of Nuclear Reactor Fuel Elements*, Technical Info. Center, 1976. Sec. 15.6

31. T. Hirabayashi, M. Saeki, and E. Tachikawa, ''A Thermal Desorption Study of the Surface Interaction Between Tritium and Type 316 Stainless Steel,'' *J. of Nucl. Mat.*, vol. 126, pp. 38-43, 1984.

32. K. Erents and G. M. McCracken, ''Trapping and Re-emission of Fast Deuterium Ions From Nickel II,'' *Radiation Effects*, vol. 3, pp. 123-129, 1970.

33. T. Otsubo, S. Goto, and H. Sato, ''Proc. 2nd JIM Int. Symposium on Hydrogen in Metals,'' *Supplement to Trans. JIM*, vol. 21, p. 241, 1980.

34. K. L. Wilson and M. I. Baskes, ''Deuterium Re-emission from 304LN Stainless Steel,'' *J. Nucl. Mat.*, vol. 111 & 112, pp. 622- 627, 1982.

35. S. K. Erents, ''The Effect of Bombardment Induced Damage on The Trapping and Thermal Re-emission of Deuterium from Tungsten and Molybdenum,'' The 8th Symposium on Fusion Technology, p. EEC EUR 5782e, Nordwijkerhout, Netherlands, June, 1974.

36. D. K. Brice and B. L. Doyle, ''A Trap Activation Model for Hydrogen Retention and Isotope Exchange in Some Refractory Materials,'' *J. Nucl. Mat.*, vol. 103 & 104, pp. 503-508, 1981.

37. D. K. Brice, ''Hydrogen Trapping in Fusion Materials due to Ion Irradiation: Implications for Neutron Irradiation,'' *J. Nucl. Mat.*, vol. 108 & 109, pp. 389-394, 1982.

38. B. L. Doyle, ''A Simple Theory for Maximum Inventory and Release: A New Transport Parameter,'' *J. Nucl. Mat.*, vol. 111 & 112, pp. 628-635, 1982.

39. D. F. Holland and B. J. Merrill, ''Analysis of Tritium Migration and Deposition in Fusion Reactor Systems,'' EGG-M-10281, 1981.

40. W.Th.M. Buters and A. Van den Beukel, ''Trapping and Re-Trapping of Mobile Particles by Uniformly Distributed Non-Saturable Traps,'' *J. Nucl. Mat.*, vol. 137, pp. 51-62, 1985.

LAWRENCE BERKELEY LABORATORY
TECHNICAL INFORMATION DEPARTMENT
UNIVERSITY OF CALIFORNIA
BERKELEY, CALIFORNIA 94720